Maia Haugen Tømmerbakk

Ship Tracking Based on Fiber Optic Cable Data

Master's thesis in Applied Physics and Mathematics

Supervisor: Jo Eidsvik

June 2020

Master's thesis

NTNU
Norwegian University of Science and Technology
Faculty of Information Technology and Electrical Engineering
Department of Mathematical Sciences

NTNU
Norwegian University of
Science and Technology

Maia Haugen Tømmerbakk

Ship Tracking Based on Fiber Optic Cable Data

Master's thesis in Applied Physics and Mathematics
Supervisor: Jo Eidsvik
June 2020

Norwegian University of Science and Technology
Faculty of Information Technology and Electrical Engineering
Department of Mathematical Sciences

NTNU
Norwegian University of
Science and Technology

Summary

On the ocean floor around the world there is a network of fiber optic cables, and combined with a technology called distributed acoustic sensing, it may be possible to utilize data from these cables for ship tracking. Tracking a ship means to estimate the state of the ship at several time steps, where the state of the ship at a time step is given by the position and the velocity of the ship at that time step. The goal of this project is to track a ship based on simulated and real fiber optic cable data.

As the ship travels on the surface of the ocean, it creates vibrations that are measured using distributed acoustic sensing and fiber optic cables. These vibrations can be represented using direct waves, and curves of travel time and energy of a direct wave have been extracted from the real fiber optic cable data. However, it turned out that these extracted curves do not behave as expected. The simulated data consists of travel time and energy curves that are given by the equations of a direct wave, in addition to normally distributed noise.

The curves of travel time and energy have been used as input for two statistical methods, sequential importance resampling and the ensemble Kalman particle filter. Both of these methods are particle filters that at each time step use particles, which are samples of possible states of the ship, to estimate the distribution of the state of the ship given the measured data from the current and the previous time steps. Three evaluation metrics are used to compare the methods. These metrics are root mean square error, minimal effective sample size and mean continuous ranked probability score.

For the simulated data the methods are used to track a ship for four different simulation cases, and for all cases the ensemble Kalman particle filter has the best performance. The results for the ensemble Kalman particle filter for the simulation cases are good; at most time steps both the position and the velocity of the ship is well estimated with low bias and low variance, and the effective sample size is reasonable. For all cases, the sequential importance resampling method struggles with degeneracy.

For the real data the results are not as good as the results for the simulated data. Because of the good performance of the ensemble Kalman particle filter for the simulated data, it is assumed that the reason for the inferior results for the real data is the quality of the data, along with the extraction procedures that are used to extract the travel time and energy curves from the data.

From further analysis of the performance of the methods, it is clear that the ensemble Kalman particle filter is more robust than the sequential importance resampling method. To a certain degree, the performance of the ensemble Kalman particle filter is not significantly affected by choosing parameters that are not optimal, and the results from the ensemble Kalman particle filter are not negatively affected by using only a small amount of particles for the estimation procedures.

Based on the good results for the simulated data, it might be possible to use the ensemble Kalman particle filter for ship tracking based on fiber optic cable data at some point in the future. However, the quality and the processing of the data must be improved. In addition, the method needs to be developed such that it is possible to track several ships at the same time.

Samandrag

På havbotnen rundt om i verda finns det eit nettverk av fiberoptiske kablar. Ved å kombinera desse kablane med ein teknologi kalla distribuert akustisk måling, kan det kanskje vera mogleg å bruka data frå kablane til å spora skip. Å spora eit skip vil seia å estimera tilstanden til skipet ved fleire tidssteg, der tilstanden til eit skip i dette tilfellet er posisjonen og farten til skipet. Målet med dette prosjektet er å spora eit skip basert på simulert og reell data frå fiberoptiske kablar.

Medan skipet flyttar seg på havoverflata lagar det vibrasjonar som vert måla med distribuert akustisk måling. Vibrasjonane kan bli representert av direktebølgjer, som igjen er representert av gangtidskurver og energikurver. Slike kurver har blitt henta ut frå det reelle datasettet, men frå analyse av desse kurvene viste det seg at dei ikkje oppfører seg slik ein kunne forventa. Simulert data er laga av kurver for gangtid og energi som er gitt av likningane for direktebølgjer, i tillegg til normalfordelt støy.

Gangtidskurvene og energikurvene har blitt brukt som input til to statistiske metodar kalla sekvensiell viktigheitsomsampling og ensemble Kalman partikkelfilter. Begge desse metodane er partikkelfilter som for kvart tidssteg brukar partiklar, som er eit utval av moglege skipstilstandar, til å estimera fordelinga av skipstilstanden gitt målt data frå det aktuelle tidssteget og tidlegare tidssteg. For å samanlikna resultata frå dei to metodane har tre ulike evalueringsmål blitt nytta. Desse måla er rota av den gjennomsnittlege kvadratiske feilen, minimal effektiv utvalsstorleik og gjennomsnittleg kontinuerleg rangert sannsynspoengsum.

For simulert data har metodane blitt brukt til å spora eit skip i fire ulike simuleringssituasjonar, og i alle situasjonane var resultata best for ensemble Kalman partikkelfilteret. Resultata for denne metoden er gode; for dei fleste tidsstega er både posisjonen og farten til skipet estimert på ein god måte med lite feil og lite varians. I tillegg er den effektive utvalsstorleiken rimeleg. I alle situasjonane har den sekvensielle viktigheitsomsamplingsmetoden problem med forfall grunna låg effektiv utvalsstorleik.

For det reelle datasettet er ikkje resultata like gode som for simulert data. På grunn av dei gode resultata for ensemble Kalman partikkelfilteret for simulert data, er det antatt at grunnen til at resultata ikkje er like gode for reelle data som for simulert data at kvaliteten av det reelle datasettet og kvaliteten av kurveuthentingsmetodane ikkje er bra nok.

Frå vidare analyse av prestasjonen til metodane er det kome fram til at ensemble Kalman partikkelfilteret er ein meir robust metode enn den sekvensielle viktigheitsomsamplingsmetoden. Resultata frå ensemble Kalman partikkelfilteret vert til ei viss grad ikkje påverka på ein negativ måte dersom valet av parametrar ikkje er optimalt, eller om metoden brukar få partiklar til å estimera fordelinga av tilstanden til skipet.

Basert på dei gode resultata for simulert data kan det konkluderast med at det ein gong i framtida kanskje kan vera mogleg å bruka ensemble Kalman partikkelfilteret saman med data frå fiberoptiske kablar til å spora skip. For at dette skal kunna skje, må kvaliteten av det reelle datasettet og kvaliteten av dataprosesseringa forbetrast. Det er også ein fordel om metoden vert utvikla slik at det er mogleg å spora fleire skip på same tid.

Preface

This project is the final part of the Master of Science in Applied Physics and Mathematics at NTNU. The work presented here has been carried out during the spring semester of 2020, and it constitutes my master thesis. I would like to thank Izzie Yi Liu and Martin Landrø at Sintef for providing data, code, information about the problem and guidance. I would also like to thank Jo Eidsvik for excellent supervision throughout the semester.

Table of Contents

Chapter 1

Introduction

During the last decades, the use of fiber optic cable data has grown in importance. As discussed by Baldwin (2014) the oil and gas industry has used data from fiber optic cables for several applications, varying from temperature measurements to production monitoring in the wells. More recently, as documented by Ajo-Franklin et al. (2019), it has shown possible to use fiber optic cable data to detect earthquakes and to monitor the groundwater level. One way of retrieving data from fiber optic cables is to use a technology called distributed acoustic sensing, or DAS for short.

Vibrations created on the surface of the earth travel through the soil as waves of energy, and by using DAS in combination with fiber optic cables in the ground these waves of energy can be measured. The DAS installation sends pulses of laser light through a fiber optic cable, and as these pulses interact with the fiber optic cable, reflections are sent back through the cable. The interactions happen because of the vibrations in the fiber optic cable, which are caused by the vibrations created on the surface. The time it takes before the reflections reach the DAS installation determines the position along the cable where the laser pulse interacted with the cable. Consequently, it is possible to measure vibrations along the entire cable using DAS (Silixia, 2019).

Anything that happens on the surface of the earth creates vibrations that affect fiber optic cables below the surface. However, the magnitude of these vibrations differ based on their source. A person walking around will create vibrations in the soil, but these vibrations are much smaller than the vibrations created by a landslide or an earthquake. Similarly, noisy events in the water cause vibrations. If a fiber optic cable is placed on the ocean floor, then the vibrations caused by a ship can be measured by DAS.

According to Kystverket (2019) all civilian ships are obliged to use a system of identification called the automatic identification system, or AIS for short. AIS is a satellite based technology that gives authorities and ships in traffic information on the position, velocity and routes of other ships, and the technology helps ships avoid collisions. The AIS technology is a supplement to the radar technology.

It is possible for ships to turn off the AIS-transponder, and consequently it can be difficult to track these ships. If a ship turns off the AIS-transponder it might be because the

ship is involved in secret activities, and an alternative to AIS is needed to detect for instance illegal activities. As the network of fiber optic cables around the world is extensive, one alternative might be to use data from fiber optic cables to track these ships. A map of the fiber optic cables on the ocean floor around the world is shown in Figure 1.1, indicating locations where coverage is reasonable and ship tracking could be possible.
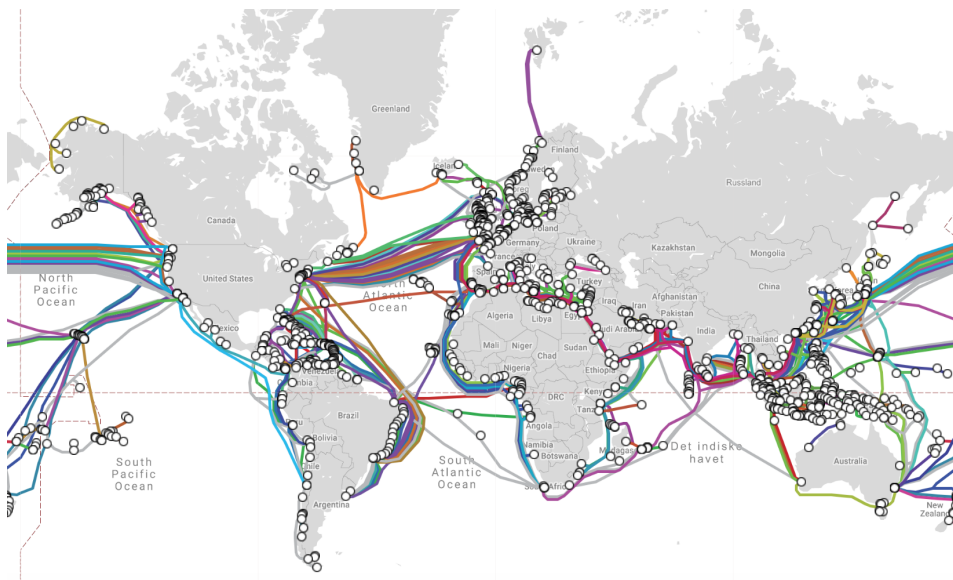
Figure 1.1: The network of offshore fiber optic cables around the world (TeleGeography, 2019).

The goal of this project is to apply two statistical methods in combination with data from DAS to track a ship. These methods are the particle filters called sequential importance resampling (SIR) and the ensemble Kalman particle filter (EnKPF). The SIR method is a basic particle filter, while the EnKPF method is a more advanced particle filter. Traditionally, according to Arulampalam et al. (2002), Kalman filters have been applied to tracking problems, but these filters are not applicable when the tracking problem is non-linear, which is the case in this project. Particle filters, on the other hand, can be implemented such that non-linearity is not a problem, and consequently, particle filters have become a popular choice for non-linear tracking problems.

In previous applications of data from DAS, the data has not been used in combination with statistical methods, however, this does not necessarily mean that data from DAS is not suitable for use in combination with statistical methods, it just means that DAS is a relatively new type of data, not yet introduced in current-day workflows, at least not for statistical modeling and spatio-temporal monitoring. The data that will be used in this project is both simulated data and real data, where the real data originates from fiber optic cables in the North Sea.

In chapter 2 of this project the experimental setup of the project will be presented, and the physical procedure for simulating data will be explained. In the last part of the chapter the real data will be explored. In chapter 3 the statistical methods along with algorithms

of how the methods are applied to the fiber optic cable data will be presented. The results from applying the statistical methods to the data from DAS are given in chapter 4. For the simulated data, the results are presented for four different simulation cases. The results will be discussed in chapter 5, and possible extensions of the project are discussed in chapter 6. In the end, in chapter 7, a conclusion of the project will be provided.

Chapter 2

Experimental setup and data analysis

This chapter aims to clarify the experimental setup of the project. In addition, data exploration will be performed on both simulated and real data.

2.1 Experimental setup

In the simplest setup for this project, the fiber optic cable on the ocean floor is assumed to be straight, and the cable defines a coordinate system with origin in one of the ends of the cable. The x-axis goes along the cable, and the y- and z-axes are perpendicular to the cable. Hence, the coordinates for the cable are defined by the x-coordinate as $y = z = 0$ along the cable. The z-coordinate is zero on the ocean floor and increases towards the surface of the ocean.

  The potential ship positions at time step t used in the implementation of the statistical methods are given by the coordinates x_t, y_t and z_t which are defined relative to the coordinate system defined by the cable. $z_t = z_{\text{true}}$ is fixed as the depth of the ocean around the fiber optic cable. The position that is to be estimated for each time step t, $t = 0, \ldots, \tau$, is defined by the coordinates $x_{\text{true},t}$, $y_{\text{true},t}$ and $z_{\text{true},t}$, but since it is assumed that $z_{\text{true},t} = z_{\text{true}}$ for all t, only $x_{\text{true},t}$ and $y_{\text{true},t}$ needs to be estimated for $t = 0, \ldots, \tau$. The experimental setup is shown in Figure 2.1. The bold x-axis in the figure represents the cable, and the true position of the ship is marked for the time steps t and $t + 1$.

2.2 Wave data

Vibrations from ships are represented as waves, and according to Sheriff and Geldart (1995) several different types of waves exist in physical models of the phenomena. Two of these wave types are direct waves and head waves. The different types of waves describe
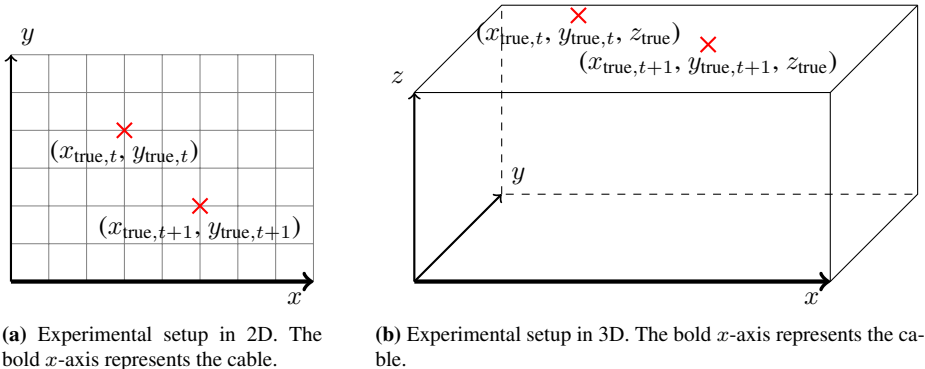
(a) Experimental setup in 2D. The bold x-axis represents the cable.

(b) Experimental setup in 3D. The bold x-axis represents the cable.

Figure 2.1: Experimental setup.

the different ways the vibrations can spread throughout the water. For instance, direct waves describe how the vibrations spread directly and naturally from the source. When the vibrations reach the ocean floor the direct waves describe how the vibrations continue to spread through the layers of the earth under the ocean. Head waves, on the other hand, describes how, when the vibrations reach the ocean floor, the vibrations spread along the ocean floor. Direct waves and head waves are illustrated in Figure 2.2. The red dot in the figure represents the source of the wave, which in this case is a ship. The green dot represents the point at which the wave is registered, which in this case is a point on the fiber optic cable.

(a) Direct wave.
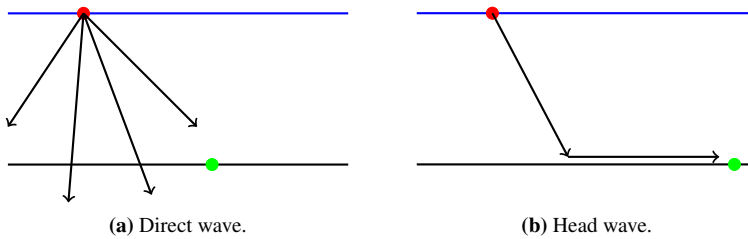
(b) Head wave.

Figure 2.2: Illustration of the difference between direct waves and head waves. The blue line defines the surface of the ocean, while the horizontal black line defines the floor of the ocean. The red dot represents the source from which the vibrations have originated, and the green dot represents the point at which the vibrations are measured. The black arrows represent waves.

Figure 2.2 illustrates that as a head wave reaches the ocean floor, some of its energy is transferred to the ground. This indicates that the energy of a direct wave is larger than the energy of a head wave. The texture of the ground affects which kind of waves the cable will measure, and which kind of waves that most accurately represents the vibrations from the ship. If the ground is made of rock, then the head wave will move fast along the ground, and the cable will measure a head wave before it measures a direct wave. If the

ground is muddy, then the head wave will move slowly along the ground and the direct wave will be measured by the cable before it measures the head wave. It is also possible that the vibrations that are created by the ship are more precisely represented by a mixture of wave types, than by only one of the wave types.

For each of the wave types there are equations for the travel time of the wave between two locations, and the associated energy of the wave. These equations are expressed in terms of cable coordinates $x_{\text{cable}}, y_{\text{cable}}$ and z_{cable} and the ship position from which the wave originated x_t, y_t and z_{true} for $t = 0, \dots, \tau$. In this project only direct waves will be considered, and the input to the statistical methods is given by the travel time and energy of a direct wave resulting from vibrations created by a ship for time steps $t = 0, \dots, \tau$. The travel time and energy is measured at discretized locations along the cable. The equation for the travel time T_t at time step t for the direct wave is given by

$$T_t = \frac{\sqrt{(x_{\text{cable}} - x_t)^2 + (y_{\text{cable}} - y_t)^2 + (z_{\text{cable}} - z_{\text{true}})^2}}{v_p}, \tag{2.1}$$

where v_p is a constant, and in saltwater $v_p = 1500$ m/s. The energy P_t^2 for the direct wave at time step t is given by

$$P_t^2 = \left[\frac{s(x_{\text{cable}} - x_t)}{(x_{\text{cable}} - x_t)^2 + (y_{\text{cable}} - y_t)^2 + (z_{\text{cable}} - z_{\text{true}})^2} \right]^2, \tag{2.2}$$

where s is a normalization constant defined by the source signature. These equations reflect the linear pathways of direct waves, and the vibrations of the crossline component of the cable stretching as a function of the passing wave. Calculating T_t and P_t^2 at all locations along the cable results in travel time curves and energy curves, respectively. Such curves for $y_{\text{cable}} = z_{\text{cable}} = 0$ and $(x_t, y_t, z_{\text{true}}) = (270, 120, 50)$ for a cable of length 700 m are shown in Figure 2.3. For these curves there are 701 equally spaced locations along the cable for which Equations (2.1) and (2.2) are calculated.

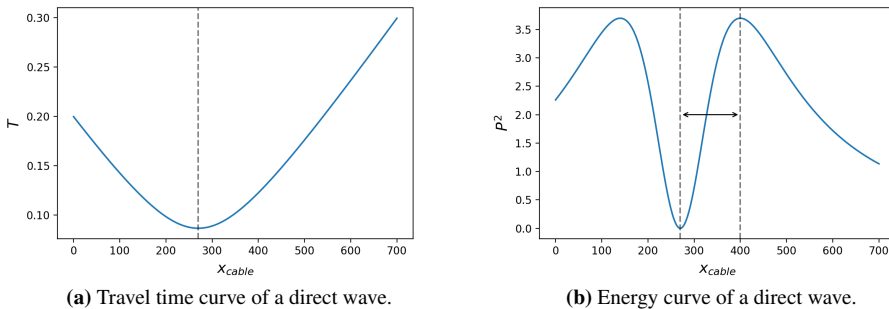**(a)** Travel time curve of a direct wave. **(b)** Energy curve of a direct wave.

Figure 2.3: Curves for travel time and energy for a direct wave from position $(x_t, y_t, z_{\text{true}}) = (270, 120, 50)$ with $s = 500$. The vertical dashed line in the plot on the left is placed at the x-coordinate of the ship. The double sided arrow in the plot on the right illustrates the distance a_t.

The derivative of T_t with respect to x_{cable} is given by

$$\frac{\partial T_t}{\partial x_{\text{cable}}} = \frac{2(x_{\text{cable}} - x_t)}{2v_p \sqrt{(x_{\text{cable}} - x_t)^2 + (y_{\text{cable}} - y_t)^2 + (z_{\text{cable}} - z_{\text{true}})^2}}. \qquad (2.3)$$

Setting this expression equal to zero and solving for x_{cable} gives $x_{\text{cable}} = x_t$. This result is confirmed by Figure 2.3a as the minimum of the curve is given by $x_{\text{cable}} = x_t = 270$.

The derivative of P_t^2 with respect to x_{cable} is given by

$$\frac{\partial P_t^2}{\partial x_{\text{cable}}} = \frac{2s^2(x_{\text{cable}} - x_t)((x_{\text{cable}} - x_t)^2 + (y_{\text{cable}} - y_t)^2 + (z_{\text{cable}} - z_{\text{true}})^2)^2}{((x_{\text{cable}} - x_t)^2 + (y_{\text{cable}} - y_t)^2 + (z_{\text{cable}} - z_{\text{true}})^2)^4}$$
$$- \frac{s^2(x_{\text{cable}} - x_t)^2 2((x_{\text{cable}} - x_t)^2 + (y_{\text{cable}} - y_t)^2 + (z_{\text{cable}} - z_{\text{true}})^2)2(x_{\text{cable}} - x_t)}{((x_{\text{cable}} - x_t)^2 + (y_{\text{cable}} - y_t)^2 + (z_{\text{cable}} - z_{\text{true}})^2)^4}.$$
$$(2.4)$$

Setting this expression equal to zero and solving for x_{cable} gives

$$x_{\text{cable}} = x_t \pm \sqrt{(y_{\text{cable}} - y_t)^2 + (z_{\text{cable}} - z_{\text{true}})^2}. \qquad (2.5)$$

In combination with Figure 2.3b it is clear that this means that the distance from the minimum value of the energy curve as a function of x_{cable} to the maximum value of the curve is given by $a_t = \sqrt{(y_{\text{cable}} - y_t)^2 + (z_{\text{cable}} - z_{\text{true}})^2}$. In the case of the displayed curve which is plotted for $y_{\text{cable}} = z_{\text{cable}} = 0$, the expression for the distance a_t is reduced to $a_t = \sqrt{y_t^2 + z_{\text{true}}^2}$. If the depth of the ocean, z_{true}, is considered known, then the distance a_t is determined only by y_t.

From the calculations of the derivatives of the curves for the direct wave it is clear that, for a known z_{true}, the shapes of the curves are determined by x_t and y_t. If x_t is set from Equation (2.3), then y_t can be found from Equation (2.5). Note that y_t can only be determined in absolute value.

It should be mentioned that in practice it can be quite difficult to solve Equations (2.3) and (2.4). In reality, the cable can be curved such that y_{cable} is a function of x_{cable}. Also, the depth of the ocean can vary such that z_{true} is not constant for all t. In that case, z_{true} would also be a function of x_{cable}. In addition, the measurements from the fiber optic cable contain noise, such that the curves that are measured will not be as smooth as the curves in Figure 2.3.

2.3   Simulated data

A reason for simulating data is to study the properties of the statistical methods in an idealized situation. If the statistical methods give satisfactory results for the simulated data, then it is expected that the methods are suitable for ship tracking, and it is reasonable to try to implement the methods using real data. However, if the results from using the statistical methods with simulated data are poor, then the methods may not be suited for ship tracking, and it might not be necessary to try to implement the methods using real data. Hence, the use of the simulated data combined with the statistical methods may indicate whether or not the methods are suitable for ship tracking.

2.3.1   The simulation procedure

For the simulation procedure it is assumed that a ship is traveling on the surface of the ocean in proximity to an imaginary straight cable on the ocean floor, and the outcome of this procedure is travel time curves and energy curves with added noise. The first step of the simulation procedure is to determine the true path of the ship. The true path is defined by a set of states, $\mathbf{x}_{\text{true},t}$ for $t = 0, \ldots, \tau$, where each true state is given by

$$\mathbf{x}_{\text{true},t} = \left[x_{\text{true},t}, y_{\text{true},t}, v_{\text{true},x,t}, v_{\text{true},y,t} \right]^T. \tag{2.6}$$

At time t, $v_{\text{true},x,t}$ is the true velocity of the ship in the x-direction and $v_{\text{true},y,t}$ is the true velocity of the ship in the y-direction.

The next step of the simulation procedure consists of calculating the n-dimensional vectors $\mathbf{T}_{\text{data},t}$ and $\mathbf{P}^2_{\text{data},t}$ for $t = 0, \ldots, \tau$, where n is equal to the number of points along the cable at which the energy and travel time is registered. These vectors are given by

$$\mathbf{T}_{\text{data},t} = f_{\mathbf{T}}(\mathbf{x}_{\text{true},t}) + \boldsymbol{\eta}_{\mathbf{T},t} \tag{2.7}$$

and

$$\mathbf{P}^2_{\text{data},t} = f_{\mathbf{P}}(\mathbf{x}_{\text{true},t}) + \boldsymbol{\eta}_{\mathbf{P},t}, \tag{2.8}$$

where the noise vectors $\boldsymbol{\eta}_{\mathbf{T},t}$ and $\boldsymbol{\eta}_{\mathbf{P},t}$ are assumed to be distributed according to

$$\boldsymbol{\eta}_{\mathbf{T},t} \sim \mathcal{N}_n(\mathbf{0}, \sigma_{\mathbf{T}}^2 I_n) \quad \text{and} \quad \boldsymbol{\eta}_{\mathbf{P},t} \sim \mathcal{N}_n(\mathbf{0}, \sigma_{\mathbf{P}}^2 I_n), \tag{2.9}$$

with I_n equal to the identity matrix of dimensions $n \times n$. $\mathcal{N}_n$ denotes the n-dimensional Gaussian distribution.

As can be observed from Equations (2.7)-(2.9) it is assumed that the noise of the simulated data is normally distributed. It is also assumed that the noise at each point along the curves is uncorrelated with the noise at all other points along the curves. In addition, the noise of the travel time curve is uncorrelated with the noise of the energy curve, and the amount of noise for the curves is independent of the time step. These assumptions are present in the project as they simplify the implementation of the statistical methods. It would also be possible to assume some bias in the curves, meaning that a measured curve is larger or smaller at each element compared to the true curve. However, such an assumption would make the problem more complicated.

Each element of $\mathbf{T}_{\text{data},t}$ is the measured travel time for a wave from position $(x_{\text{true},t}, y_{\text{true},t})$ to each of the n points on the cable, and the output of $f_{\mathbf{T}}(\mathbf{x}_{\text{true},t})$ is a n-dimensional vector where each element is given by Equation (2.1). Similarly, $\mathbf{P}^2_{\text{data},t}$ is the measured energy of a wave from position $(x_{\text{true},t}, y_{\text{true},t})$ to each of the n points on the cable, and the output of $f_{\mathbf{P}}(\mathbf{x}_{\text{true},t})$ is a n-dimensional vector where each element is given by Equation (2.2). The simulated curves based on the curves in Figure 2.3 are shown in Figure 2.4.

(a) Simulated travel time curve of a direct wave.

(b) Simulated energy curve of a direct wave.

Figure 2.4: Simulated curves for travel time and energy for a direct wave from position $(x_{\text{true},t}, y_{\text{true},t}, z_{\text{true}}) = (270, 120, 50)$. In this case $s = 500$, $\sigma_{\mathbf{T}}^2 = 0.001$ and $\sigma_{\mathbf{P}}^2 = 2$.

When the ship is close to the cable, the values of $f_{\mathbf{P}(\mathbf{x}_{\text{true},t})}$ are larger than when the ship is far away from the cable. Consequently, the signal to noise ratio is larger in this situation. Simulated data for a ship in position $(x_{\text{true},t}, y_{\text{true},t}, z_{\text{true}}) = (270, 60, 50)$ is shown in Figure 2.5. The signal to noise ratio is larger in Figure 2.5 than in Figure 2.4. The consequence is that it might be easier for the statistical methods to estimate a state that fits the measured data close to the cable than further away from the cable.

(a) Simulated travel time curve of a direct wave for a ship close to the cable.

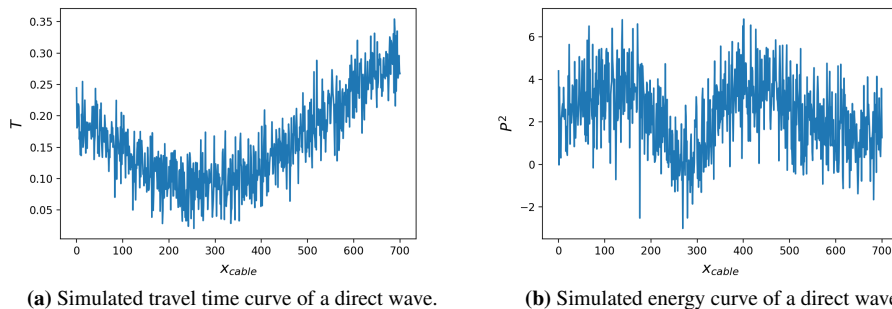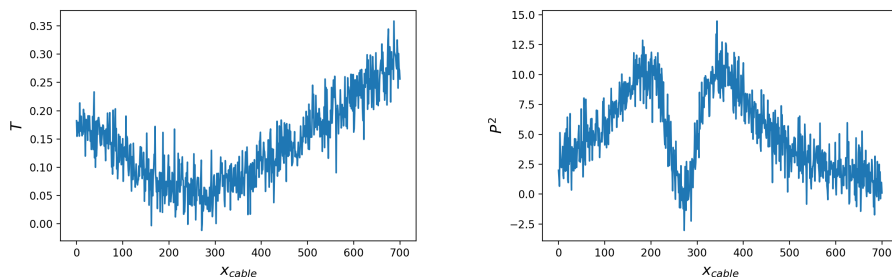**(b)** Simulated energy curve of a direct wave for a ship close to the cable.

Figure 2.5: Simulated curves for travel time and energy for a direct wave from position $(x_{\text{true},t}, y_{\text{true},t}, z_{\text{true}}) = (270, 60, 50)$. The normalization constant is $s = 500$, in addition $\sigma_{\mathbf{T}}^2 = 0.001$ and $\sigma_{\mathbf{P}}^2 = 2$.

2.4 Real data

The real data is provided by Tampnet, which is responsible for the fiber optic cables in the North Sea (Tampnet, 2019). The real data from the North Sea contains much noise, and the signal to noise ratio is low. Moreover, the real data shows repetitions of source signatures over time, representing the frequency of the boat engine. The data used in this project was collected in March of 2018 from a cable positioned outside the east coast of England. Preprocessed data from Tampnet has been provided by Sintef. The data is shown in Figure 2.6. Curves of travel time and energy are to be extracted from this data.
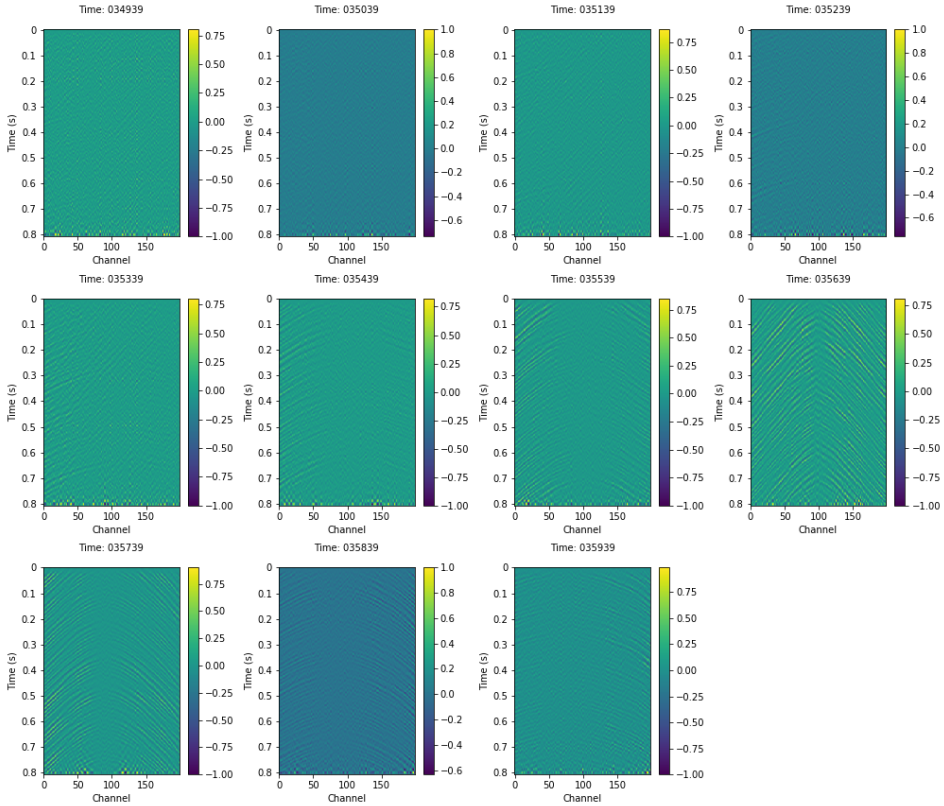
Figure 2.6: The real data collected for 0.8 seconds at eleven different time stamps.

Figure 2.6 shows 0.8 seconds of data for 11 different time stamps. There is one time stamp for each minute, and the first time stamp is at 03:49. For each minute the data is retrieved 39 seconds into the current minute. The x-axis of the plots in Figure 2.6 is given by the points along the cable at which the travel time curves and the energy curves are measured. The structure in the data represents the travel time curve of the vibrations of the ship. At time stamp *Time: 035639* the structure is clear, and it can be observed that the travel time decreases towards the center of the plot. This indicates that the vibrations of the ship reach the middle part of the cable before they reach the ends of the cable, and

consequently, it is expected that at time stamp *Time: 035639* the x-coordinate of the ship is quite similar to the x-coordinate of the center of the cable.

The data from Tampnet is a constant stream of measurements along the cable and each of the plots in Figure 2.6 is taken from this constant stream of measurements. This means that one of the differences between the simulated curves and the curves that will be extracted from the real data, is that for the simulated curves there is no aspect of time. The curves that are to be extracted from the real data are extracted from data that is measured over time, and the resulting curves are based on measurements for not only one exact position, but on the positions that the ship visited during the time that the data was measured. Since the interval of time during which the curves are extracted is very short, 0.8 seconds to be exact, the ship is approximately only in one position during the interval.

The cable that the data in this project is taken from is represented by a list of 31 coordinates. These coordinates are transformed to a Cartesian coordinate system, such that the coordinate system that is used for state estimation is defined by the cable. The 31 coordinates of the cable are used as input to an interpolation algorithm, and the cable that is used in this project is given by the interpolated curve which consists of 28800 points. These points will be referred to as channels. Only data associated with the 199 channels placed closest to the point at which the ship crosses the cable will be used in this project. These 199 channels constitute the x-axis of each of the plots in Figure 2.6.

For each of the eleven time stamps shown in Figure 2.6 the real data is given as a matrix of dimensions $501 \times n$, with $n = 199$. The matrix of data associated with time stamp t is denoted by Q_t and column j of matrix Q_t is denoted by $\mathbf{q}_{t,j}$ for $j = 0, \ldots, n - 1$. In this case $t = 0, \ldots, 10$ where $t = 0$ corresponds to time stamp *Time: 034939*. $\mathbf{q}_{t,j}$ is a time series which represent the vibrations from a ship registered by channel j. The first dimension of each matrix Q_t is transformed into a time axis by multiplying with the time scale $\lambda = 0.0016$ s. This creates the vertical axis of the data displayed in Figure 2.6.

2.4.1 Extracting travel time curves

When it comes to extracting travel time curves from the real data, there are many ways in which this can be done. The structure of the data in Figure 2.6 indicates how the travel time curve is shaped. This means that if the structure of the data consists of steep curves, then also the travel time curve is expected to be a steep curve. It also means that if the structure of the data has its peaks at column $\mathbf{q}_{t,j}$, then the minimum of the extracted travel time curve is expected to be around channel j. Based on this, it seems reasonable to exploit the structure of the wave data when travel time curves are to be extracted. One way to do so is to use a technique called dynamic time warping (Keogh and Pazzani, 2001), or DTW for short. This technique aims to shift the data such that the structure is flattened, and then use the shifts to define a travel time curve. These are the principles that are used for the travel time extraction in this project.

Another way of extracting travel time curves is for instance to try to follow one of the lines in the structure of the data through all columns of the data. This technique is quite simple, but a major disadvantage is that the technique only utilizes a small part of the data, namely the line that it tries to follow. Other techniques are those that are based on image recognition or neural networks. The problem with such techniques is that they need to be trained on a large amount of data. The technique that is used in this project is quite simple

to implement, and no training is needed. Also, with this technique it is possible to utilize all of the data, not just a small part of the data.

For each matrix Q_t the procedure for travel time extraction used in this project iterates through the columns of the matrix. The first part of the procedure aims to find a time shift for which each column should be shifted in order to minimize the squared difference between the elements of columns $j - 1$ and j. In order to do this, l elements of $\mathbf{q}_{t,j-1}$ are compared to l elements of $\mathbf{q}_{t,j}$. More precisely, the squared difference between $\mathbf{q}_{t,j-1}[\text{start}_0 : \text{start}_0 + l]$ and $\mathbf{q}_{t,j}[\text{start}_k : \text{start}_k + l]$ is calculated for $k = 0, \ldots, M$. start_k is the smallest index of the elements that are part of the comparison for the kth interval. Furthermore, $\mathbf{q}_{t,j}[a : b]$ denotes the elements of $\mathbf{q}_{t,j}$ with indexes in the interval $[a, b)$. The scheme for calculating the time shifts at time step t is illustrated in Figure 2.7 and the same scheme is presented in Algorithm 1. In the figure and in the algorithm, δ is a parameter that represents the number of indexes between start_{k-1} and start_k for all k.
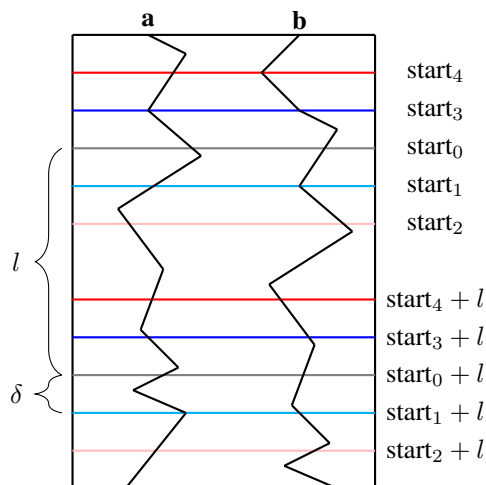
Figure 2.7: The framework for time shifting of time series. **a** and **b** are two time series. Two horizontal lines of matching color define an interval of elements that is used for time series comparison.

The two black curves in Figure 2.7 are two time series, **a** and **b**. By using Algorithm 1 to find the best time shift for **b** compared to **a**, $M + 1 = 5$ different intervals of the two time series are compared. At first the squared difference between all elements of the two time series between the two horizontal gray lines is calculated. Next, the squared difference between the elements of **a** between the two horizontal gray lines and the elements of **b** between the horizontal light blue lines is calculated. Furthermore, this calculation is carried out for the remaining horizontal lines. During all calculations the relevant elements of **a** are those elements between the two horizontal gray lines, while the relevant elements of **b** are those elements between two horizontal lines of matching color.

For Figure 2.7 **b** is a shifted version of **a**, and **b** is shifted downwards by 2δ. Hence, the squared difference between the elements of the two time series in Figure 2.7 is at its smallest if **b** is shifted upwards by 2δ. This means that by applying Algorithm 1 to the time series in Figure 2.7 the vector $\texttt{shifts}_t = [0, 2\delta]$ is created.

Algorithm 1: Procedure for calculating time shifts.

1 Initialize the n-dimensional vector $\texttt{shifts}_t$ as a vector of zeros
2 **for** $j = 1, \ldots, n-1$ **do**
3   Initialize $\texttt{diff}$ as a $(M+1)$-dimensional vector of zeros
4   **for** $k = 0, \ldots, M$ **do**
5   **if** $k \leq M/2$ **then**
6 $\text{start}_k = \text{start}_0 + k\delta$
7   **else**
8 $\text{start}_k = \text{start}_0 - (k - M/2)\delta$
9   **end**
10 $\texttt{diff}[k] = \text{sum}((\mathbf{q}_{t,j-1}[\text{start}_0 : \text{start}_0 + l] - \mathbf{q}_{t,j}[\text{start}_k : \text{start}_k + l])^2)$
11   **end**
12 $\texttt{shift} = \text{argmin}(\texttt{diff})$
13   **if** $shift \leq M/2$ **then**
14 $\texttt{shifts}_t[j] = \texttt{shift} \cdot \delta$
15   **else**
16 $\texttt{shifts}_t[j] = -(\texttt{shift} - M/2) \cdot \delta$
17   **end**
18 **end**

The next part of the procedure of extracting travel time curves is to use the time shifts to create travel time curves. At time step t the goal is to create the n-dimensional vector $\mathbf{T}_{\text{data},t}$. The first element of this vector is set as $\mathbf{T}_{\text{data},t}[0] = 0.4$. It is not very important what value the first element has since it is the shape of the travel time curve that is important, not the magnitude of the curve. The remaining elements of $\mathbf{T}_{\text{data},t}$ is given by

$$\mathbf{T}_{\text{data},t}[j] = \mathbf{T}_{\text{data},t}[j-1] + \texttt{shifts}_t[j] \cdot \lambda \quad \text{for} \quad j = 1, \ldots, n-1. \tag{2.10}$$

Finally, since the shape of the travel time curve is the most essential, the minimum value of $\mathbf{T}_{\text{data},t}$ is subtracted from all elements of the travel time curve.

2.4.2 Extracting energy curves

The procedure that is used to extract energy curves is much simpler than the procedure that is used to extract travel time curves. The extracted energy curve at time step t is given by the n-dimensional vector $\mathbf{P}^2_{\text{data},t}$. The jth element of this vector is given by the root mean square (RMS) of $\mathbf{q}_{t,j}$, and in order to reduce the noise in the energy curves, smoothing is applied.

At first the vector $\hat{\mathbf{P}}^2_{\text{data},t}$ is created using

$$\hat{\mathbf{P}}^2_{\text{data},t}[j] = \sqrt{\frac{1}{501} \sum_{i=0}^{500} (\mathbf{q}_{t,j}[i])^2} \quad \text{for} \quad j = 0, \ldots, n-1. \tag{2.11}$$

For elements $j = 3, \ldots, n-4$ the smoothing is then carried out by

$$\begin{aligned}
\mathbf{P}^2_{\text{data},t}[j] = {} & 0.1(\hat{\mathbf{P}}^2_{\text{data},t}[j-3] + \hat{\mathbf{P}}^2_{\text{data},t}[j-2] + \hat{\mathbf{P}}^2_{\text{data},t}[j-1]) \\
& + 0.4 \cdot \hat{\mathbf{P}}^2_{\text{data},t}[j] \\
& + 0.1(\hat{\mathbf{P}}^2_{\text{data},t}[j+1] + \hat{\mathbf{P}}^2_{\text{data},t}[j+2] + \hat{\mathbf{P}}^2_{\text{data},t}[j+3]),
\end{aligned} \tag{2.12}$$

while $\mathbf{P}^2_{\text{data},t}[j] = \hat{\mathbf{P}}^2_{\text{data},t}[j]$ for $j = 0, 1, 2$ and $j = n-3, n-2, n-1$. Finally, the minimum of $\mathbf{P}^2_{\text{data},t}$ is subtracted from all elements of $\mathbf{P}^2_{\text{data},t}$ for all t.

2.4.3 Extracted curves

In this subsection, some curves that are extracted from the real data using the extraction procedures described above will be analyzed. Curves that are extracted from two different time stamps in Figure 2.6 will be presented. These time stamps are *Time: 035639* and *Time: 035839*. At time stamp *Time: 035639* the ship is close to the cable, and at time stamp *Time: 035839* the ship is farther away from the cable. Both of the travel time curves that are analyzed in this subsection are scaled such that the magnitude of the extracted curves fit the magnitude of the travel time curves given by Equation (2.1) for the relevant positions of the ship.

At time stamp *Time: 035639* the data has the highest signal to noise ratio. Consequently, it is expected that among the extracted curves for all time stamps the extracted

curves from this time stamp are the curves with the smallest amount of noise. The blue curve in Figure 2.8a show the extracted travel time curve associated with the data at time stamp *Time: 035639*, while the blue curve in Figure 2.8b show the extracted energy curve associated with the data at time stamp *Time: 035639*.

The extracted travel time curve in Figure 2.8a does not contain much noise, and the curve fits well with the travel time curve given by Equation (2.1) for the position in which the ship is located at time stamp *Time: 035639*. This position is given by AIS. The travel time curve that is given by Equation (2.1) is shown as an orange curve in Figure 2.8a and such travel time curves will be referred to as analytical travel time curves. The extracted travel time curve in Figure 2.8a is extracted using the procedure described previously in this chapter, and for the extraction $M + 1 = 7$, $l = 200$, $\text{start}_0 = 250$ and $\delta = 1$. The extracted travel time curve reaches its minimum around channel 100. This is what is expected from the plot of the data at time stamp *Time: 035639* in Figure 2.6.

The extracted energy curve in Figure 2.8b displays much noise, but the curve fits somewhat well with the energy curve which is calculated from Equation (2.2) for the position in which the ship is placed at time stamp *Time: 035639*. The energy curve which is given by Equation (2.2) is shown as an orange curve in Figure 2.8b and such energy curves will be referred to as analytical energy curves.
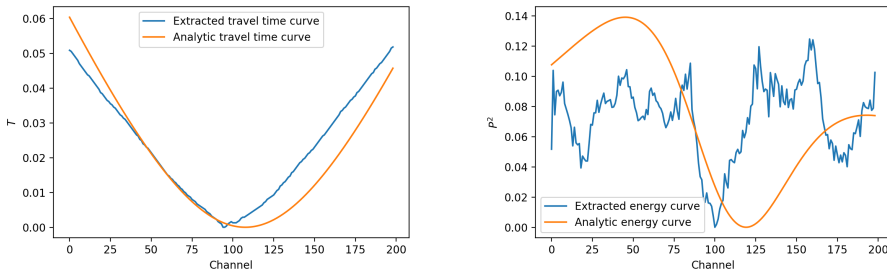
(a) Extracted and analytical travel time curve at time stamp *Time: 035639*.

(b) Extracted and analytical energy curve at time stamp *Time: 035639*.

Figure 2.8: Extracted and analytical travel time and energy curves at time stamp *Time: 035639*.

A snippet of the original data and the shifted data at time stamp *Time: 035639* is shown in Figure 2.9. From the figure it can be observed that the curvature of the structure of the original data has been flattened in the shifted data. This indicates that the result of applying Algorithm 1 to the data at time stamp *Time: 035639* is as intended.
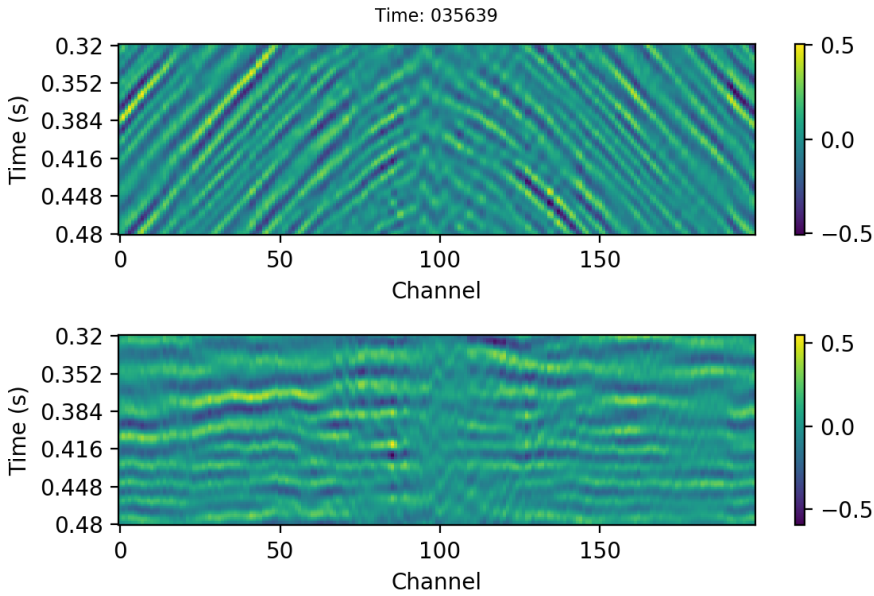
Figure 2.9: Original and shifted data at time stamp *Time: 035639*.

At time stamp *Time: 035839* the signal to noise ratio is quite low, but it is possible to see some structure in the data. The blue curve in Figure 2.10a show the extracted travel time curve associated with the data at time stamp *Time: 035839*, while the blue curve in Figure 2.10b show the extracted energy curve associated with the data at time stamp *Time: 035839*.

The extracted travel time curve in Figure 2.10a has the expected shape, but it also contains some noise. The minimum of the curve is located around channel 110, but according to Figure 2.6 it is expected that the curve would reach its minimum for a channel in the interval $[75, 100]$. It can also be observed that the extracted travel time curve does not fit the analytical travel time curve very well as the number of channels between the minimum of the two curves is large. The travel time curve is extracted using the procedure described previously in this chapter, and for the extraction $M + 1 = 7$, $l = 200$, $start_0 = 250$ and $\delta = 1$.

The extracted energy curve in Figure 2.10b does not have the expected shape, and it seems like the curve is almost pure noise. The extracted energy curve does not fit the analytical energy curve. It is difficult to believe that such a curve will give satisfying results when used as input to the statistical methods.

A snippet of the original data and the shifted data at time stamp *Time: 035839* is shown in Figure 2.11. Also at this time stamp it can be seen that the structure of the data has been flattened, and that the shifting procedure has given the expected result. Hence, the time shifting procedure seem to work also for data with a low signal to noise ratio.
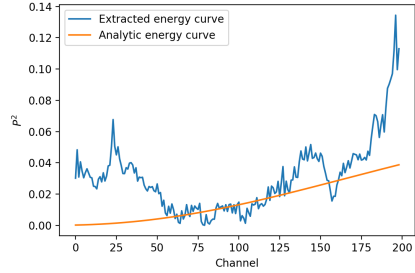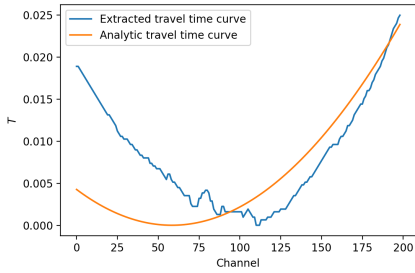
(a) Extracted and analytical travel time curve at time stamp *Time: 035839*.

(b) Extracted and analytical energy curve at time stamp *Time: 035839*.

Figure 2.10: Extracted and analytical travel time and energy curves at time stamp *Time: 035839*.
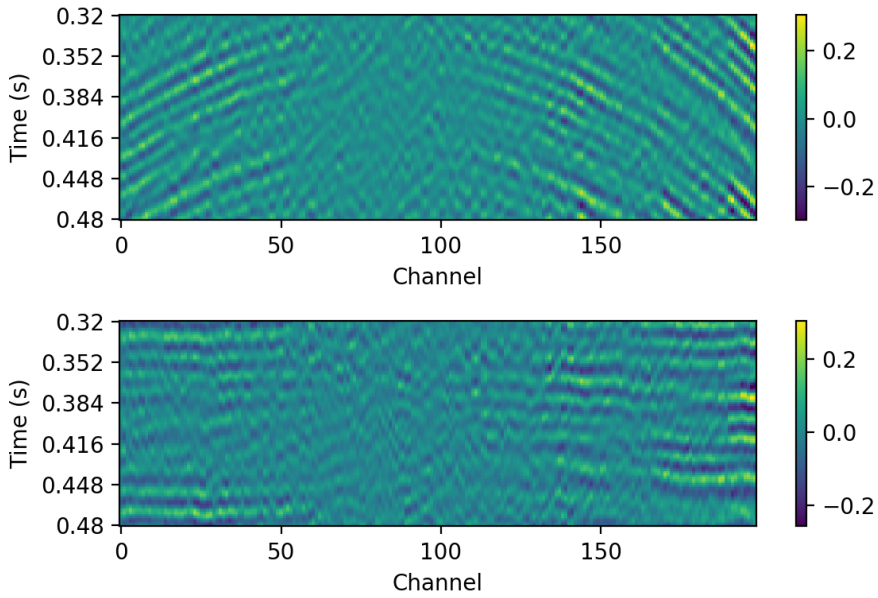
Figure 2.11: Original and shifted data at time stamp *Time: 035839*.

Based on Figures 2.8 and 2.10 the assumptions associated with the noise of the simulated curves may not be reasonable. The travel time curves from the real data seem to contain less noise on the edges of the curves, compared to the middle part of the curves. This contradicts the assumption of uncorrelated noise along the simulated travel time curves. For the energy curves there seem to be the same amount of noise along the entire curves. This fits well with the assumption of the noise of the simulated energy curves. Both curves in Figure 2.10 seem to contain more noise than the curves in Figure 2.8. However, for the simulated curves it is assumed that there is no correlation between the noise of the travel time curve and the energy curve at time step t. For the simulated data it is assumed that the amount of noise is uncorrelated with the time step. This does not seem to be a reasonable assumption as the amount of noise seems to be larger for the time steps when the ship is far away from the cable.

Chapter 3

Methods and implementation

In order to track a ship, a state-space model for the movement of the ship is considered. By using this model, the statistical methods can be applied to the ship tracking problem. The state-space model and the statistical methods will be introduced in this chapter. Evaluation metrics which will be used to compare the results from the methods are also introduced in this chapter.

3.1 State-space representation

State-space models consist of a state equation and an observation equation, and such models are used as a framework for sequential methods in tracking problems (Brockwell and Davis, 2016). In this project the movement of a ship can be represented by a nonlinear state-space model (Arulampalam et al., 2002), where the state equation is given by

$$\mathbf{x}_{t+1} = g(\mathbf{x}_t) + \boldsymbol{\eta}_{\mathbf{x},t}, \quad t = 0, \ldots, \tau - 1. \tag{3.1}$$

$\mathbf{x}_t$ is the state of the system at time t, which, in the case of the ship, is a 4-dimensional vector given by

$$\mathbf{x}_t = [x_t, y_t, v_{x,t}, v_{y,t}]^T, \tag{3.2}$$

where (x_t, y_t) is the position of the ship at time t, $v_{x,t}$ is the velocity of the ship in the x-direction at time t and $v_{y,t}$ is the velocity of the ship in the y-direction at time t. Tracking a ship consists of estimating the state of the ship at all time steps $t = 0, \ldots, \tau$.

In the simplest version of the ship tracking problem, the goal is to track a ship with constant velocity, and in that case the function $g(\mathbf{x}_t)$ is the linear function defined by

$$g(\mathbf{x}_t) = G_t \mathbf{x}_t = \begin{bmatrix} 1 & 0 & \Delta_t & 0 \\ 0 & 1 & 0 & \Delta_t \\ 0 & 0 & 1 & 0 \\ 0 & 0 & 0 & 1 \end{bmatrix} \begin{bmatrix} x_t \\ y_t \\ v_{x,t} \\ v_{y,t} \end{bmatrix} = \begin{bmatrix} x_t + \Delta_t v_{x,t} \\ y_t + \Delta_t v_{y,t} \\ v_{x,t} \\ v_{y,t} \end{bmatrix}, \tag{3.3}$$

where Δ_t is the change in time from step t to $t + 1$. In this project $\boldsymbol{\eta}_{\mathbf{x},t}$ is a noise vector of dimension 4 given by

$$\boldsymbol{\eta}_{\mathbf{x},t} \sim \mathcal{N}_4(\mathbf{0}, V_t), \tag{3.4}$$

where V_t is the 4×4 diagonal covariance matrix given by

$$V_t = \begin{bmatrix} \sigma_{\text{pos},t}^2 & 0 & 0 & 0 \\ 0 & \sigma_{\text{pos},t}^2 & 0 & 0 \\ 0 & 0 & \sigma_{\text{vel},t}^2 & 0 \\ 0 & 0 & 0 & \sigma_{\text{vel},t}^2 \end{bmatrix}. \tag{3.5}$$

The function $g(\mathbf{x}_t)$ models a ship that moves with constant velocity. Consequently, Equation (3.1) models a ship that is moving with approximately constant velocity. The effect of $\boldsymbol{\eta}_{\mathbf{x},t}$ is that according to the model the ship might move with slightly different velocity at time step t than at time step $t + 1$, and that the ship might move slightly shorter or longer than $x_t + \Delta_t v_{x,t}$ in the x-direction and slightly shorter or longer than $y_t + \Delta_t v_{y,t}$ in the y-direction at time step $t + 1$. Because of this, $\boldsymbol{\eta}_{\mathbf{x},t}$ can be interpreted as the acceleration of the ship at time step t.

Another way of interpreting $\boldsymbol{\eta}_{\mathbf{x},t}$ is that its variance can be used as a tuning parameter to control the complexity of the state equation. By this interpretation the model given by Equation (3.3) can also be used when a ship with non-constant velocity is to be tracked. In that case the elements of V_t should be large.

The state of the ship at time step $t = 0$ is given by the initial condition $p(\mathbf{x}_0)$ which in this project is given by

$$p(\mathbf{x}_0) = \mathcal{N}_4(\mathbf{x}_0, V_0), \tag{3.6}$$

where $\mathbf{x}_0$ needs to be chosen by the user of the statistical methods. A natural choice for $\mathbf{x}_0$ is $\mathbf{x}_{\text{true},0}$, or alternatively the best guess one has of $\mathbf{x}_{\text{true},0}$. The values of the elements of V_0 indicate the amount of knowledge one has about the state of the ship at time step $t = 0$. If the elements of V_0 are large, then the the amount of knowledge concerning the ship is limited and consequently the guess one has of $\mathbf{x}_{\text{true},0}$ might be poor.

In this project the observation equation of the state-space model is two-fold, and these equations are given by

$$\mathbf{T}(\mathbf{x}_t) = f_{\mathbf{T}}(\mathbf{x}_t) + \boldsymbol{\eta}_{\mathbf{T},t}, \tag{3.7}$$

$$\mathbf{P}^2(\mathbf{x}_t) = f_{\mathbf{P}}(\mathbf{x}_t) + \boldsymbol{\eta}_{\mathbf{P},t}. \tag{3.8}$$

$\mathbf{T}(\mathbf{x}_t)$ and $\mathbf{P}^2(\mathbf{x}_t)$ are n-dimensional vectors, structured in the same manner as $\mathbf{T}_{\text{data},t}$ in Equation (2.7) and $\mathbf{P}_{\text{data},t}^2$ in Equation (2.8), respectively. As previously mentioned, the elements of the vectors produced by $f_{\mathbf{T}}(\mathbf{x}_t)$ and $f_{\mathbf{P}}(\mathbf{x}_t)$ are given by Equations (2.1) and (2.2), which means that $f_{\mathbf{T}}(\mathbf{x}_t)$ and $f_{\mathbf{P}}(\mathbf{x}_t)$ are nonlinear functions. $\boldsymbol{\eta}_{\mathbf{T},t}$ and $\boldsymbol{\eta}_{\mathbf{P},t}$ are noise vectors given by Equation (2.9).

As for the simulation procedure in chapter 2, it is assumed that the noise of the travel time curves and the noise of the energy curves is normally distributed noise. It is assumed that there is no correlation between the amount of noise and the position along the curve, and there is no correlation between the amount of noise for the two different kinds of curves. There is also no correlation between the noise of the curves and the time step. These assumptions are made to simplify the implementation of the statistical methods, but the analysis of the real data showed that some of these assumptions may not be reasonable.

3.2 A Bayesian framework for filtering

The statistical methods will utilize the state-space model to estimate a filtering distribution at each time step t. The filtering distribution at time step t uses all available data up to and at time step t, and represents the distribution of the state of the ship given the available data. The filtering distribution is derived and discussed in this section.

The distribution of the state of the ship at time step t given its previous state is denoted by $p(\mathbf{x}_t|\mathbf{x}_{t-1})$. This distribution is defined by the state equation, Equation (3.1), and since there is assumed to be no correlation between $\boldsymbol{\eta}_{\mathbf{x},t}$ for different time steps, it is clear that the state-space model used in this project defines a Markov chain. Also because of the assumption of independence between $\boldsymbol{\eta}_{\mathbf{T},t}$ and $\boldsymbol{\eta}_{\mathbf{P},t}$, the distribution of the observation given the state at time step t is given by $p(\mathbf{T}_{\text{data},t}, \mathbf{P}^2_{\text{data},t}|\mathbf{x}_t) = p(\mathbf{T}_{\text{data},t}|\mathbf{x}_t)p(\mathbf{P}^2_{\text{data},t}|\mathbf{x}_t)$. This distribution is given by the observation equations of the state-space model, that is, Equations (3.7) and (3.8).

Figure 3.1 shows the relationship between the states of the ship and the measured data. The figure shows that each state $\mathbf{x}_t$ is only dependent on the previous state $\mathbf{x}_{t-1}$ and that the measured data at time step t is only dependent on the state of the ship at time step t. Consequently, $\mathbf{T}_{\text{data},t}$ and $\mathbf{P}^2_{\text{data},t}$ are conditionally independent of previous states. The line going from state $\mathbf{x}_{t-1}$ to state $\mathbf{x}_t$ in the figure represents the probability $p(\mathbf{x}_t|\mathbf{x}_{t-1})$, while the two lines from state $\mathbf{x}_t$ to $\mathbf{T}_{\text{data},t}$ and $\mathbf{P}^2_{\text{data},t}$ represent the probability $p(\mathbf{T}_{\text{data},t}, \mathbf{P}^2_{\text{data},t}|\mathbf{x}_t)$. The figure also shows another important assumption, namely the assumption that the measured travel time and the measured energy are conditionally independent. This assumption may not be reasonable since for instance the minimum of both the travel time curve and the energy curve should be located at the x-coordinate of the ship.
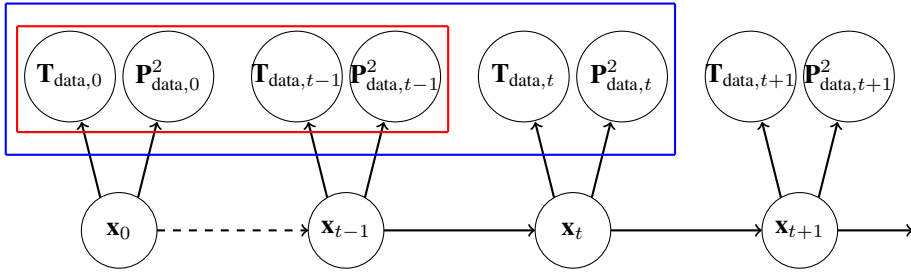
Figure 3.1: Illustration of the relationship between the states of the ship and the measured data. The red box surrounds the data that is used for prediction at time step t, while the blue box surrounds the data that is used for filtering at time step t.

At each time step t, the goal for the statistical methods is to estimate the filtering distribution $p(\mathbf{x}_t|\mathbf{T}_{\text{data},t}, \mathbf{P}^2_{\text{data},t}, \dots, \mathbf{T}_{\text{data},0}, \mathbf{P}^2_{\text{data},0}) = p(\mathbf{x}_t|\mathbf{T}_{\text{data},0:t}, \mathbf{P}^2_{\text{data},0:t})$. Filtering methods, according to Särkkä (2013), use directly observed measurements that contain noise to estimate the states of a system. The measurements gives information about the states of the system such that the states are observed indirectly through the measurements. Such a situation, with travel time and energy being the measurements, is shown in Figure 3.1. In combination with the non-linearity of the tracking problem in this project, this indicates that particle filters are suitable methods for ship tracking based on fiber optic cable data.

According to Bayes' theorem, the assumption of conditional independence between $\mathbf{T}_{\text{data},t}$ and $\mathbf{P}^2_{\text{data},t}$ and previous states, and the assumptions related to $\boldsymbol{\eta}_{\mathbf{x},t}$, $\boldsymbol{\eta}_{\mathbf{T},t}$ and $\boldsymbol{\eta}_{\mathbf{P},t}$, the filtering distribution can be written as

$$p(\mathbf{x}_t|\mathbf{T}_{\text{data},0:t}, \mathbf{P}^2_{\text{data},0:t}) \propto p(\mathbf{T}_{\text{data},t}, \mathbf{P}^2_{\text{data},t}|\mathbf{x}_t)p(\mathbf{x}_t|\mathbf{T}_{\text{data},0:t-1}, \mathbf{P}^2_{\text{data},0:t-1}), \qquad (3.9)$$

where

$$p(\mathbf{x}_t|\mathbf{T}_{\text{data},0:t-1}, \mathbf{P}^2_{\text{data},0:t-1}) = \int p(\mathbf{x}_t|\mathbf{x}_{t-1})p(\mathbf{x}_{t-1}|\mathbf{T}_{\text{data},0:t-1}, \mathbf{P}^2_{\text{data},0:t-1})d\mathbf{x}_{t-1}. \quad (3.10)$$

Equation (3.9) is a correction step that updates the state of the system using the measurements at time step t, while Equation (3.10), called the one-step prediction, uses the measurements of the previous time steps along with the state equation to predict the next state of the ship (Shen and Tang, 2015). The red and blue boxes in Figure 3.1 respectively show the difference in what amount of data the prediction distributions and the filtering distributions are based on. For the rest of the project, the distribution $p(\mathbf{x}_t|\mathbf{T}_{\text{data},0:t-1}, \mathbf{P}^2_{\text{data},0:t-1})$ will be referred to as the prior at time step t.

Because of the non-linearity of $f_{\mathbf{T}}(\mathbf{x}_t)$ and $f_{\mathbf{P}}(\mathbf{x}_t)$ the integral in Equation (3.10) is not on closed form. This means that the integral is difficult to solve analytically, and consequently, the statistical methods that will be used in this project approximate the solution of Equation (3.9). The approximations use samples of states, called particles, to estimate $p(\mathbf{x}_t|\mathbf{T}_{\text{data},0:t}, \mathbf{P}^2_{\text{data},0:t})$ at each time step t.

3.3 SIR

Particle filters are sequential methods that use Monte Carlo sampling to estimate the state of the system at time t given observations up to the same time. Each particle follows the state-space model defined by Equations (3.1)-(3.8) and, in this project the particles can be considered to be plausible ships.

The basic particle filter that will be used in this project is called SIR (Doucet et al., 2001; Arulampalam et al., 2002). This method compares the observation associated with each of the particles at time step t to the measured data at time step t, and computes a weight based on how probable it is that the measured data could have been observed for any of the particles at time t. The next step is to resample based on the weights, and finally, the particles are moved according to Equation (3.1).

More precisely, the first step of the SIR method is to draw the state of N particles from the initial distribution, which can be written as

$$\mathbf{x}_0^{(i)} \sim \mathcal{N}_4(\mathbf{x}_0, V_0), \quad i = 1, \ldots, N. \qquad (3.11)$$

At each time step t the SIR method aims to estimate $p(\mathbf{x}_t|\mathbf{T}_{\text{data},0:t}, \mathbf{P}^2_{\text{data},0:t})$ and $p(\mathbf{x}_{t+1}|\mathbf{T}_{\text{data},0:t}, \mathbf{P}^2_{\text{data},0:t})$. At time step $t = 0$ this means to estimate $p(\mathbf{x}_0|\mathbf{T}_{\text{data},0}, \mathbf{P}^2_{\text{data},0})$ and $p(\mathbf{x}_1|\mathbf{T}_{\text{data},0}, \mathbf{P}^2_{\text{data},0})$.

Assuming that there exist N samples, denoted $\mathbf{x}_t^{(i)}$, from $p(\mathbf{x}_t|\mathbf{T}_{\text{data},0:t-1}, \mathbf{P}^2_{\text{data},0:t-1})$ at time step t, then for each of the N particles the n-dimensional vectors $\mathbf{T}(\mathbf{x}_t^{(i)})$ and $\mathbf{P}^2(\mathbf{x}_t^{(i)})$

are computed from Equations (3.7) and (3.8) respectively, and consequently

$$\mathbf{T}(\mathbf{x}_t^{(i)})|\mathbf{x}_t^{(i)} \sim \mathcal{N}_n(f_\mathbf{T}(\mathbf{x}_t^{(i)}), \sigma_\mathbf{T}^2 I_n), \quad i = 1, \dots, N, \tag{3.12}$$

$$\mathbf{P}^2(\mathbf{x}_t^{(i)})|\mathbf{x}_t^{(i)} \sim \mathcal{N}_n(f_\mathbf{P}(\mathbf{x}_t^{(i)}), \sigma_\mathbf{P}^2 I_n), \quad i = 1, \dots, N. \tag{3.13}$$

According to the SIR method each of the N particles will be assigned a weight. The weight of the ith particle at time step t is given by

$$\mathrm{w}_t^{(i)} = \frac{p(\mathbf{T}_{\text{data},t}, \mathbf{P}_{\text{data},t}^2|\mathbf{x}_t^{(i)})}{\sum_{i=1}^N p(\mathbf{T}_{\text{data},t}, \mathbf{P}_{\text{data},t}^2|\mathbf{x}_t^{(i)})} = \frac{p(\mathbf{T}_{\text{data},t}|\mathbf{x}_t^{(i)})p(\mathbf{P}_{\text{data},t}^2|\mathbf{x}_t^{(i)})}{\sum_{i=1}^N p(\mathbf{T}_{\text{data},t}|\mathbf{x}_t^{(i)})p(\mathbf{P}_{\text{data},t}^2|\mathbf{x}_t^{(i)})}, \tag{3.14}$$

where $p(\mathbf{T}_{\text{data},t}|\mathbf{x}_t^{(i)})$ and $p(\mathbf{P}_{\text{data},t}^2|\mathbf{x}_t^{(i)})$ represent the probability of observing the measured data given the state of the ith particle. These probabilities are given by

$$p(\mathbf{T}_{\text{data},t}|\mathbf{x}_t^{(i)}) \propto \exp(-\frac{1}{2\sigma_\mathbf{T}^2}(f_\mathbf{T}(\mathbf{x}_t^{(i)}) - \mathbf{T}_{\text{data},t})^T(f_\mathbf{T}(\mathbf{x}_t^{(i)}) - \mathbf{T}_{\text{data},t})) \tag{3.15}$$

and

$$p(\mathbf{P}_{\text{data},t}^2|\mathbf{x}_t^{(i)}) \propto \exp(-\frac{1}{2\sigma_\mathbf{P}^2}(f_\mathbf{P}(\mathbf{x}_t^{(i)}) - \mathbf{P}_{\text{data},t}^2)^T(f_\mathbf{P}(\mathbf{x}_t^{(i)}) - \mathbf{P}_{\text{data},0}^2)). \tag{3.16}$$

The SIR method uses the weights for resampling. The resampling scheme consists of creating a discretized cumulative distribution of the weights, and drawing a sample, $u^{(i)}$, from the uniform distribution on the interval $[0, 1]$ for each of the N particles. $W_t^{(k)}$ denotes the sum of the k first weights at time step t, and if $u^{(i)} \in (W_t^{(k-1)}, W_t^{(k)}]$ then the ith particle is resampled as a particle with the same state as the kth particle. This resampling scheme, which is based on the weights of the particles, is called importance resampling. The consequence of importance resampling is that the particles with high weights are duplicated, while the particles with low weights are likely removed from the probabilistic representation.

The resampled particles estimate the filtering distribution of the state of the ship given the measurements of the previous steps and the current step. This means that the posterior mean of the state of the ship at time step t is estimated by

$$\hat{\mathrm{E}}(\mathbf{x}_t|\mathbf{T}_{\text{data},0:t}, \mathbf{P}_{\text{data},0:t}^2) = \bar{\mathbf{x}}_{t+} = \frac{1}{N}\sum_{i=1}^N \mathbf{x}_{t+}^{(i)}, \tag{3.17}$$

while the posterior covariance matrix at time step t is estimated by

$$\widehat{\mathrm{Cov}}(\mathbf{x}_t|\mathbf{T}_{\text{data},0:t}, \mathbf{P}_{\text{data},0:t}^2) = \frac{1}{N-1}\sum_{i=1}^N (\mathbf{x}_{t+}^{(i)} - \bar{\mathbf{x}}_{t+})(\mathbf{x}_{t+}^{(i)} - \bar{\mathbf{x}}_{t+})^T, \tag{3.18}$$

where $\mathbf{x}_{t+}^{(i)}$, $i = 1, \dots, N$ denotes the states of the resampled particles at time step t which estimate $p(\mathbf{x}_t|\mathbf{T}_{\text{data},0:t}, \mathbf{P}_{\text{data},0:t}^2)$.

Finally, the resampled particles are moved according to Equation (3.1), and the new states $\mathbf{x}_{t+1}^{(i)}$ $i = 1, \dots, N$, which estimate $p(\mathbf{x}_{t+1}|\mathbf{T}_{\text{data},0:t}, \mathbf{P}_{\text{data},0:t}^2)$, are used by the method for the next time step. The SIR method repeats the procedure described above for a given number of time steps, $\tau + 1$, and the method for all time steps is given in Algorithm 2.

Algorithm 2: SIR for ship tracking

---

1 Draw initial states: $\mathbf{x}_0^{(i)} \sim \mathcal{N}_4(\mathbf{x}_0, V_0), i = 1, \ldots, N$

2 for $t = 0, \ldots, \tau$ **do**

3 $\quad$ Use Equations (2.1) and (2.2) to calculate $f_{\mathbf{T}}(\mathbf{x}_t^{(i)})$ and $f_{\mathbf{P}}(\mathbf{x}_t^{(i)})$ for each of the states $\mathbf{x}_t^{(i)}, i = 1, \ldots, N$

4 $\quad$ Calculate $w_t^{(i)}$ for $i = 1, \ldots, N$ using Equation (3.14)

5 $\quad$ Resample the particles using the weights and produce $\mathbf{x}_{t+}^{(i)}, i = 1, \ldots, N$

6 $\quad$ Use the resampled particles to estimate the distribution $p(\mathbf{x}_t | \mathbf{T}_{\text{data},0:t}, \mathbf{P}_{\text{data},0:t}^2)$

7 $\quad$ **if** $t \leq \tau - 1$ **then**

8 $\quad\quad$ Move the particles according to Equation (3.1) to produce $\mathbf{x}_{t+1}^{(i)}$ for $i = 1, \ldots, N$

9 $\quad$ **end**

10 end

The SIR method is illustrated in Figure 3.2. The first of the four frames of this figure shows the prior distribution of $\mathbf{x}_t$ approximated by ten particles. The second frame shows the estimated filtering distribution of $\mathbf{x}_t$ given the measured data at time step t. The points in this frame are found by resampling of the points in the first frame, and the size of these points indicates that several points are resampled to the positions of these points. In this case the weights of five states are larger than the weights of the other five states, and all the particles are resampled to the five states with large weights. It seems like the weights of these five states are approximately equal since the number of unique states is reduced from ten to five. The second frame also indicates that the data that is measured at time step t fits well with the waves created by a ship with x-coordinate close to $x = 200$.
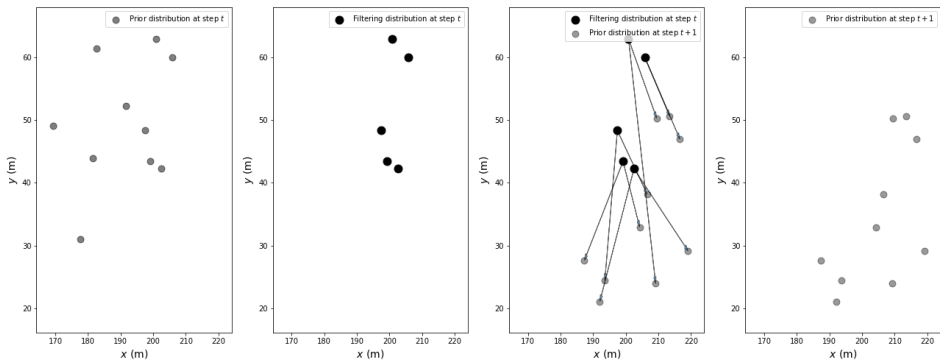

Figure 3.2: Illustration of the SIR method. The first frame shows the approximated prior distribution of $\mathbf{x}_t$ and the second frame shows the resampled particles which are used to approximate the filtering distribution of $\mathbf{x}_t$. The third frame shows how the particles are moved, and consequently how the prior of $\mathbf{x}_{t+1}$ is approximated.

The third frame in Figure 3.2 shows how the particles are moved according to Equation (3.1), and the fourth frame shows the resulting distribution of the particles after they are moved. These particles constitute the approximation of the distribution of $\mathbf{x}_{t+1}$ prior to the collection of data at time step $t+1$.

3.3.1 Properties of the SIR method

There are several positive aspects of using the SIR method. One of these is the fact that Algorithm 2 is quite simple to implement. At least this is true when the problem is Gaussian, which is the case in this project. Another advantage of the SIR method is that the particle filter has proved to be exact when the number of particles goes to infinity (Skare et al., 2003).

A common problem with the SIR method is degeneracy (Arulampalam et al., 2002). This is a problem that occurs when one of the weights is much larger than the others. The consequence is that almost all resampled particles are equal to the particle with the dominant weight. If most of the particles are in the same state, then the correlation between the particles is large, which means that the effective sample size, or ESS for short, is small. As a consequence, the statistical inference performed for the particles may not be valid.

In order to detect the degeneracy the ESS can be monitored as the method is executed. The ESS at time step t is given by

$$\text{ESS}_t = \frac{1}{\sum_{i=1}^{N}(\mathbf{w}_t^{(i)})^2}, \tag{3.19}$$

and $\text{ESS}_t \in [1, N]$. ESS close to 1 indicates that the variance of the weights is large, which may indicate that one weight is much larger than the other weights. In the case of ship tracking, this means that the observations associated with one of the particles is very similar to the measured data, and consequently most particles will be resampled with state equal to the state of that particle. This will lead to degeneracy. If the ESS is closer to N then the variance of the weights is small, which indicates that the weights are of similar size. This means that several of the observations are similar to the measured data, and the particles are resampled with a wide variety of states.

In order to overcome the problem of degeneracy it is possible to combine the SIR method with the Ensemble Kalman Filter, or EnKF for short (Evensen, 2009; Shen and Tang, 2015). EnKF is a filtering method which is known to not have problems with degeneracy, and it is suitable for large-scale state-space problems. Combining the SIR method and the EnKF method gives the EnKPF method (Rezaie and Eidsvik, 2012; Frei and Künsch, 2013; Shen and Tang, 2015).

3.4 EnKF

For EnKF and EnKPF it is convenient to introduce the $2n$-dimensional vectors $\mathbf{d}(\mathbf{x}_t^{(i)})$ and $\mathbf{d}_{\text{data},t}$ given by

$$\mathbf{d}(\mathbf{x}_t^{(i)}) = \begin{bmatrix} \mathbf{T}(\mathbf{x}_t^{(i)}) \\ \mathbf{P}^2(\mathbf{x}_t^{(i)}) \end{bmatrix} \quad \text{and} \quad \mathbf{d}_{\text{data},t} = \begin{bmatrix} \mathbf{T}_{\text{data},t} \\ \mathbf{P}^2_{\text{data},t} \end{bmatrix}. \tag{3.20}$$

$\mathbf{d}(\mathbf{x}_t^{(i)})$ is the observed data associated with state $\mathbf{x}_t^{(i)}$ and $\mathbf{d}_{\text{data},t}$ is the measured data at time step t. Furthermore,

$$\mathbf{d}(\mathbf{x}_t^{(i)})|\mathbf{x}_t^{(i)} \sim \mathcal{N}_{2n}(f(\mathbf{x}_t^{(i)}), R), \quad i = 1, \ldots, N, \tag{3.21}$$

where R is a diagonal matrix of dimensions $2n \times 2n$. The n first elements on the diagonal are equal to $\sigma_{\mathbf{T}}^2$, and the n last elements on the diagonal are equal to $\sigma_{\mathbf{P}}^2$. $f(\mathbf{x}_t^{(i)})$ is the $2n$-dimensional expectation vector of $\mathbf{d}(\mathbf{x}_t^{(i)})$ given by

$$f(\mathbf{x}_t^{(i)}) = \mathrm{E}[\mathbf{d}(\mathbf{x}_t^{(i)})] = \begin{bmatrix} f_{\mathbf{T}}(\mathbf{x}_t^{(i)}) \\ f_{\mathbf{P}}(\mathbf{x}_t^{(i)}) \end{bmatrix}. \tag{3.22}$$

EnKF is a method that uses the correlation between samples from a prior and the data, to update the samples from the prior in order to approximate the filtering distribution. At time step $t = 0$, the prior is given by Equation (3.11). According to EnKF, samples from the filtering distribution $p(\mathbf{x}_t|\mathbf{d}_{\text{data},0:t})$ are given by the formula

$$\mathbf{x}_{t+}^{(i)} = \mathbf{x}_t^{(i)} + C_{\mathbf{x}f_{\mathbf{x}}}(t)C_{f_{\mathbf{x}}f_{\mathbf{x}}}^{-1}(t)(\mathbf{d}_{\text{data},t} - f(\mathbf{x}_t^{(i)})), \quad i = 1, \ldots, N, \tag{3.23}$$

where $\mathbf{x}_t^{(i)}$ for $i = 1, \ldots, N$ are samples from the prior. Here, $C_{\mathbf{x}f_{\mathbf{x}}}(t)$ is the sample covariance matrix between the samples from the prior and the observed data associated with those samples at time step t, and $C_{f_{\mathbf{x}}f_{\mathbf{x}}}(t)$ is the sample covariance matrix of the observed data associated with the samples from the prior at time step t. These matrices are given by

$$C_{\mathbf{x}f_{\mathbf{x}}}(t) = \frac{1}{N-1}\sum_{i=1}^{N}(\mathbf{x}_t^{(i)} - \bar{\mathbf{x}}_t)(f(\mathbf{x}_t^{(i)}) - \bar{f}_{\mathbf{x}_t})^T \tag{3.24}$$

and

$$C_{f_{\mathbf{x}}f_{\mathbf{x}}}(t) = R + \frac{1}{N-1}\sum_{i=1}^{N}(f(\mathbf{x}_t^{(i)}) - \bar{f}_{\mathbf{x}_t})(f(\mathbf{x}_t^{(i)}) - \bar{f}_{\mathbf{x}_t})^T, \tag{3.25}$$

where

$$\bar{\mathbf{x}}_t = \frac{1}{N}\sum_{i=1}^{N}\mathbf{x}_t^{(i)} \quad \text{and} \quad \bar{f}_{\mathbf{x}_t} = \frac{1}{N}\sum_{i=1}^{N}f(\mathbf{x}_t^{(i)}). \tag{3.26}$$

The matrix product $C_{\mathbf{x}f_{\mathbf{x}}}(t)C_{f_{\mathbf{x}}f_{\mathbf{x}}}^{-1}(t)$ is called the Kalman gain. The theory of the nonlinear use of the EnKF method is based on the work presented by Shen and Tang (2015), and the EnKF method is shown in Algorithm 3.

An illustration of the EnKF method with ten particles is displayed in Figure 3.3. The first frame shows the approximated prior distribution of $\mathbf{x}_t$. The second frame shows the updated states which approximates the filtering distribution of $\mathbf{x}_t$ given the measured data at time step t. These states are given by Equation (3.23), and it can be seen from the figure that the affect of the data is that the spread of the particles is reduced.

Algorithm 3: EnKF for ship tracking

---
1 Draw initial states: $\mathbf{x}_0^{(i)} \sim \mathcal{N}_4(\mathbf{x}_0, V_0), i = 1, \ldots, N$
2 **for** $t = 0, \ldots, \tau$ **do**
3   Use Equations (2.1) and (2.2) to calculate $f(\mathbf{x}_t^{(i)})$ for each of the states $\mathbf{x}_t^{(i)}$,
       $i = 1, \ldots, N$
4   Use Equation (3.23) to update the state of the particles
5   Use the updated particles to estimate the distribution $p(\mathbf{x}_t | \mathbf{d}_{\text{data},0:t})$
6   **if** $t \leq \tau - 1$ **then**
7   Move the particles according to Equation (3.1) to produce $\mathbf{x}_{t+1}^{(i)}$ for
          $i = 1, \ldots, N$
8   **end**
9 **end**

The third frame shows how the updated states are moved according to Equation (3.1). The approximated prior distribution of $\mathbf{x}_{t+1}$ is shown in the fourth frame. Figure 3.2 and Figure 3.3 show the differences between the SIR method and the EnKF method. The SIR method reduces the number of unique states and moves the particles that does not fit the data to states which fits the data better. The EnKF method, on the other hand, updates all states, not just the ones that provide a poor fit to the data.
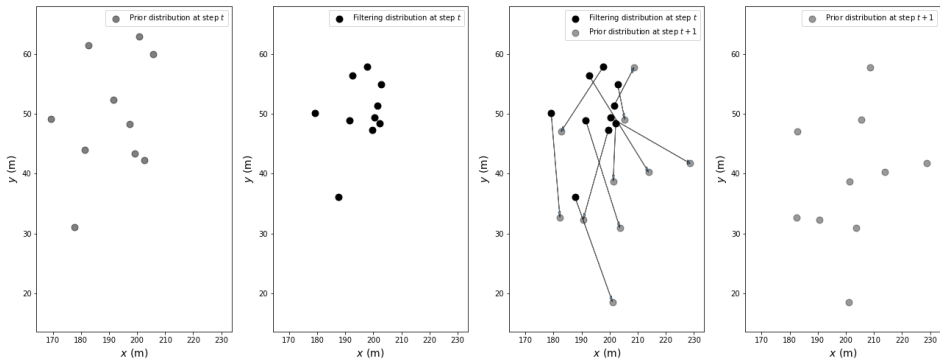
Figure 3.3: Illustration of the EnKF method. The first frame shows the approximated prior distribution of $\mathbf{x}_t$ and the second frame shows the updated particles which are used to approximate the filtering distribution of $\mathbf{x}_t$. The third frame shows how the particles are moved, and consequently how the prior of $\mathbf{x}_{t+1}$ is approximated.

In this project the EnKF method will not be used to track the ship. However, the EnKPF method is based on the principles of the EnKF method that have been presented in this section.

3.4.1 Properties of the EnKF method

According to Evensen (2009), the EnKF method has proved to be exact for linear Gaussian problems when $N \to \infty$. However, unlike the SIR method, the EnKF method is not exact for non-linear or non-Gaussian problems when the number of particles goes to infinity. Despite this, the EnKF method has turned out to be a good choice for state estimation in many large size, practical applications (Evensen, 2003). Another advantage of the EnKF method is that, as with the SIR method, the method is quite simple to implement.

The EnKF method is known to have difficulties with solving problems that have more than one valid answer. For instance, if there are several states that gives the same observations, all of these states are valid answers to the problem of state estimation. In this project it can be problematic to use the EnKF method for state estimation. The analysis of the travel time and energy functions in section 2.2 showed that the observed data of a ship in position (x_t, y_t) is the same as the observed data of the same ship in position $(x_t, -y_t)$. Hence, if the states in the prior include both of the states that fits the observation, then the EnKF method may not be able to give a satisfying result.

3.5 EnKPF

By combining the SIR method and the EnKF method into the EnKPF method it may be possible to overcome the problems of both of the methods. The level of influence that the SIR method and the EnKF method has on the EnKPF method is controlled by the tuning parameter $\gamma \in [0, 1]$, where $\gamma = 0$ corresponds to the SIR method, and $\gamma = 1$ corresponds to the EnKF method. The EnKPF method will hopefully be able to avoid degeneracy, and at the same time be able to estimate the state of the ship in a satisfying manner even if the prior includes states with different y-coordinates that fits the observation.

The implementation of EnKPF that will be used in this project is based on the work presented by Shen and Tang (2015). The EnKPF method has also been implemented in other articles, such as (Rezaie and Eidsvik, 2012; Frei and Künsch, 2013), but in the implementation by Shen and Tang (2015) the observation equation of the state-space model is non-linear, which is also the case in this project.

As with the SIR method and the EnKF method, at time step $t = 0$, the samples from the prior are given by Equation (3.11). The EnKPF method can be divided into four steps at each time step t. The first step is an EnKF step, and the purpose of the step is to compute the temporary state vectors $\mathbf{v}_t^{(i)}$, $i = 1, \ldots, N$ in addition to the 4-dimensional vectors $\boldsymbol{\omega}_t^{(i)}$, $i = 1, \ldots, N$. $\mathbf{v}_t^{(i)}$ is given by

$$\mathbf{v}_t^{(i)} = \mathbf{x}_t^{(i)} + K_1(t, \gamma)(\mathbf{d}_{\text{data},t} - f(\mathbf{x}_t^{(i)})), \quad i = 1, \ldots, N, \tag{3.27}$$

where $K_1(t, \gamma)$ is the Kalman gain matrix of dimensions $4 \times 2n$ for the first EnKF step. This matrix is given by $K_1(t, \gamma) = C_{\mathbf{x} f_{\mathbf{x}}}(t) C_{f_{\mathbf{x}} f_{\mathbf{x}}}(t, \gamma)^{-1}$ with $C_{\mathbf{x} f_{\mathbf{x}}}(t)$ given by Equation (3.24) and $C_{f_{\mathbf{x}} f_{\mathbf{x}}}(t, \gamma)$ given by

$$C_{f_{\mathbf{x}} f_{\mathbf{x}}}(t, \gamma) = \frac{R}{\gamma} + \frac{1}{N-1} \sum_{i=1}^{N} (f(\mathbf{x}_t^{(i)}) - \bar{f}_{\mathbf{x}_t})(f(\mathbf{x}_t^{(i)}) - \bar{f}_{\mathbf{x}_t})^T. \tag{3.28}$$

The vectors $\boldsymbol{\omega}_t^{(i)}$, $i = 1, \ldots, N$ are given by

$$\boldsymbol{\omega}_t^{(i)} = \frac{K_1(t, \gamma)\boldsymbol{\epsilon}_{1,t}^{(i)}}{\sqrt{\gamma}}, \tag{3.29}$$

where $\boldsymbol{\epsilon}_{1,t}^{(i)} \sim \mathcal{N}_{2n}(\mathbf{0}, R)$ for $i = 1, \ldots, N$.

The second step of the EnKPF method is a SIR step, and the goal is to calculate the weights, $\mathrm{w}_t^{(i)}$ for each of the particles $i = 1, \ldots, N$ at time step t. A weight is given by

$$\mathrm{w}_t^{(i)} = \frac{\hat{\mathrm{w}}_t^{(i)}}{\sum_{i=1}^{N} \hat{\mathrm{w}}_t^{(i)}}, \tag{3.30}$$

with

$$\hat{\mathrm{w}}_t^{(i)} \propto \exp(-\frac{1}{2}(f(\mathbf{v}_t^{(i)}) - \mathbf{d}_{\text{data},t})^T \Sigma^{-1}(f(\mathbf{v}_t^{(i)}) - \mathbf{d}_{\text{data},t})), \tag{3.31}$$

where

$$f(\mathbf{v}_t^{(i)}) = \begin{bmatrix} f_{\mathbf{T}}(\mathbf{v}_t^{(i)}) \\ f_{\mathbf{P}}(\mathbf{v}_t^{(i)}) \end{bmatrix}. \tag{3.32}$$

Furthermore, the matrix Σ of dimensions $2n \times 2n$ is given by

$$\Sigma = \frac{R}{1 - \gamma} + \frac{1}{N - 1} \sum_{i=1}^{N}(f(\boldsymbol{\omega}_t^{(i)}) - \bar{f}_{\boldsymbol{\omega}_t})(f(\boldsymbol{\omega}_t^{(i)}) - \bar{f}_{\boldsymbol{\omega}_t})^T, \tag{3.33}$$

where

$$f(\boldsymbol{\omega}_t^{(i)}) = \begin{bmatrix} f_{\mathbf{T}}(\boldsymbol{\omega}_t^{(i)}) \\ f_{\mathbf{P}}(\boldsymbol{\omega}_t^{(i)}) \end{bmatrix}, \quad \text{and} \quad \bar{f}_{\boldsymbol{\omega}_t} = \frac{1}{N} \sum_{i=1}^{N} f(\boldsymbol{\omega}_t^{(i)}). \tag{3.34}$$

The third step of the EnKPF method is also a SIR step, and it consists of resampling the state vectors $\mathbf{v}_t^{(i)}$ based on the weights $\mathrm{w}_t^{(i)}$, $i = 1, \ldots, N$. The resampling is performed in the same way as in the SIR method by drawing a sample from the uniform distribution and comparing the sample to the cumulative weights. The resampled temporary state vectors are denoted by $\mathbf{v}_{t+}^{(i)}$, and for each particle $i = 1, \ldots, N$ the new vector given by

$$\boldsymbol{\xi}_t^{(i)} = \mathbf{v}_{t+}^{(i)} + \boldsymbol{\omega}_t^{(i)} \tag{3.35}$$

is created.

The fourth, and final, step of the EnKPF method is an EnKF step. The result of this step are updated state vectors which will be used to estimate the filtering distribution $p(\mathbf{x}_t|\mathbf{d}_{\text{data},0:t})$. The updated state vectors are given by

$$\mathbf{x}_{t+}^{(i)} = \boldsymbol{\xi}_t^{(i)} + K_2(t, \gamma)(\mathbf{d}_{\text{data},t} - \frac{\boldsymbol{\epsilon}_{2,t}^{(i)}}{\sqrt{1 - \gamma}} - f(\boldsymbol{\xi}_t^{(i)})), \tag{3.36}$$

where $K_2(t, \gamma)$ is a Kalman gain matrix of dimensions $4 \times 2n$ given by $K_2(t, \gamma) = C_{\boldsymbol{\omega} f_{\boldsymbol{\omega}}}(t)C_{f_{\boldsymbol{\omega}} f_{\boldsymbol{\omega}}}(t, \gamma)^{-1}$. The matrix $C_{\boldsymbol{\omega} f_{\boldsymbol{\omega}}}(t)$ is given by

$$C_{\boldsymbol{\omega} f_{\boldsymbol{\omega}}}(t) = \frac{1}{N - 1} \sum_{i=1}^{N}(\boldsymbol{\omega}_t^{(i)} - \bar{\boldsymbol{\omega}}_t)(f(\boldsymbol{\omega}_t^{(i)}) - \bar{f}_{\boldsymbol{\omega}_t})^T, \tag{3.37}$$

where

$$\bar{\boldsymbol{\omega}}_t = \frac{1}{N} \sum_{i=1}^{N} \boldsymbol{\omega}_t^{(i)}. \tag{3.38}$$

Furthermore, $C_{f_\omega f_\omega}(t, \gamma) = \Sigma$ which is presented in Equation (3.33). $\boldsymbol{\epsilon}_{2,t}^{(i)}$ is a sample from a Normal distribution, namely $\boldsymbol{\epsilon}_{2,t}^{(i)} \sim \mathcal{N}_{2n}(\mathbf{0}, R)$, and $f(\boldsymbol{\xi}_t^{(i)})$ is given by

$$f(\boldsymbol{\xi}_t^{(i)}) = \begin{bmatrix} f_{\mathbf{T}}(\boldsymbol{\xi}_t^{(i)}) \\ f_{\mathbf{P}}(\boldsymbol{\xi}_t^{(i)}) \end{bmatrix}. \tag{3.39}$$

The posterior mean and the posterior covariance matrix of the state of the ship at time step t can then be estimated using Equations (3.17) and (3.18), respectively. The ESS will be monitored during the execution of the EnKPF method. For each time step t, ESS_t is calculated from Equation (3.19) using the weights calculated from Equations (3.30) and (3.31). The EnKPF method is summarized in Algorithm 4.

Algorithm 4: EnKPF for ship tracking

---

1 Draw initial states: $\mathbf{x}_0^{(i)} \sim \mathcal{N}_4(\mathbf{x}_0, V_0), i = 1, \ldots, N$
2 **for** $t = 0, \ldots, \tau$ **do**
3   For $i = 1, \ldots, N$ calculate the temporary states $\mathbf{v}_t^{(i)}$ using Equation (3.27), and the vectors $\boldsymbol{\omega}_t^{(i)}$ using Equation (3.29)
4   Use Equations (3.30) and (3.31) to calculate the weights $\mathbf{w}_t^{(i)}$ for the temporary states $\mathbf{v}_t^{(i)}$ for $i = 1, \ldots, N$
5   Calculate ESS_t from Equation (3.19)
6   Resample the temporary states $\mathbf{v}_t^{(i)}$ and calculate $\boldsymbol{\xi}_t^{(i)}$ using Equation (3.35) for $i = 1, \ldots, N$
7   Calculate the updated states $\mathbf{x}_{t^+}^{(i)}$ using Equation (3.36) for $i = 1, \ldots, N$
8   Use the updated states to estimate the distribution $p(\mathbf{x}_t | \mathbf{d}_{\text{data},0:t})$
9   **if** $t \leq \tau - 1$ **then**
10   Move the particles according to Equation (3.1) to produce $\mathbf{x}_{t+1}^{(i)}$ for $i = 1, \ldots, N$
11   **end**
12 **end**

3.5.1 Properties of the EnKPF method

The parameter γ decides how much the particle filter is affected by the EnKF method. If $\gamma = 0$ both of the Kalman gain matrices $K_1(t, \gamma)$ and $K_2(t, \gamma)$ are matrices of zeros. In that case, the EnKPF method reduces to the SIR method. On the other hand, if $\gamma = 1$, all the weights are equal, and the EnKPF method reduces to the EnKF method.

The EnKPF method tries to combine the SIR method and the EnKF method such that the resulting method includes advantages of both methods. Hence, γ can be used to find

the balance between the SIR method and the EnKF method which works best to track a ship. If γ is large then EnKPF may not suffer from degeneracy, but if γ is too large it might be difficult to estimate the state of the ship if there is more than one state that fits the data perfectly. If $\gamma \to 0$ then the EnKPF method is exact as $N \to \infty$, but if $\gamma \to 1$ then this is not true unless the problem is linear and Gaussian.

The EnKPF method is not quite as simple to implement as the SIR method and the EnKPF method. The EnKPF method consists of several steps, and at each step, vectors and matrices must be calculated correctly based on many different parameters.

3.6 Evaluation metrics

In order to assess the performance of the SIR method and the EnKPF method for fiber optic cable data a few evaluation metrics will be monitored. These evaluation metrics are root mean square error (RMSE), minimal ESS and mean continous ranked probability score (CRPS).

3.6.1 RMSE

The RMSE quantifies the error made by the methods, and in this project the RMSE is used to calculate the error associated with the estimated positions and the estimated velocities. The formula for calculating the RMSE of the x-coordinate of the estimated positions is given by

$$\text{RMSE}(x) = \sqrt{\frac{1}{\tau + 1} \sum_{t=0}^{\tau} (x_{\text{true},t} - \bar{x}_{t+})^2}, \tag{3.40}$$

where $\bar{x}_{t+}$ is the first element of $\bar{\mathbf{x}}_{t+}$ given by Equation (3.17) based on particles from either the SIR method or the EnKPF method. $\text{RMSE}(y)$, $\text{RMSE}(v_x)$ and $\text{RMSE}(v_y)$ are also given by Equation (3.40), but $x_{\text{true},t}$ is replaced by either the true y-coordinate or the true velocity at time step t, and $\bar{x}_{t+}$ is replaced by the relevant element of $\bar{\mathbf{x}}_{t+}$. For the preferred statistical method, the RMSE is small for all of the four elements of the state vector.

3.6.2 ESS

The minimal ESS of the methods can be compared, and if one of the methods displays a minimal ESS close to one then that method may have problems with degeneracy. The minimal ESS is given by

$$\min(\text{ESS}) = \min_{t=0,\ldots,\tau} \text{ESS}_t, \tag{3.41}$$

where ESS_t is given by Equation (3.19). If the choice of method is based on minimal ESS, then the method with the largest minimal ESS should be chosen.

3.6.3   CRPS

The CRPS (Hersbach, 2000) measures the uncertainty of an estimate. In this project the CRPS is used to examine the accuracy of the estimated positions and the estimated velocities. The CRPS is calculated for each of the time steps, and the mean over the time steps is used as an evaluation metric. For the estimated x-coordinate of a position the mean CRPS is given by

$$\text{CRPS}(x) = \frac{1}{\tau + 1} \sum_{t=0}^{\tau} \widehat{\text{CRPS}}_t(x), \tag{3.42}$$

where $\widehat{\text{CRPS}}_t(x)$ is an estimate of $\text{CRPS}_t(x)$ which is given by

$$\text{CRPS}_t(x) = \int_{-\infty}^{\infty} (I(x \geq x_{\text{true},t}) - F(x))^2 dx. \tag{3.43}$$

$I(x \geq x_{\text{true},t})$ is an identity function given by

$$I(x \geq x_{\text{true},t}) = \begin{cases} 1, & \text{if} \quad x \geq x_{\text{true},t} \\ 0, & \text{otherwise}, \end{cases} \tag{3.44}$$

and $F(x)$ is the cumulative density function, CDF for short, of x. The estimate $\widehat{\text{CRPS}}_t(x)$ is given by

$$\widehat{\text{CRPS}}_t(x) = \frac{1}{N} \sum_{i=1}^{N} (x_{\text{true},t} - x_{t+}^{(i)})^2. \tag{3.45}$$

The CRPS at each time step can be considered as the area between the CDF of the estimated quantity and the identity function given by Equation (3.44). Consequently, the estimate of the CRPS at each time step is an estimate of this area. This is shown in Figure 3.4. In the case of the figure $x_{\text{true},t} = 200$, and $N = 100$ particles are used. The particles that are used to make the figure are iid normally distributed with expectation given by $x_{\text{true},t}$ and standard deviation equal to 50 m.

The empirical CDF which is shown in Figure 3.4 is an estimate of $F(x)$ and it is given by

$$\hat{F}(x) = \frac{1}{N} \sum_{i=1}^{N} I(x \geq x_{t+}^{(i)}). \tag{3.46}$$

The area between $\hat{F}(x)$ and the identity function is estimated by the length of each of the gray horizontal lines in Figure 3.4 times the distance between the lines, which is $1/N$. Hence, the area is estimated by the area of several small rectangles, whose area is given by the empirical CDF. If the CRPS at a time step is large, then the area between the CDF and the identity function is large, which means that the uncertainty of the estimate is high. Hence, a preferred method has a small value of CRPS for all of the quantities of the state vector.

For the y-coordinate of the estimated position at time step t the estimated CRPS, $\widehat{\text{CRPS}}_t(y)$, is given by Equation (3.45) where $x_{\text{true},t}$ is replaced by $y_{\text{true},t}$ and $y_{t+}^{(i)}$ is used instead of $x_{t+}^{(i)}$ for $i = 1, \ldots, N$. For the estimated velocity, both in the x-direction and
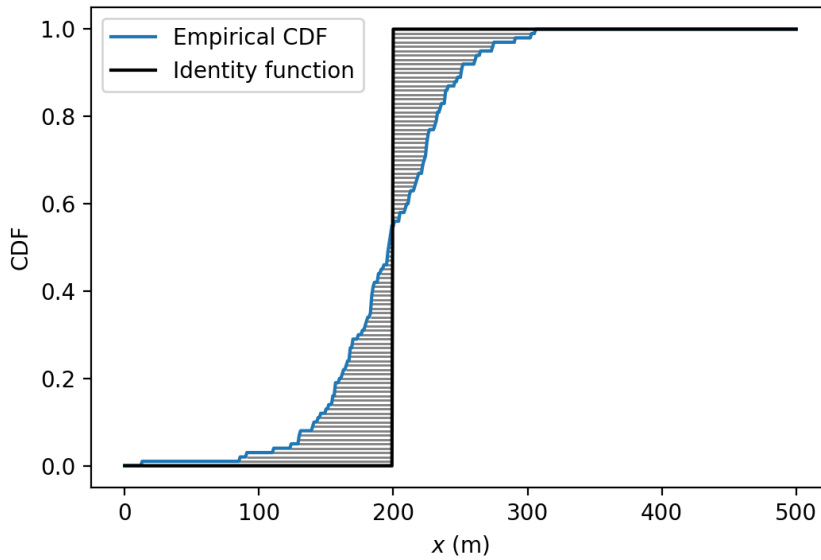
Figure 3.4: Illustration of the estimated CRPS. The area between the blue curve and the black curve is estimated based on the length of each of the horizontal gray lines and the distance between these lines.

in the y-direction, the estimated CRPS at time step t is given by Equation 3.45, but $x_{\text{true},t}$ and $x_{t+}^{(i)}$ are replaced by the relevant quantities.

Chapter 4

Results

In this chapter, the results from applying the statistical methods to the simulated and the real data will be presented. The results for the simulated data will be presented as the solution to four different cases.

4.1 Case 1: Tracking a ship with constant velocity

In order to apply the statistical methods to the simulated data, a path consisting of $\tau+1 = 9$ time steps is created. It is assumed that the true path of the ship crosses the imaginary cable of length 700 m on the ocean floor, and the path is shown in Figure 4.1.
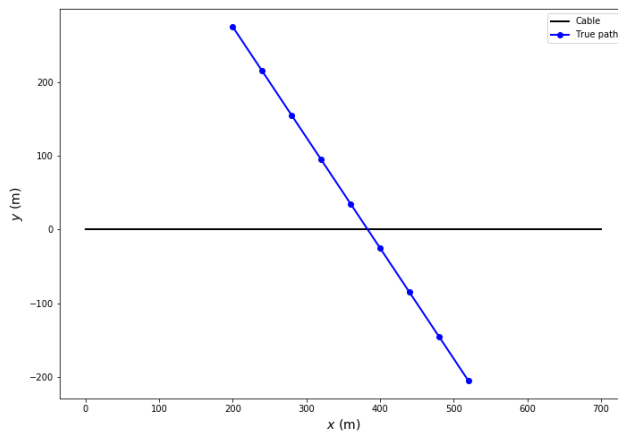

Figure 4.1: The true path of the ship in case 1. The dots along the path indicate the position of the ship at each time step.

The path is created by deciding the starting position, which in this case is given by $(x_{\text{true},0}, y_{\text{true},0}) = (200, 275)$. Further, the constant velocity of the ship is set, $v_{\text{true},x,t} = 4$ m/s and $v_{\text{true},y,t} = -6$ m/s for all t. Finally, the state of the ship for all remaining time steps is given by $\mathbf{x}_{t+1} = g(\mathbf{x}_t)$ with $g(\mathbf{x}_t)$ given by Equation (3.3) and $\Delta_t = 10$ s for all t. The true depth of the imaginary ocean is $z = 50$ m and $n = 701$. For each of the time steps $t = 0, \ldots, \tau$ along the true path the data is simulated using Equations (2.7) and (2.8) with $s = 500$, $\sigma_{\mathbf{T}}^2 = 0.001$ and $\sigma_{\mathbf{P}}^2 = 2$.

4.1.1 Summary of results

The results of applying the SIR method and the EnKPF method to the first simulation case are summarized by the monitored evaluation metrics in Table 4.1 and Table 4.2. In the tables, the mean of the RMSE and CRPS based on three runs of the methods are reported. Also, the standard deviations of the RMSE and the CRPS based on the three runs are reported in the tables. For the ESS, the minimal and the maximal value of the minimal ESS for the three runs of the methods is given. These two values gives the bounds of an interval in which it can be assumed that the minimal ESS of the methods is contained. The EnKPF method is applied with three different values of γ, namely $\gamma = 0.1$, $\gamma = 0.5$ and $\gamma = 0.9$. In the tables $\gamma = 0$ indicates that the results are those given by the SIR method for the first simulation case.

For all three runs the SIR method and the EnKPF method is applied with $N = 10000$ particles. For all of the different values of γ the standard deviations of the noise in Equation (3.1) are given by $\sigma_{\text{pos},0} = 60$ m and $\sigma_{\text{pos},t} = 50$ m for $t = 1, \ldots, \tau$, $\sigma_{\text{vel},0} = 15$ m/s and $\sigma_{\text{vel},t} = 1$ m/s for $t = 1, \ldots, \tau$. The expectation of the distribution of the initial state is given by $\mathbf{x}_0 = \mathbf{x}_{\text{true},0}$. Further, the variance of the noise in Equations (3.7) and (3.8) are given by $\sigma_{\mathbf{T}}^2 = 0.001$ and $\sigma_{\mathbf{P}}^2 = 2$, which are the same values that are used for simulation. The specifications given in this paragraph are the same for all three runs of the methods.

γ	RMSE(x)		RMSE(y)		RMSE(v_x)		RMSE(v_y)		min(ESS)	
	Mean	Std.	Mean	Std.	Mean	Std.	Mean	Std.	Min	Max
0	2.10	0.11	9.51	10.93	4.61	1.51	3.73	0.52	1.00	1.19
0.1	4.20	0.05	4.86	0.86	0.46	0.03	0.48	0.08	172.9	247.52
0.5	2.69	0.02	4.58	2.81	0.43	0.21	0.55	0.07	16.96	56.49
0.9	3.84	0.08	3.77	0.32	0.99	0.43	0.50	0.10	2.49	4.83

Table 4.1: RMSE and minimal ESS of SIR and EnKPF for the first simulation case.

γ	CRPS(x)		CRPS(y)		CRPS(v_x)		CRPS(v_y)	
	Mean	Std.	Mean	Std.	Mean	Std.	Mean	Std.
0	9.06	0.23	810.23	1115.18	45.42	17.38	36.65	8.23
0.1	122.95	1.75	319.93	25.56	34.53	0.20	33.84	0.43
0.5	44.57	1.84	238.73	180.10	33.67	0.90	34.72	1.88
0.9	44.53	0.37	112.89	21.77	32.99	1.08	32.96	0.81

Table 4.2: Mean CRPS of SIR and EnKPF for the first simulation case.

Tables 4.1 and 4.2 show that for most methods, for most of the evaluation metrics the

standard deviation of the evaluation metric is of reasonable size compared to the value of the mean of the evaluation metric. Some exceptions are RMSE(y) and CRPS(y) for SIR and EnKPF with $\gamma = 0.5$. This indicate that the results are more variable for these methods than for the EnKPF method with $\gamma = 0.1$ and $\gamma = 0.9$. Since the standard deviations are large for some of the evaluation metrics, it makes sense to calculate the evaluation metrics based on several runs. This way it is less likely that one of the methods is chosen as the best method for a case just because one single run of the method gives promising results.

Table 4.1 shows that the minimal ESS is close to one for all runs of the SIR method. This indicates that for all runs the method struggles with degeneracy. Hence, the SIR method does not seem to be the best choice for state estimation for simulation case 1. For $\gamma = 0.9$ the interval for the minimal ESS has a lower bound close to one. This means that degeneracy is a problem also for EnKPF with $\gamma = 0.9$ for the first simulation case. Since the lower bound of the interval for minimal ESS for $\gamma = 0.1$ and $\gamma = 0.5$ is much larger than one EnKPF with $\gamma = 0.1$ and EnKPF with $\gamma = 0.5$ do not experience degeneracy for the first simulation case. Since the minimal value of the minimal ESS is lower for $\gamma = 0.5$ than for $\gamma = 0.1$, EnKPF with $\gamma = 0.1$ seems to be the best alternative for state estimation for simulation case 1. The results of using EnKPF with $\gamma = 0.1$ are presented below. The results are based on one of the runs of the method. The run that the results are based on is chosen randomly among the three runs.

Table 4.2 indicates that the EnKPF method with $\gamma = 0.9$ gives the results with the least amount of uncertainty associated with the estimated states. Table 4.1 shows that the results from the EnKPF alternatives contain a lower amount of bias than the results from the SIR method. Furthermore, the results associated with $\gamma = 0.1, \gamma = 0.5$ and $\gamma = 0.9$ seem to be approximately equally biased. Based on these observations, EnKPF with $\gamma = 0.9$ seem to be the best alternative for state estimation, but it is not wise to choose this as the best alternative because of the low value of minimal ESS. EnKPF with $\gamma = 0.9$ is highly influenced by the EnKF method, and when the cable is assumed to be straight, it is expected that the EnKF method will struggle to estimate the correct y-coordinate of the position of the ship. This might be the reason why EnKPF with $\gamma = 0.9$ has a very low value of minimal ESS.

4.1.2 Best alternative: EnKPF with $\gamma = 0.1$

By using the EnKPF method with $\gamma = 0.1$ the estimated filtering distributions of the positions of the ship are given in Figure 4.2. For some time steps the estimated filtering distribution surrounds the true position of the ship, but the estimated filtering distribution of the position of the ship at time steps $t = 1, t = 3, t = 4, t = 5$ and $t = 6$ has two modes, with some particles positioned on the wrong side of the cable. This indicates that it is difficult to estimate the y-coordinate of the position of the ship.

It should be noticed that the spread of the particles decreases from time step $t = 2$ to time step $t = 3$. Since noise is added to the movement of the particles in Equation (3.1), one could expect that the spread of the particles would increase from one time step to the next. However, the EnKPF method with $\gamma = 0.1$ seems to be able to decrease the uncertainty of the estimated distribution from one time step to the next. At other time steps, the spread of the particles increases from one time steep to the next. This is true for

the distributions at time step $t = 7$ and $t = 8$. For these time steps the method is not able to make the uncertainty associated with the movement of the particles insignificant.
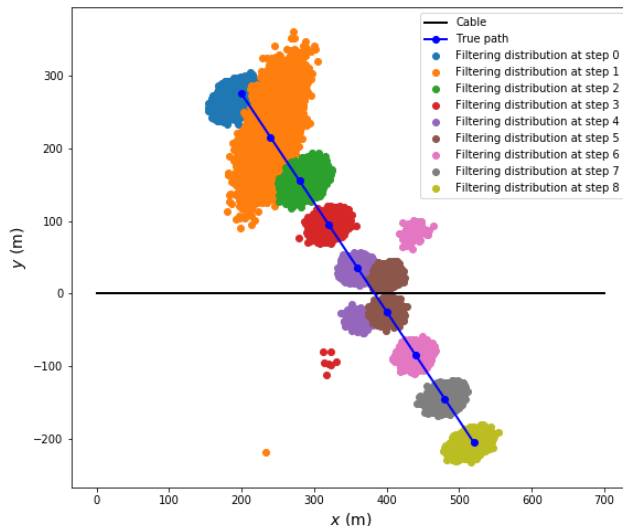

Figure 4.2: Estimated filtering distribution of the positions of the ship according to the EnKPF method with $\gamma = 0.1$.

The ESS at all time steps for the EnKPF method with $\gamma = 0.1$ is shown in Figure 4.3. With $\gamma = 0.1$ the EnKPF method is slightly influenced by the EnKF method, and the result is that degeneracy is not a problem. The ESS is large at all time steps, and it is never close to one. The ESS is at its smallest at time steps $t = 4$ and $t = 5$. This makes sense since these are the time steps at which the ship is closest to the cable. At these time steps the signal to noise ratio is large, and the observations associated with a few states fit very well to the data, while it is clear that for many states the observations do not fit the measured data. Hence, the weights associated with some states are much larger than the weights associated with other states.

The expected path and the associated uncertainty of the ship provided by the EnKPF method with $\gamma = 0.1$ is shown in Figure 4.4. The expected path fits the true path of the ship very well. At all time steps the true position of the ship lays on the inside of the uncertainty bounds of the estimate. The low bias of the estimated path fits well with the values of RMSE(x) and RMSE(y) given in Table 4.1.

At each time step, the estimated position, which is represented by the red dots along the expected path in Figure 4.4, is given by $(\bar{x}_{t^+}, \bar{y}_{t^+})$. The uncertainty bounds are created by adding and subtracting the estimated posterior standard deviation associated with the estimated filtering distribution of the positions of the ship. The estimated states and the associated posterior standard deviations are given by Equations (3.17) and (3.18), respec-
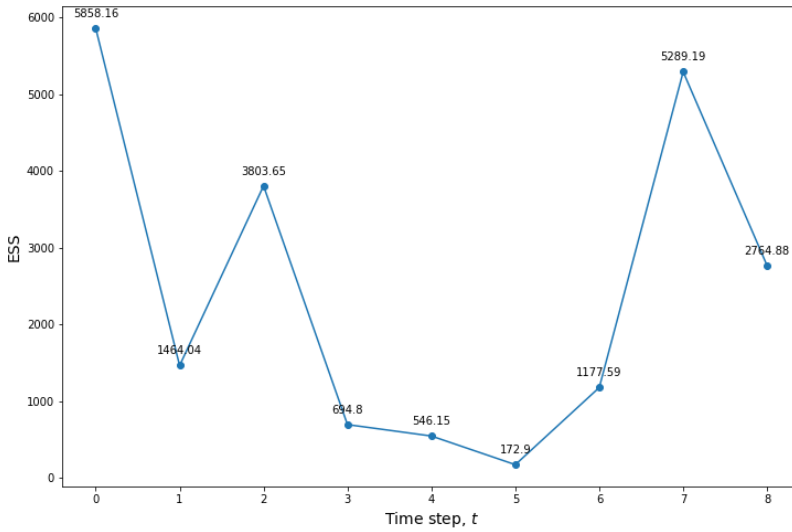
Figure 4.3: ESS at each time step using EnKPF with $\gamma = 0.1$.

tively.

The estimated velocity of the ship based on the EnKPF method with $\gamma = 0.1$ is shown in Figure 4.5 together with the uncertainty of the the estimate. The true velocity lays inside the uncertainty bounds for all time steps, and it can be seen that for all time steps the velocity estimate is very close to the true velocity both in the x-direction and in the y-direction. This confirms the results for RMSE(v_x), RMSE(v_y), CRPS(v_x) and CRPS(v_y) for $\gamma = 0.1$ given in Table 4.1 and Table 4.2.

Overall, Figures 4.2, 4.3, 4.4 and 4.5 confirms that the choice of EnKPF with $\gamma = 0.1$ is a good choice for state estimation for simulation case 1. From the results presented in this subsection, it seems like EnKPF with $\gamma = 0.1$ is influenced with the right amount of EnKF. The ESS is large, but the method has problems with estimating the correct y-coordinate of the positions of the ship. For a larger γ the problems related to the estimated y-coordinates would probably be worse, and consequently, the ESS would be smaller.
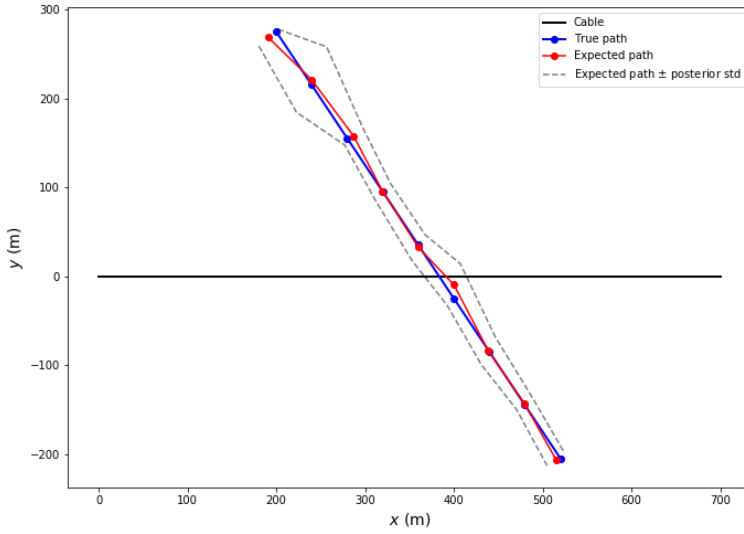
Figure 4.4: The expected path of the ship according to EnKPF with $\gamma = 0.1$.
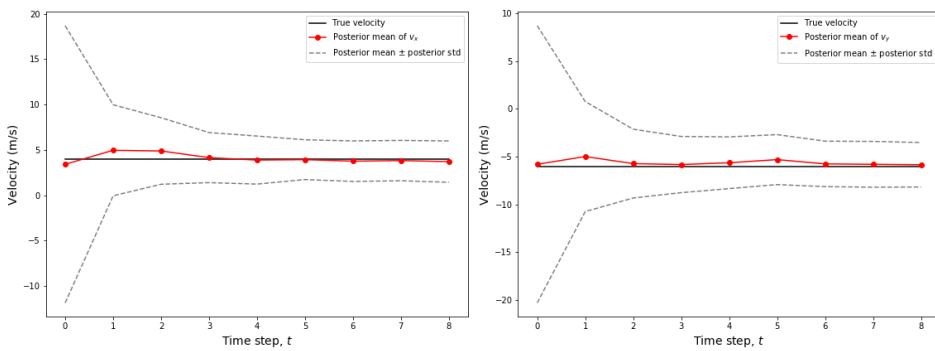

Figure 4.5: The estimated velocity of the ship according to EnKPF with $\gamma = 0.1$. The estimate of v_x is shown on the left, while the estimate of v_y is shown on the right.

4.2 Case 2: Adding curvature to the cable

In order to overcome the problem of estimating the position of the ship with wrong y-coordinate some curvature is added to the cable. This curvature is given by

$$y_{\text{cable}}(x_{\text{cable}}) = 60\sin(0.01x_{\text{cable}}). \tag{4.1}$$

The path in this case is created in the same way, with the same parameters, as in the previous case, and the setup is shown in Figure 4.6. The data in this case is simulated in the same manner as in the previous case. The parameter n is still given by $n = 701$ since this is the number of points along the cable at which the energy and travel time is calculated.
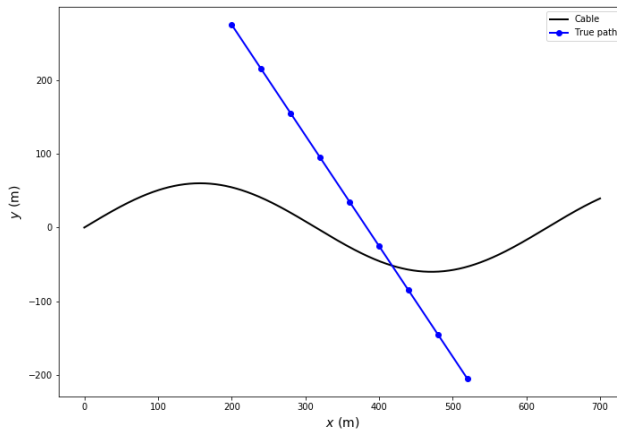
Figure 4.6: The true path of the ship in case 2. The dots along the path indicate the position of the ship at each time step.

4.2.1 Summary of results

The results of applying the SIR method and the EnKPF method to the second simulation case are summarized by the monitored evaluation metrics in Table 4.3 and Table 4.4. As in the previous case, the EnKPF method is applied with three different values of γ, namely $\gamma = 0.1$, $\gamma = 0.5$ and $\gamma = 0.9$, and in the tables $\gamma = 0$ indicates that the results are those given by the SIR method for the second simulation case. The evaluation metrics that are presented in Table 4.3 and Table 4.4 are based on three runs of the methods. The parameters for the methods are the same as those that were specified in simulation case 1.

From Table 4.3 it can be observed that the minimal ESS for the SIR method is close to one for all runs, which means that degeneracy is a problem for SIR for simulation case 2. The minimal ESS of the EnKPF method with $\gamma = 0.1$ is low, but not close to one. These methods may not be a good alternative for state estimation for the second simulation case.

γ	RMSE(x)		RMSE(y)		RMSE(v_x)		RMSE(v_y)		min(ESS)	
	Mean	Std.	Mean	Std.	Mean	Std.	Mean	Std.	Min	Max
0	2.69	0.26	1.26	0.07	4.43	2.55	2.27	1.08	1.00	1.16
0.1	2.25	0.16	2.95	0.11	0.42	0.09	0.76	0.13	5.16	7.27
0.5	3.83	0.06	3.45	0.16	0.48	0.04	0.76	0.09	41.35	72.84
0.9	3.25	0.12	1.94	0.05	0.44	0.01	0.33	0.08	52.27	57.61

Table 4.3: RMSE and minimal ESS of SIR and EnKPF for the second simulation case.

γ	CRPS(x)		CRPS(y)		CRPS(v_x)		CRPS(v_y)	
	Mean	Std.	Mean	Std.	Mean	Std.	Mean	Std.
0	10.26	2.06	3.36	0.39	69.76	20.80	27.36	3.28
0.1	228.56	2.59	421.42	6.30	35.06	0.69	36.60	0.63
0.5	68.10	1.95	135.69	8.43	35.18	0.25	34.28	1.54
0.9	44.84	0.66	111.36	2.76	33.11	0.45	34.14	0.82

Table 4.4: Mean CRPS of SIR and EnKPF for the second simulation case.

The minimal ESS of EnKPF with $\gamma = 0.5$ and $\gamma = 0.9$ is high for all of the runs of the method. Since the minimum of the minimal ESS is smaller for EnKPF with $\gamma = 0.5$ than for EnKPF with $\gamma = 0.9$, EnKPF with $\gamma = 0.9$ is chosen as the best alternative for state estimation for simulation case 2.

The high values of minimal ESS of EnKPF with $\gamma = 0.5$ and $\gamma = 0.9$ reported in Table 4.3 indicate that the curvature added to the cable makes the problems of estimating the correct y-coordinates of the ship less significant. Consequently, the influence of the EnKF method makes the ESS large, and not small which was an issue in the first simulation case.

From Table 4.3 it can be observed that for $\gamma = 0.1$, $\gamma = 0.5$ and $\gamma = 0.9$ the bias associated with the estimated states is quite similar. It can also be observed that the estimated velocities based on the SIR method seem to contain more bias than the estimated velocities based on the EnKPF alternatives. Table 4.4 indicates that the uncertainty associated with the estimated states from EnKPF with $\gamma = 0.9$ is smaller than the uncertainty associated with the estimated states of the other methods. Tables 4.3 and 4.4 indicate that, as in the first simulation case, the SIR method seems to give results that vary more than the results from the EnKPF alternatives.

The results from applying EnKPF with $\gamma = 0.9$ to the second simulation case are presented in the following subsection. The results are based on one of the three runs of the method, and this run is chosen randomly among the three runs.

4.2.2 Best alternative: EnKPF with $\gamma = 0.9$

Using EnKPF with $\gamma = 0.9$ for simulation case 2 gives the estimated filtering distributions of the positions of the ship shown in Figure 4.7. The spread of the particles seems reasonable, and the estimated filtering distributions surround the true position of the ship at all time steps. At most time steps it can be observed that the spread of the distributions is at its largest in a north-east direction. For most time steps, this was not the case in simulation case 1, and the reason for these shapes of the distribution is probably related to the curva-

ture of the cable. At time step $t = 5$ the estimated filtering distribution covers both sides of the cable, but the distribution has only one mode. This indicates that adding curvature to the cable makes it easier for EnKPF to estimate the correct y-coordinates of the ship.
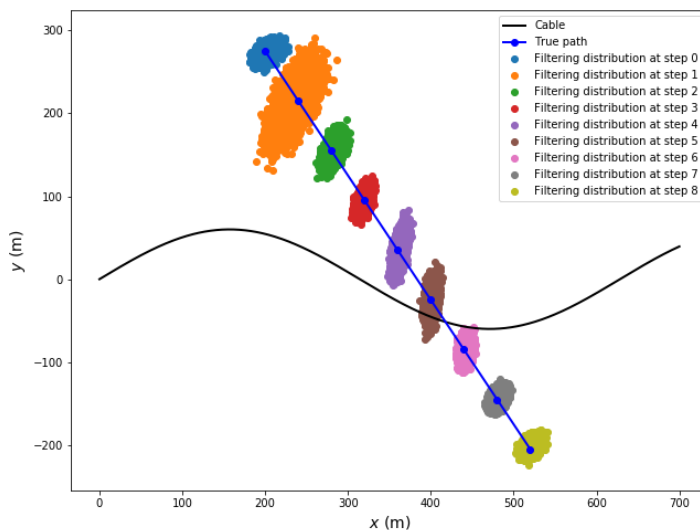

Figure 4.7: Estimated filtering distribution of the positions of the ship according to the EnKPF method with $\gamma = 0.9$.

The ESS for all time steps for EnKPF with $\gamma = 0.9$ is given in Figure 4.8. The ESS is high for all time steps, and the ESS is never close to one. Consequently, degeneracy is not a problem for the EnKPF method with $\gamma = 0.9$ for simulation case 2.

The expected path of the ship given by the EnKPF method with $\gamma = 0.9$ for the second simulation case is shown in Figure 4.9. The estimates of the positions of the ship fit well with the true positions of the ship, and the associated uncertainties are small. The true positions lays on the inside or on the edge of the uncertainty bound of the estimated positions at all time steps. This figure fits well with the values of RMSE and CRPS for x and y given in Tables 4.3 and 4.4.

The estimate of the velocity of the ship made by the EnKPF method with $\gamma = 0.9$ for the second simulation case is shown in Figure 4.10. The estimated velocity fits very well with the true velocity of the ship. For all time steps the true velocity lays on the inside of the uncertainty bound of the estimated velocity. In addition, the estimated velocity is close to the true velocity at all time steps.

Overall, the results from using EnKPF with $\gamma = 0.9$ are good for the second simulation case. Figures 4.7, 4.8, 4.9 and 4.10 confirm the indication from Table 4.3 and Table 4.4 that EnKPF with $\gamma = 0.9$ is a satisfying method for state estimation for simulation case 2.
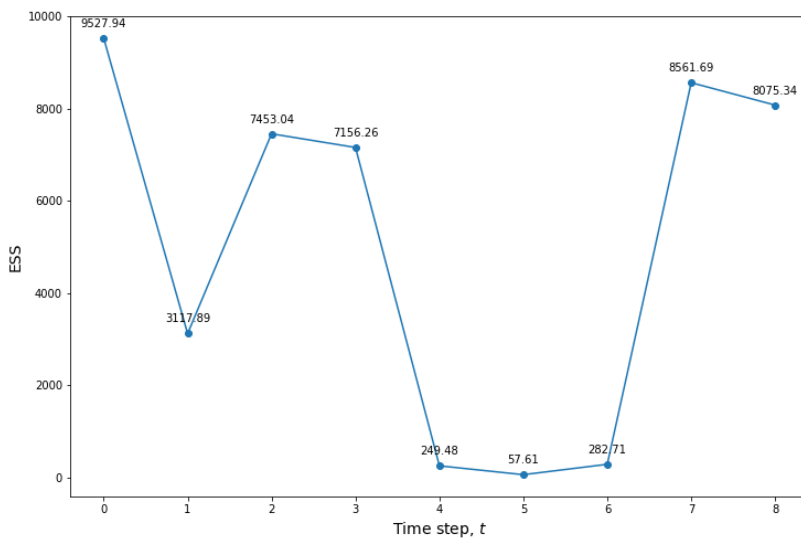
Figure 4.8: ESS at each time step using EnKPF with $\gamma = 0.9$.
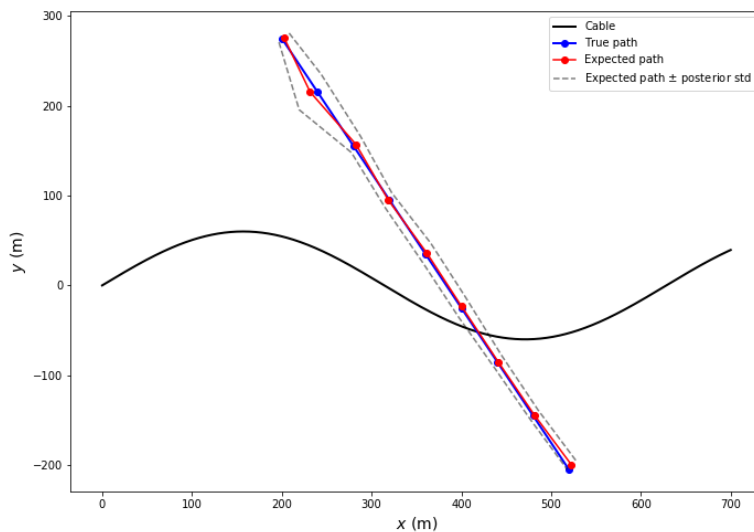

Figure 4.9: The expected path of the ship according to EnKPF with $\gamma = 0.9$.
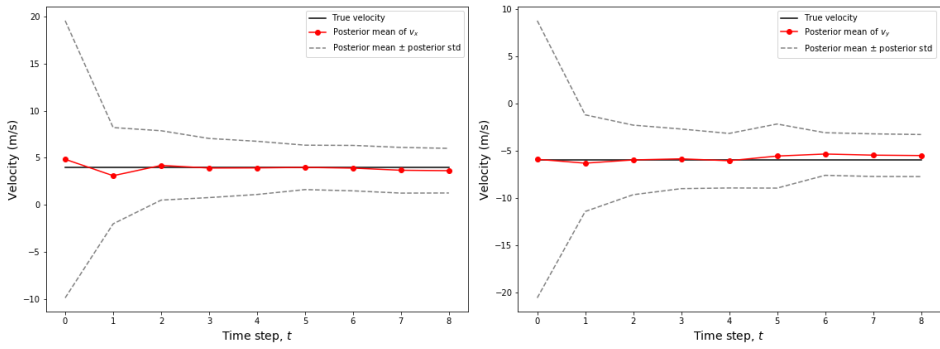
Figure 4.10: The estimated velocity of the ship according to EnKPF with $\gamma = 0.9$. The estimate of v_x is shown on the left, while the estimate of v_y is shown on the right.

4.3 Case 3: Tracking a ship with non-constant velocity

In this case, the curvature of the imaginary cable is given by Equation (4.1), and the setup is presented in Figure 4.11.
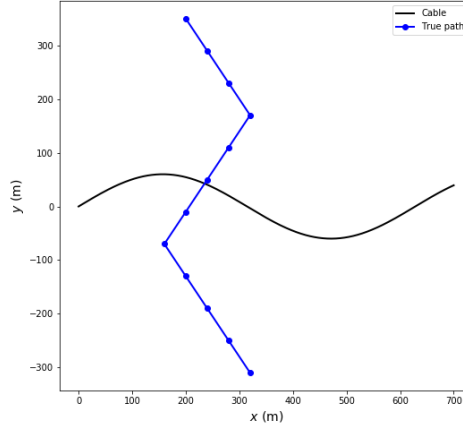

Figure 4.11: The true path of the ship in case 3. The dots along the path indicate the position of the ship at each time step.

In this case the number of time steps is $\tau + 1 = 12$. The starting position is given by $(x_{\text{true},0}, y_{\text{true},0}) = (200, 350)$, and for $t = 0, 1, 2$ and $t = 7, 8, 9, 10, 11$ $v_{\text{true},x,t} = 4$ m/s and $v_{\text{true},y,t} = -6$ m/s. For $t = 3, 4, 5, 6$, on the other hand, $v_{\text{true},x,t} = -4$ m/s and $v_{\text{true},y,t} = -6$ m/s. Also in this case $\Delta_t = 10$ s for all t, and the positions along the path are given by

$$x_{\text{true},t+1} = x_{\text{true},t} + \Delta_t v_{\text{true},x,t} \tag{4.2}$$

and

$$y_{\text{true},t+1} = y_{\text{true},t} + \Delta_t v_{\text{true},y,t} \tag{4.3}$$

for $t = 0, \ldots, \tau - 1$. These equations together with the defined velocities at each time step define the state equations of the state-space model for the third simulation case. However, also for the third simulation case Equations (3.1) and (3.3) are used in the implementation of SIR and EnKPF. By using a larger $\sigma_{\text{vel},t}$ for simulation case 3 than for simulation cases 1 and 2 the methods should be able to give satisfying estimates of the path of the ship. The true depth of the imaginary ocean is $z = 50$ m, and as before, $n = 701$. The simulation procedure in this case is the same as the procedure in case 1.

This case is more difficult to solve than simulation cases 1 and 2. According to the state-space model it is assumed that the ship is moving with constant velocity, but this is not true. Hence, even though the value of $\sigma_{\text{vel},t}$ is large, it is expected that for this case, the results may not be as good as the results for the previous cases.

4.3.1 Summary of results

The results of applying the SIR method and the EnKPF method to the third simulation case are summarized by the monitored evaluation metrics in Table 4.5 and Table 4.6. As in the previous cases, the EnKPF method is applied with three different values of γ, namely $\gamma = 0.1$, $\gamma = 0.5$ and $\gamma = 0.9$, and in the tables $\gamma = 0$ indicates that the results are those given by the SIR method for the third simulation case. The evaluation metrics are based on three runs of the methods. The parameters for the methods are the same as those that were specified in simulation case 1, except that $\sigma_{\text{vel},t} = 4$ m/s for $t = 1, \ldots, \tau$.

γ	RMSE(x)		RMSE(y)		RMSE(v_x)		RMSE(v_y)		min(ESS)	
	Mean	Std.	Mean	Std.	Mean	Std.	Mean	Std.	Min	Max
0	279.63	45.78	163.47	100.15	8.60	0.52	6.72	1.21	NaN	NaN
0.1	3.84	0.07	4.10	0.27	3.79	0.22	1.65	0.83	1.16	2.98
0.5	2.62	0.08	2.42	0.07	3.84	0.10	0.95	0.33	4.77	12.14
0.9	5.08	0.05	3.35	0.07	3.79	0.04	0.55	0.04	42.20	51.58

Table 4.5: RMSE and minimal ESS of SIR and EnKPF for the third simulation case.

γ	CRPS(x)		CRPS(y)		CRPS(v_x)		CRPS(v_y)	
	Mean	Std.	Mean	Std.	Mean	Std.	Mean	Std.
0	80294.95	26920.62	36752.78	26917.58	99.15	7.83	68.36	13.92
0.1	191.62	5.12	208.39	9.88	59.72	2.69	47.91	2.91
0.5	64.94	0.40	91.34	2.12	62.59	4.31	46.05	2.15
0.9	66.65	0.74	90.13	2.96	61.17	0.85	46.41	1.04

Table 4.6: Mean CRPS of SIR and EnKPF for the third simulation case.

From Table 4.5 it can be observed that the minimal ESS is NaN for all runs of the SIR method. This means that during all runs the method has collapsed due to degeneracy. Consequently, the SIR method is not the best alternative for state estimation for the third simulation case. The high values of RMSE and CRPS for SIR for both the x-coordinate and the y-coordinate given in Tables 4.5 and 4.6 also indicates that as the method has collapsed, it has not been able to estimate the path of the ship in a satisfying manner. This is not the case in simulation case 1 and 2, where the values of these evaluation metrics are closer to the values of the evaluation metrics related to the other values of γ.

According to table 4.5 the minimal value of the minimal ESS is quite small for both EnKPF with $\gamma = 0.1$ and EnKPF with $\gamma = 0.5$. This indicates that EnKPF with $\gamma = 0.1$ and EnKPF with $\gamma = 0.5$ are not the best alternatives for state estimation for the third simulation case. Tables 4.5 and 4.6 indicate that for $\gamma = 0.9$ the minimal ESS is high and that the values of RMSE and CRPS are low compared to the values of these evaluation metrics for the other methods. Hence, EnKPF with $\gamma = 0.9$ is chosen as the best alternative for state estimation for simulation case 3. The results presented in the following subsection are those of one of the three runs of the method, and the run that the results are based on is chosen randomly among the three runs.

Tables 4.5 and 4.6 show that also for the third simulation case the standard deviation of the RMSE and the CRPS seems to be of reasonable size compared to the mean of the

evaluation metrics. It can be observed that the SIR method seems to give more variable results than the EnKPF alternatives.

4.3.2 Best alternative: EnKPF with $\gamma = 0.9$

EnKPF with $\gamma = 0.9$ gives the estimated filtering distributions of the positions of the ship for the third simulation case shown in Figure 4.12. The estimated distributions seem to surround the true position at all time steps, but the shape of the estimated distribution at time step $t = 5$ is peculiar in the way that it has a heavy tail. Also in this simulation case some of the filtering distributions are tilted, such that the spread of the particles are larger in one direction than the others.
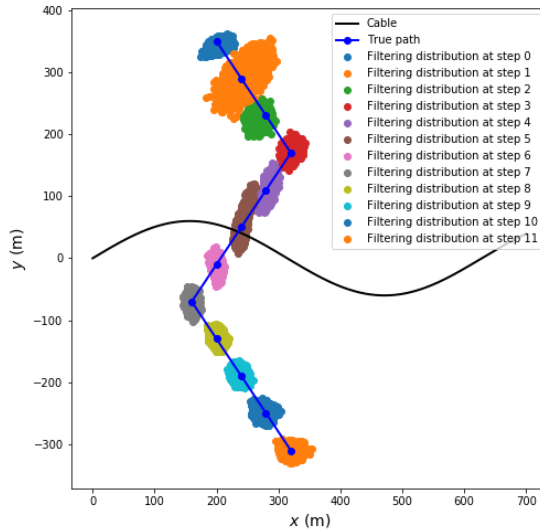
Figure 4.12: Estimated filtering distribution of the positions of the ship according to the EnKPF method with $\gamma = 0.9$.

The ESS for all time steps for EnKPF with $\gamma = 0.9$ for the third simulation case is given in Figure 4.13. The ESS is at its lowest at time step $t = 5$, but it is not close to one at this time step. At all other time steps the ESS is large. This confirms that degeneracy is not a problem for EnKPF with $\gamma = 0.9$ for simulation case 3.

Based on the EnKPF method with $\gamma = 0.9$ the expected path of the ship for simulation case 3 is shown in Figure 4.14. The estimated path fits well with the true path of the ship. The bias of the estimated path is small, and the true path of the ship lays on the inside or on the edge of the uncertainty bound of the estimated path at all time steps. This figure fits well with the low values of RMSE(x), RMSE(y), CRPS(x) and CRPS(y) in Tables 4.5 and 4.6.

Figure 4.13: ESS at each time step using EnKPF with $\gamma = 0.9$.

The estimated velocity of the ship in simulation case 3 according to EnKPF with $\gamma = 0.9$ is shown in Figure 4.15. The estimated velocity of the ship in the y-direction fits very well with the true velocity of the ship. The true velocity is close to the estimated velocity at all time steps. The estimated velocity in the x-direction does not fit the true velocity very well. At time steps $t = 3$ and $t = 7$ the true velocity lays on the outside of the uncertainty bound of the estimated velocity.

The reason why the true velocity lays on the outside of the uncertainty bound of the estimated velocity in the x-direction is most likely given by Equations (4.2) and (4.3) which indicate that the velocity of the ship at time step $t - 1$ affects the path of the ship not at time step $t - 1$, but at time step t. This fits well with Figure 4.15 which shows that the estimated velocity in the x-direction is shifted one time step compared to the true velocity. Hence, it might be too much to expect that the methods should be able to estimate the velocity in the x-direction correctly for all time steps. Also, the change in velocity from $v_{\text{true},x,t} = 4$ m/s to $v_{\text{true},x,t+1} = -4$ m/s is radical, and the results could maybe have been better if the change in velocity was smaller.

EnKPF with $\gamma = 0.9$ seems to provide a reasonable estimate of the states of the ship for simulation case 3. The estimated path fits well to the true path, and the quality of the estimated velocity is not very bad considering the affect a change in velocity has on the path of the ship. Hence, Figures 4.12, 4.13, 4.14 and 4.15 confirms that EnKPF with $\gamma = 0.9$ is a good alternative for state estimation for the third simulation case.
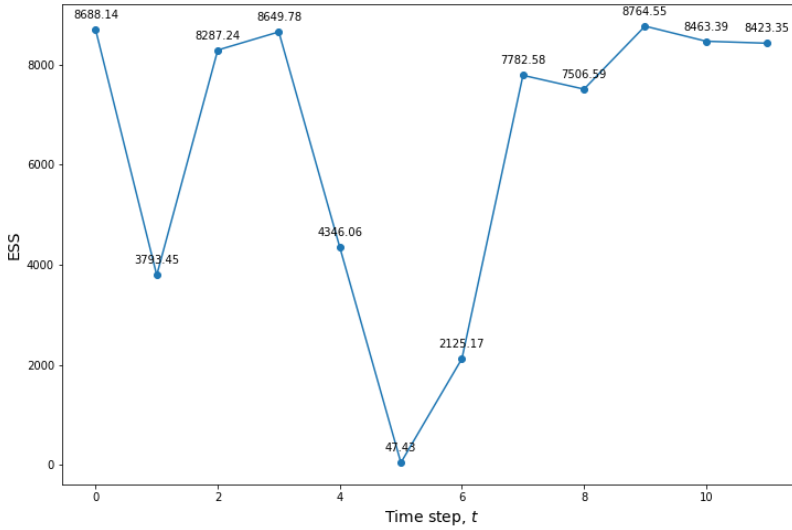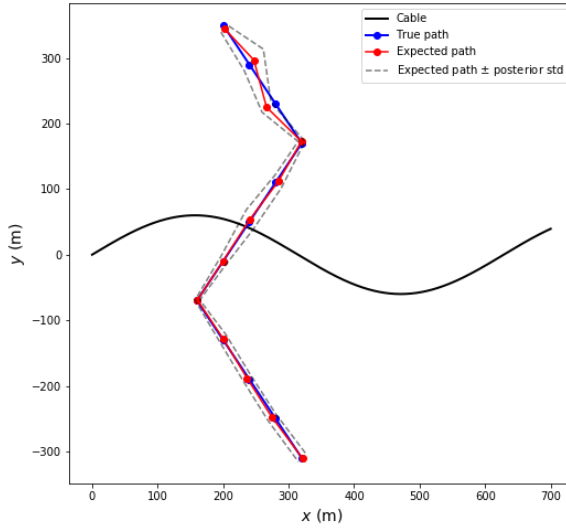
Figure 4.14: The expected path of the ship according to EnKPF with $\gamma = 0.9$.
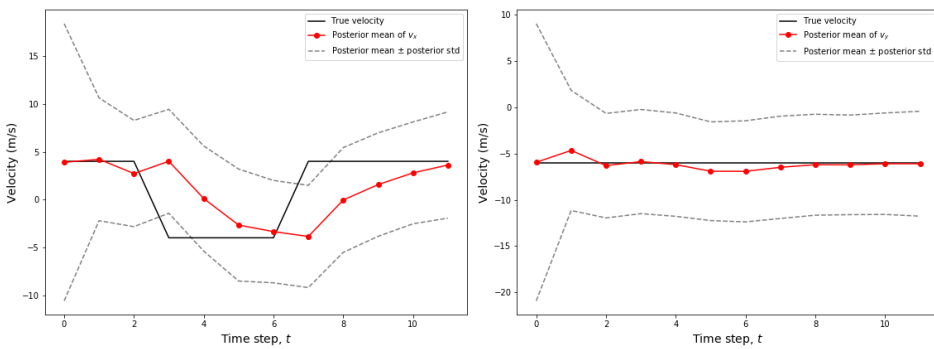

Figure 4.15: The estimated velocity of the ship according to EnKPF with $\gamma = 0.9$. The estimate of v_x is shown on the left, while the estimate of v_y is shown on the right.

4.4 Case 4: Using data from two curved cables

If the vibrations caused by a ship are registered by two cables, it might be possible to use the data from both of these cables to track the ship. The data from the two cables can be combined in many ways in order to define a filtering distribution of the estimated states. One way is to use the data from one of the cables to estimate the state of the ship, and then use this estimate along with data from the other cable as input to the statistical method to end up with a final estimate of the state. This is performed for each time step in the following subsection for SIR and EnKPF.

The two cables define two different coordinate systems. The first cable is the x-axis of a coordinate system where the origin is located in the point $(\tilde{x}, \tilde{y}) = (200, 0)$ of the coordinate system defined by the second cable. From the point of view of the second cable, the first cable is the line defined by $\tilde{y} = -500 + 2.5\tilde{x}$, and the angle between the two cables is then given by $\theta = \arctan(2.5)$. Both of the cables are 700 m long. This setup is shown in Figure 4.16, and the entire x-axes in this figure represent the cables. The coordinate system given by x and y is defined by the first cable, while the coordinate system given by $\tilde{x}$ and $\tilde{y}$ is defined by the second cable.
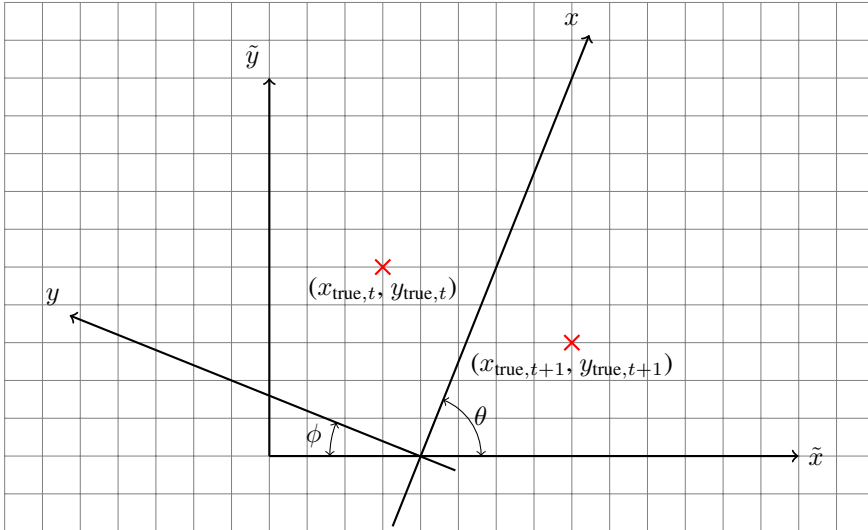
Figure 4.16: Setup for two cables. Each cable defines a coordinate system.

By using the geometry of the coordinate systems the coordinates of a point in one of the coordinate systems can be transformed to coordinates of a point in the other coordinate system. A transformation from the first coordinate system to the second coordinate system is given by

$$\tilde{x} = 200 + (0.4x - y)\cos\phi \tag{4.4}$$

and

$$\tilde{y} = 80 + (y - \sqrt{80^2 + 200^2} + 2.5x)\sin\phi, \tag{4.5}$$

where $\phi = \pi/2 - \theta$.

Since the problem of estimating the position of a ship close to the cable is solved by adding curvature the cable, this is also done in this case. For both cables, the curvature is given by Equation (4.1). In order to investigate if the statistical methods are able to estimate the velocity correctly when the change in velocity is small, a true path with non-constant velocity is created. The true path for the fourth simulation case is shown in Figure 4.17.
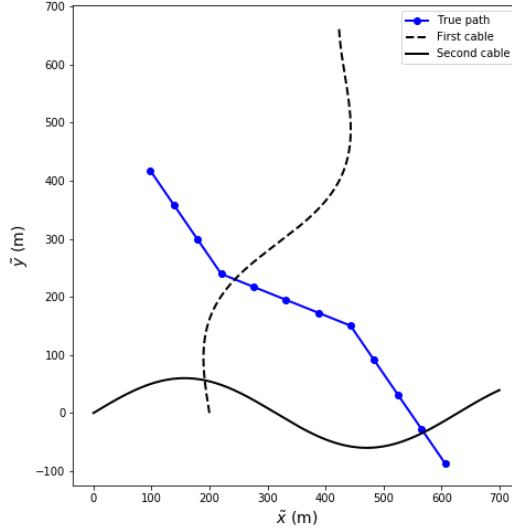
Figure 4.17: The true path of the ship in case 4. The dots along the path indicate the true position of the ship at each time step.

In this case the number of time steps is $\tau + 1 = 12$. For the first cable the initial position is given by $(x_{\text{true},0}, y_{\text{true},0}) = (350, 250)$. For time steps $t = 0, 1, 2$ and time steps $t = 7, 8, 9, 10, 11$ the velocity is given by $v_{\text{true},x,t} = -4$ m/s and for time steps $t = 3, 4, 5, 6$ the velocity is given by $v_{\text{true},x,t} = 0$ m/s. For all time steps $v_{\text{true},x,t} = -6$ m/s. As before, $\Delta_t = 10$ s for all t and the positions along the path in the first coordinate system are given by Equations (4.2) and (4.3). The transformed positions, $(\tilde{x}_{\text{true},t}, \tilde{y}_{\text{true},t})$, for all t are given by Equations (4.4) and (4.5), and the initial position is $(\tilde{x}_{\text{true},0}, \tilde{y}_{\text{true},0}) = (97.87, 417.81)$. Consequently, the velocities of the transformed path are given by

$$v_{\text{true},\tilde{x},t} = \frac{\tilde{x}_{\text{true},t+1} - \tilde{x}_{\text{true},t}}{\Delta_t}, \tag{4.6}$$

$$v_{\text{true},\tilde{y},t} = \frac{\tilde{y}_{\text{true},t+1} - \tilde{y}_{\text{true},t}}{\Delta_t}. \tag{4.7}$$

For time steps $t = 0, 1, 2$ and time steps $t = 7, 8, 9, 10, 11$ the velocity is given by $v_{\text{true},\tilde{x},t} = 4.09$ m/s and $v_{\text{true},\tilde{y},t} = -5.94$ m/s. For time steps $t = 3, 4, 5, 6$ the veloc-

ity is $v_{\text{true},\tilde{x},t} = 5.57$ m/s and $v_{\text{true},\tilde{y},t} = -2.23$ m/s. The true depth of the imaginary ocean is $z = 50$ m, and $n = 701$ for both cables. The simulation procedure presented in case 1 is performed for both coordinate systems.

The procedure for estimating the state of the ship using two cables consists of using data sequentially from the two cables at each time step. Since the data from the first cable estimates positions in the coordinate system of the first cable, the estimates need to be transformed before the data from the second cable is used. The transformation between the two coordinate systems is given by Equation (4.4) and (4.5). The procedure for state estimation based on data from two cables is presented in Algorithm 5.

Algorithm 5: Ship tracking based on data from two cables

---

1 Draw initial states: $\mathbf{x}_0^{(i)} \sim \mathcal{N}_4(\mathbf{x}_{\text{true},0}, V_0)$ for $i = 1, \dots, N$

2 **for** $t = 0, \dots, \tau$ **do**

3   Perform one step of SIR or EnKPF with prior defined by the particles
     $\mathbf{x}_t^{(i)}, i = 1, \dots, N$ and data from the first cable to estimate
     $p(\mathbf{x}_t | \mathbf{T}_{\text{data},0:t}, \mathbf{P}^2_{\text{data},0:t}, \tilde{\mathbf{T}}_{\text{data},0:t-1}, \tilde{\mathbf{P}}^2_{\text{data},0:t-1})$

4   Transform the estimated $p(\mathbf{x}_t | \mathbf{T}_{\text{data},0:t}, \mathbf{P}^2_{\text{data},0:t}, \tilde{\mathbf{T}}_{\text{data},0:t-1}, \tilde{\mathbf{P}}^2_{\text{data},0:t-1})$ to be
     defined in the second coordinate system. That is, compute
     $p(\tilde{\mathbf{x}}_t | \mathbf{T}_{\text{data},0:t}, \mathbf{P}^2_{\text{data},0:t}, \tilde{\mathbf{T}}_{\text{data},0:t-1}, \tilde{\mathbf{P}}^2_{\text{data},0:t-1})$

5   Perform one step of SIR or EnKPF with prior
     $p(\tilde{\mathbf{x}}_t | \mathbf{T}_{\text{data},0:t}, \mathbf{P}^2_{\text{data},0:t}, \tilde{\mathbf{T}}_{\text{data},0:t-1}, \tilde{\mathbf{P}}^2_{\text{data},0:t-1})$ and data from the second cable
     to compute the final estimate of the state given by
     $p(\tilde{\mathbf{x}}_t | \mathbf{T}_{\text{data},0:t}, \mathbf{P}^2_{\text{data},0:t}, \tilde{\mathbf{T}}_{\text{data},0:t}, \tilde{\mathbf{P}}^2_{\text{data},0:t})$

6   Transform the estimated filtering distribution to be defined in the first
     coordinate system. That is, compute $p(\mathbf{x}_t | \mathbf{T}_{\text{data},0:t}, \mathbf{P}^2_{\text{data},0:t}, \tilde{\mathbf{T}}_{\text{data},0:t}, \tilde{\mathbf{P}}^2_{\text{data},0:t})$

7   Move the particles according to Equation (3.1) in order to create the particles
     $\mathbf{x}_{t+1}^{(i)}, i = 1, \dots, N$ which defines the prior for the next time step

8 **end**

In the algorithm, $\tilde{\mathbf{T}}_{\text{data},0:t}, \tilde{\mathbf{P}}^2_{\text{data},0:t}$ denotes measured data from the second cable at all time steps up to and including time step t. In addition, at time step $t = 0$,
$p(\mathbf{x}_t | \mathbf{T}_{\text{data},0:t}, \mathbf{P}^2_{\text{data},0:t}, \tilde{\mathbf{T}}_{\text{data},0:t-1}, \tilde{\mathbf{P}}^2_{\text{data},0:t-1}) = p(\mathbf{x}_t | \mathbf{T}_{\text{data},0:t}, \mathbf{P}^2_{\text{data},0:t})$.

4.4.1 Summary of results

For the fourth simulation case the evaluation metrics are calculated based on both
$p(\tilde{\mathbf{x}}_t | \mathbf{T}_{\text{data},0:t}, \mathbf{P}^2_{\text{data},0:t}, \tilde{\mathbf{T}}_{\text{data},0:t-1}, \tilde{\mathbf{P}}^2_{\text{data},0:t-1})$ and $p(\tilde{\mathbf{x}}_t | \mathbf{T}_{\text{data},0:t}, \mathbf{P}^2_{\text{data},0:t}, \tilde{\mathbf{T}}_{\text{data},0:t}, \tilde{\mathbf{P}}^2_{\text{data},0:t})$.
Consequently, four tables are presented below. The monitored evaluation metrics for simulation case 4 are given in Table 4.7, Table 4.8, Table 4.9 and Table 4.10. As in the previous cases, the EnKPF method is applied with three different values of γ, namely $\gamma = 0.1$, $\gamma = 0.5$ and $\gamma = 0.9$, and in the tables $\gamma = 0$ indicates that the results are those given by the SIR method for the fourth simulation case. The evaluation metrics are based on three

runs of Algorithm 5. For both cables the parameters for the methods are the same as those that were specified in simulation case 1, except that $\sigma_{\text{vel},t} = 4$ m/s for $t = 1, \ldots, \tau$.

γ	RMSE(x)		RMSE(y)		RMSE(v_x)		RMSE(v_y)		min(ESS)	
	Mean	Std.	Mean	Std.	Mean	Std.	Mean	Std.	Min	Max
0	189.92	138.32	299.59	43.26	7.47	1.85	7.79	2.34	NaN	NaN
0.1	3.00	0.30	3.11	0.26	2.01	1.14	2.37	0.66	1.06	4.39
0.5	2.57	0.07	3.59	0.03	1.18	0.38	1.87	0.17	3.17	18.17
0.9	5.29	0.04	2.80	0.06	0.78	0.10	1.59	0.03	69.00	93.99

Table 4.7: RMSE and minimal ESS of SIR and EnKPF for the fourth simulation case based on the estimated $p(\tilde{\mathbf{x}}_t | \mathbf{T}_{\text{data},0:t}, \mathbf{P}^2_{\text{data},0:t}, \tilde{\mathbf{T}}_{\text{data},0:t-1}, \tilde{\mathbf{P}}^2_{\text{data},0:t-1})$.

γ	CRPS(x)		CRPS(y)		CRPS(v_x)		CRPS(v_y)	
	Mean	Std.	Mean	Std.	Mean	Std.	Mean	Std.
0	55200.81	56948.73	91627.17	27234.09	80.23	26.92	89.85	42.45
0.1	230.18	28.52	341.73	30.36	49.57	5.54	53.46	2.90
0.5	98.98	1.30	117.54	2.31	47.34	1.21	50.02	2.66
0.9	118.36	2.79	66.27	1.39	47.80	0.15	48.66	0.23

Table 4.8: Mean CRPS of SIR and EnKPF for the fourth simulation case based on the estimated $p(\tilde{\mathbf{x}}_t | \mathbf{T}_{\text{data},0:t}, \mathbf{P}^2_{\text{data},0:t}, \tilde{\mathbf{T}}_{\text{data},0:t-1}, \tilde{\mathbf{P}}^2_{\text{data},0:t-1})$.

γ	RMSE(x)		RMSE(y)		RMSE(v_x)		RMSE(v_y)		min(ESS)	
	Mean	Std.	Mean	Std.	Mean	Std.	Mean	Std.	Min	Max
0	189.91	138.33	299.59	43.26	7.83	1.99	7.93	2.28	NaN	NaN
0.1	2.54	0.01	2.52	0.04	2.04	1.20	2.36	0.68	4524.91	4778.78
0.5	1.46	0.01	1.96	0.01	1.25	0.38	1.76	0.15	7451.63	7485.24
0.9	2.53	0.06	1.74	0.03	0.74	0.08	1.57	0.03	9862.14	9874.13

Table 4.9: RMSE and minimal ESS of SIR and EnKPF for the fourth simulation case based on the estimated $p(\tilde{\mathbf{x}}_t | \mathbf{T}_{\text{data},0:t}, \mathbf{P}^2_{\text{data},0:t}, \tilde{\mathbf{T}}_{\text{data},0:t}, \tilde{\mathbf{P}}^2_{\text{data},0:t})$.

From Table 4.7 and Table 4.9 it can be observed that the SIR method has collapsed at at least one time step for all runs of the method. In addition, as in simulation case 3, the RMSE is large for all elements of the state vector, and Tables 4.8 and 4.10 show that also the CRPS is very large for the SIR method for all elements of the state vector. Hence, SIR is not the best method for state estimation for the fourth simulation case.

For all alternatives of the EnKPF method, Tables 4.7-4.10 show that both the RMSE and the CRPS for both the x-coordinate and the y-coordinate are smaller for the estimates based on data from both cables at time step t than for estimates based on data from only the first cable at time step t. This indicates that using data from two cables at time step t improves the quality of the estimate of the position of the ship compared to using data from only one cable at time step t. Tables 4.7-4.10 also show that the estimates of the velocities do not seem to improve much when using data from both of the cables compared to using data from only one of the cables at time step t.

γ	CRPS(x)		CRPS(y)		CRPS(v_x)		CRPS(v_y)	
	Mean	Std.	Mean	Std.	Mean	Std.	Mean	Std.
0	55199.63	56948.74	91626.1	27234.61	77.33	28.20	90.80	44.68
0.1	24.61	0.63	24.97	0.80	48.43	6.23	50.97	2.94
0.5	9.96	0.15	9.41	0.12	46.94	0.68	49.41	2.31
0.9	12.80	0.32	6.83	0.12	47.08	0.80	48.92	0.73

Table 4.10: Mean CRPS of SIR and EnKPF for the fourth simulation case based on the estimated $p(\tilde{\mathbf{x}}_t | \mathbf{T}_{\mathrm{data},0:t}, \mathbf{P}^2_{\mathrm{data},0:t}, \tilde{\mathbf{T}}_{\mathrm{data},0:t}, \tilde{\mathbf{P}}^2_{\mathrm{data},0:t})$.

Based on Table 4.7 both EnKPF with $\gamma = 0.1$ and EnKPF with $\gamma = 0.5$ seem to struggle with degeneracy. EnKPF with $\gamma = 0.9$ does not seem to have problems with degeneracy, and for many of the elements of the state vector EnKPF with $\gamma = 0.9$ has the lowest value of RMSE and CRPS in Tables 4.9 and 4.10. Hence, EnKPF with $\gamma = 0.9$ seem to be the best alternative for state estimation for simulation case 4. The results from using this method for the fourth simulation case are presented in the following subsection. The results are based on one of the three runs of the method, and the run that the results are based on is chosen randomly among the three runs.

The standard deviations of the RMSE and the CRPS seem to be of reasonable size compared to the mean of the evaluation metrics for $\gamma = 0.1$, $\gamma = 0.5$ and $\gamma = 0.9$. However, for the SIR method the standard deviation of the RMSE and the CRPS is large compared to the mean of the evaluation metrics for some of the elements of the state vector. This indicates that for simulation case 4, the results are more variable for the SIR method than for the EnKPF method.

4.4.2   Best alternative: EnKPF with $\gamma = 0.9$

The estimated filtering distributions of the positions of the ship according to EnKPF with $\gamma = 0.9$ for simulation case 4 are shown in Figure 4.18. The estimated distributions based on data from the first cable at time step t are shown on the left, while the estimated distributions based on data from both of the cables at time step t are shown on the right. At all time steps the estimated filtering distributions seem to surround the true position of the ship, and it is clear that when data from both of the cables is used then the spread of the particles is smaller than the spread of the particles when data from only the first cable is used. Also, when data from only one cable is used, the distributions seems to be tilted, as was the case in simulation case 2 and 3. However, when data from both of the cables is used, the spread of the particles seems to be approximately equal in all directions. This figure indicate that EnKPF with $\gamma = 0.9$ is suitable for the purpose of estimating the positions of the ship when data from two cables is used.

The ESS of the EnKPF method with $\gamma = 0.9$ for simulation case 4 is shown in Figure 4.19. For the EnKPF method that estimates $p(\tilde{\mathbf{x}}_t | \mathbf{T}_{\mathrm{data},0:t}, \mathbf{P}^2_{\mathrm{data},0:t}, \tilde{\mathbf{T}}_{\mathrm{data},0:t-1}, \tilde{\mathbf{P}}^2_{\mathrm{data},0:t-1})$, the ESS is at its lowest at time step $t = 4$, but it is not close to one at any time steps. The ESS associated with EnKPF that estimates $p(\tilde{\mathbf{x}}_t | \mathbf{T}_{\mathrm{data},0:t}, \mathbf{P}^2_{\mathrm{data},0:t}, \tilde{\mathbf{T}}_{\mathrm{data},0:t}, \tilde{\mathbf{P}}^2_{\mathrm{data},0:t})$ is close to N at all time steps. This makes sense since the prior that is used as input to the EnKPF method for data from the second cable is centered around the true position with
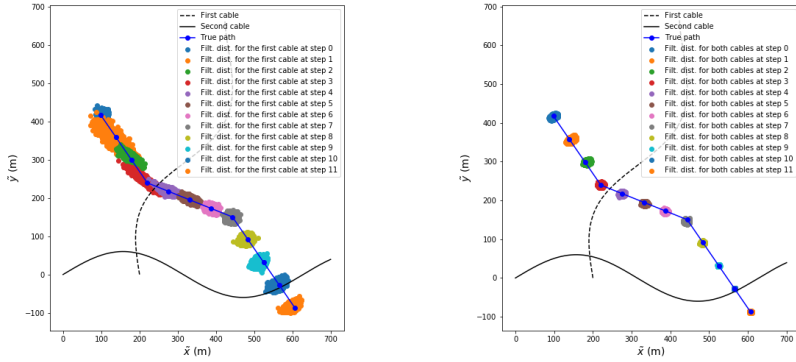
Figure 4.18: Estimated filtering distribution of the positions of the ship according to the EnKPF method with $\gamma = 0.9$. The estimated distributions based on data from the first cable at time step t are shown on the left, while the estimated distributions based on data from both of the cables at time step t are shown on the right.

low variance. This means that all particles fits well to the measured data, and consequently the variance of the weights is very low, which leads to a high ESS.
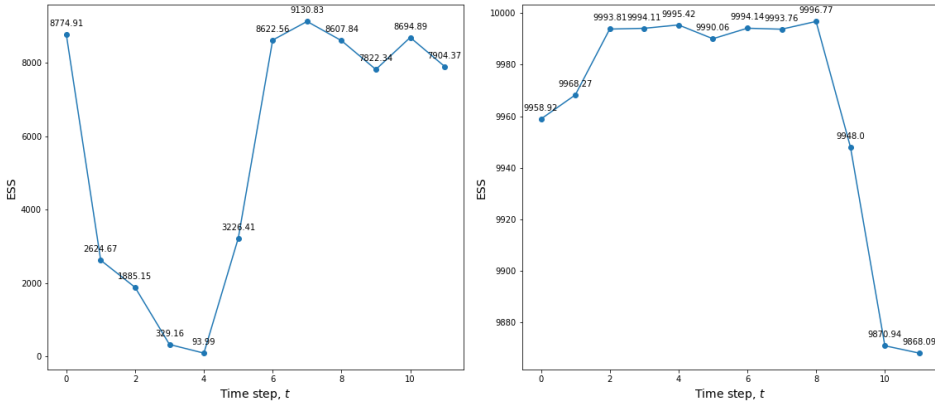

Figure 4.19: ESS at each time step using EnKPF with $\gamma = 0.9$. The ESS on the left is associated with the use of EnKPF with data from the first cable at time step t. The ESS on the right is associated with the use of EnKPF with data from both of the cables at time step t.

The estimated path of the ship in simulation case 4 given by the EnKPF method with $\gamma = 0.9$ is shown in Figure 4.20. The path on the left is the estimated path computed from the estimated distribution $p(\tilde{\mathbf{x}}_t | \mathbf{T}_{\text{data},0:t}, \mathbf{P}^2_{\text{data},0:t}, \tilde{\mathbf{T}}_{\text{data},0:t-1}, \tilde{\mathbf{P}}^2_{\text{data},0:t-1})$. The estimated path on the right is computed from the estimated distribution $p(\tilde{\mathbf{x}}_t | \mathbf{T}_{\text{data},0:t}, \mathbf{P}^2_{\text{data},0:t}, \tilde{\mathbf{T}}_{\text{data},0:t}, \tilde{\mathbf{P}}^2_{\text{data},0:t})$. It is clear that when data from both of the cables is used the uncertainty associated with the estimated path is much smaller. Also, the bias of the estimated path seems smaller for the path which is based on data from both of the

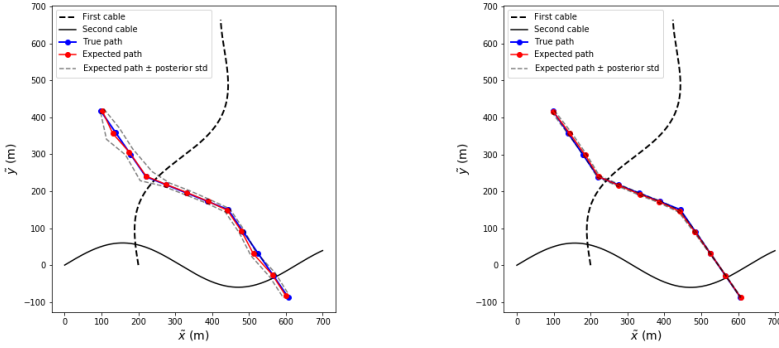cables, than for the path which is based on data from only the first cable at time step t.

Figure 4.20: The expected path of the ship according to EnKPF with $\gamma = 0.9$. The path on the left is computed based on data from the first cable at time step t, while the path on the right is computed based on data from both of the cables at time step t.

By applying EnKPF with $\gamma = 0.9$ to simulation case 4 to estimate $p(\tilde{\mathbf{x}}_t|\mathbf{T}_{\text{data},0:t}, \mathbf{P}^2_{\text{data},0:t}, \tilde{\mathbf{T}}_{\text{data},0:t-1}, \tilde{\mathbf{P}}^2_{\text{data},0:t-1})$ the estimated velocity in the second coordinate system is as given in Figure 4.21. The estimated velocity in the $\tilde{x}$-direction fits very well with the true velocity of the ship. The estimated velocity seems shifted compared to the true velocity, but the true velocity lays on the inside of the uncertainty bound of the estimated velocity at all time steps. The true velocity in the $\tilde{y}$-direction lays on the inside of the uncertainty bound of the estimated velocity at all time steps. The method seems to have detected the change in velocity, but the estimated velocity seems to be shifted compared to the true velocity.

The estimated velocity based on data from both of the cables at time step t is shown in Figure 4.22. This figure indicates that the method estimates the velocity of the ship quite well since for both directions the true velocity lays on the inside of the uncertainty bound of the estimated velocity for all time steps. The estimated velocity is shifted compared to the true velocity in both directions. The estimated velocity of the ship based on data from both of the cables at time step t does not seem to be improved compared to the estimated velocity based on data from only the first cable at time step t.

Overall, the state estimation seems to improve when data from a second cable is used in addition to data from the first cable. The evaluation metrics in Tables 4.7-4.10 indicated that using data from the second cable would result in low bias and low uncertainty in the estimated positions of the ship. Figures 4.18 and 4.20 confirms this indication. The evaluation metrics in Tables 4.7-4.10 indicated that the improvement in the estimated velocity should not be very significant. This is confirmed by Figures 4.21 and 4.22, which shows that the estimated velocity based on data from only one cable is very similar to the estimated velocity based on data from both of the cables.

Figure 4.21: The estimated velocity of the ship according to EnKPF with $\gamma = 0.9$ computed from the estimated $p(\tilde{\mathbf{x}}_t | \mathbf{T}_{\text{data},0:t}, \mathbf{P}^2_{\text{data},0:t}, \tilde{\mathbf{T}}_{\text{data},0:t-1}, \tilde{\mathbf{P}}^2_{\text{data},0:t-1})$. The estimate of $v_{\tilde{x}}$ is shown on the left, while the estimate of $v_{\tilde{y}}$ is shown on the right.

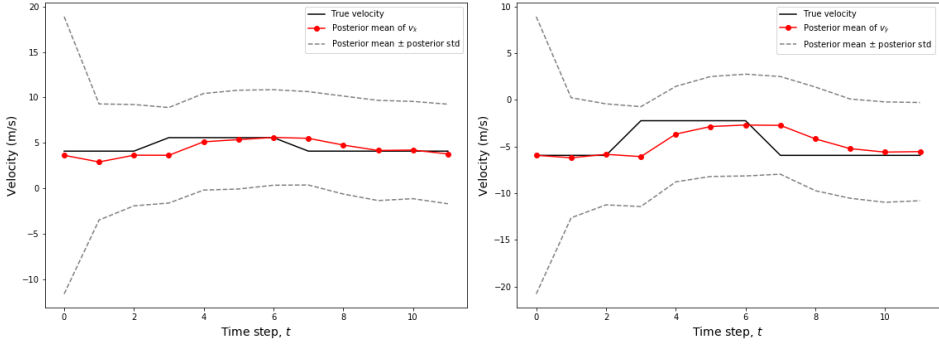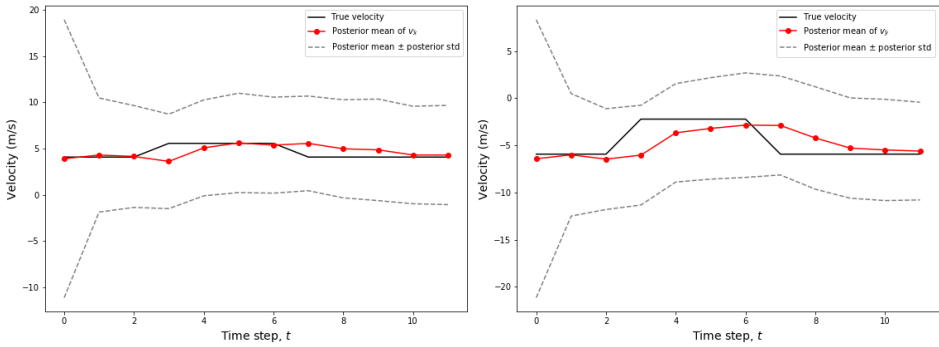**Figure 4.22:** The estimated velocity of the ship according to EnKPF with $\gamma = 0.9$ computed from the estimated $p(\tilde{\mathbf{x}}_t | \mathbf{T}_{\text{data},0:t}, \mathbf{P}^2_{\text{data},0:t}, \tilde{\mathbf{T}}_{\text{data},0:t}, \tilde{\mathbf{P}}^2_{\text{data},0:t})$. The estimate of $v_{\tilde{x}}$ is shown on the left, while the estimate of $v_{\tilde{y}}$ is shown on the right.

4.5 Real case

The true path of the ship for which the real data is measured is shown in Figure 4.23. The plot on the left shows the entire cable, while the plot on the right shows the part of the cable from which the data that is used in this project is measured.
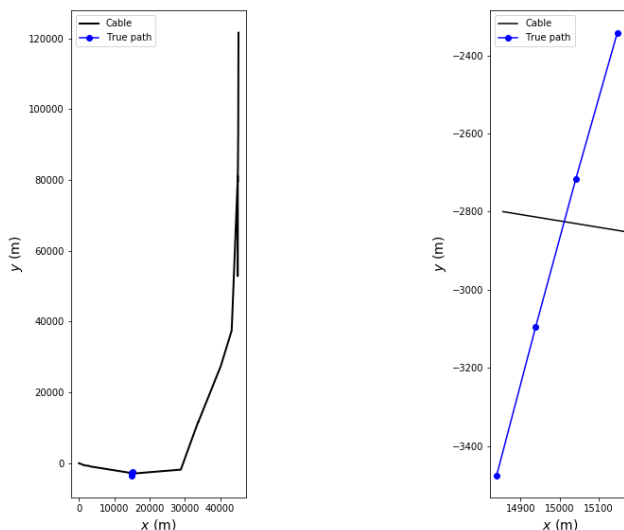

Figure 4.23: The true path of the ship for which the real data is measured. The dots along the path indicate the position of the ship at each time step. The plot on the left shows the entire cable, while the plot on the right shows the part of the cable that is used.

As mentioned in chapter 2, there are $n = 199$ channels along the part of the cable that is used in this project. $\tau + 1 = 4$ states along the path of the ship will be estimated and the first position is given by $(x_{\text{true},0}, y_{\text{true},0}) = (15148.43, -2341.87)$. The true positions are given by the coordinates of the ship which are given by AIS, and the measured data associated with these positions corresponds to the time stamps *Time: 035539-Time: 035839* in Figure 2.6. In the x-direction the true velocity of the ship is given by $v_{x,0} = -1.78$ m/s, $v_{x,1} = -1.71$ m/s, $v_{x,2} = -1.68$ m/s and $v_{x,3} = -1.78$ m/s. In the y-direction the true velocity of the ship is given by $v_{y,0} = -6.25$ m/s, $v_{y,1} = -6.29$ m/s, $v_{y,2} = -6.36$ m/s, and $v_{y,3} = -6.27$ m/s. For all time steps $\Delta_t = 60$ s, and the relationship between the positions of the ship and its velocity is given by Equations (4.2) and (4.3). The depth of the ocean around the cable is approximately $z = 30$ m. For the real data the normalization constant s is not the same for all time steps. For time steps $t = 0$ and $t = 3$ $s = 300$, for $t = 1$ $s = 75$, and for $t = 2$ $s = 175$.

4.5.1 Summary of results

The results of applying the SIR method and the EnKPF method to the real data are summarized by the monitored evaluation metrics in Table 4.11 and Table 4.12. As for the

simulation cases, the EnKPF method is applied with three different values of γ, namely $\gamma = 0.1$, $\gamma = 0.5$ and $\gamma = 0.9$, and in the tables $\gamma = 0$ indicates that the results are those given by the SIR method for the real data. The evaluation metrics that are presented in Table 4.11 and Table 4.12 are based on three runs of the methods.

Both the SIR method and the EnKPF method is applied with $N = 10000$ particles, and the remaining parameters are also the same for the SIR method and the EnKPF method. $\sigma_{\mathbf{T}}^2 = 0.0001$, $\sigma_{\mathbf{P}}^2 = 0.001$, and the expectation of the prior for the first estimated state is given by $\mathbf{x}_0 = \mathbf{x}_{\text{true},0}$. For $t = 0$, $\sigma_{\text{pos},0} = 60$ m and $\sigma_{\text{vel},0} = 15$ m/s. Furthermore, for $t = 1, \ldots, \tau$ $\sigma_{\text{pos},t} = 50$ m and $\sigma_{\text{vel},t} = 1$ m/s.

γ	RMSE(x)		RMSE(y)		RMSE(v_x)		RMSE(v_y)		min(ESS)	
	Mean	Std.	Mean	Std.	Mean	Std.	Mean	Std.	Min	Max
0	81.77	14.39	293.64	99.74	1.56	0.57	3.51	1.53	1.00	1.00
0.1	50.52	3.64	101.63	18.03	0.96	0.50	1.75	0.85	1.00	1.00
0.5	53.59	1.05	123.99	22.59	1.02	0.11	1.76	0.82	1.00	2.31
0.9	54.61	5.68	187.01	71.97	0.98	0.36	1.67	0.76	1.00	4.20

Table 4.11: RMSE and minimal ESS of SIR and EnKPF for the real data.

γ	CRPS(x)		CRPS(y)		CRPS(v_x)		CRPS(v_y)	
	Mean	Std.	Mean	Std.	Mean	Std.	Mean	Std.
0	6955.34	2507.38	96436.27	51754.65	51.19	2.38	69.08	9.52
0.1	3667.42	353.58	11107.27	3927.21	58.21	0.67	58.90	1.93
0.5	3492.85	128.62	16285.38	5439.30	59.09	1.47	61.90	4.99
0.9	3769.15	746.49	48316.99	27002.73	59.05	3.52	56.54	3.05

Table 4.12: Mean CRPS of SIR and EnKPF for the real data.

According to Table 4.11 and Table 4.12 the three EnKPF alternatives seem to give very similar results for the real data. The minimal ESS is small for all alternatives, and the values of RMSE and CRPS are very similar for all alternatives. In simulation case 1, which is very similar to the real case, the minimal ESS is at its largest for $\gamma = 0.1$, but this is not true for the real case. The results for the SIR method seem to be worse than the results for the EnKPF alternatives as the SIR method has the largest value of RMSE and CRPS for almost all elements of the state vector. For the real case the results of all four methods are quite variable, and certainly more variable than the results for the simulation cases.

Since the minimal ESS is at its largest for $\gamma = 0.9$, and the values of the other evaluation metrics are quite similar for the EnKPF alternatives, EnKPF with $\gamma = 0.9$ is chosen as the best alternative for state estimation for the real case. In the following subsection the results from using EnKPF with $\gamma = 0.9$ to track the ship based on real data are presented. The results are based on one of the three runs of the method, and which run the results are based on is chosen randomly among the three runs.

4.5.2 Best alternative: EnKPF with $\gamma = 0.9$

Figure 4.24 shows the filtering distributions of the positions of the ship for the real data according to EnKPF with $\gamma = 0.9$. At time step $t = 0$ the filtering distribution surrounds the true position of the ship, and the spread of the particles seems to be of reasonable size. At time step $t = 1$ the estimated filtering distribution of the position of the ship has two modes, which indicates that it is difficult for the EnKPF method with $\gamma = 0.9$ to estimate the correct y-coordinate of the ship when the ship is close to the cable. At time steps $t = 2$ and $t = 3$ the estimated filtering distributions of the positions of the ship are biased compared to the true positions of the ship, and the spread of the distributions is large.
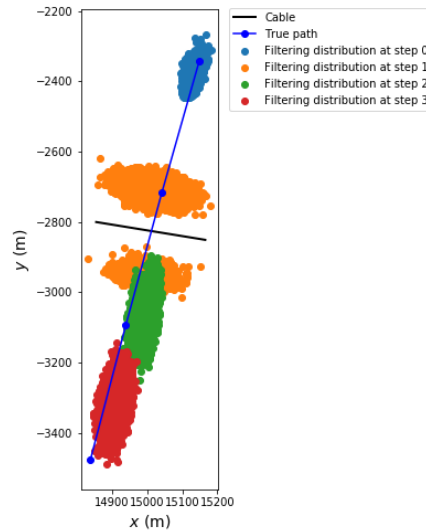
Figure 4.24: Estimated filtering distributions of the positions of the ship according to the EnKPF method with $\gamma = 0.9$.

According to Figure 4.25 the ESS for EnKPF with $\gamma = 0.9$ is quite small for all time steps of the real case. The ESS is at its smallest at time step $t = 1$, which is reasonable as Figure 4.24 shows that the estimated filtering distribution of the position of the ship at this time step is bimodal. Ideally, the ESS should be higher than the values that are given in Figure 4.25. With ESS as low as 1.98 it is not for sure that the results from EnKPF with $\gamma = 0.9$ are valid.

The expected path of the ship according to EnKPF with $\gamma = 0.9$ which is shown in Figure 4.26 does not fit very well to the true path of the ship. At time step $t = 1$ the estimated position fits well with the true position, but at the remaining time steps the estimated positions are biased compared to the true positions of the ship. At all time steps the area between the uncertainty bounds is small, and at time steps $t = 0, t = 2$ and $t = 3$ the true position of the ship lays on the outside of the uncertainty bound of the estimated
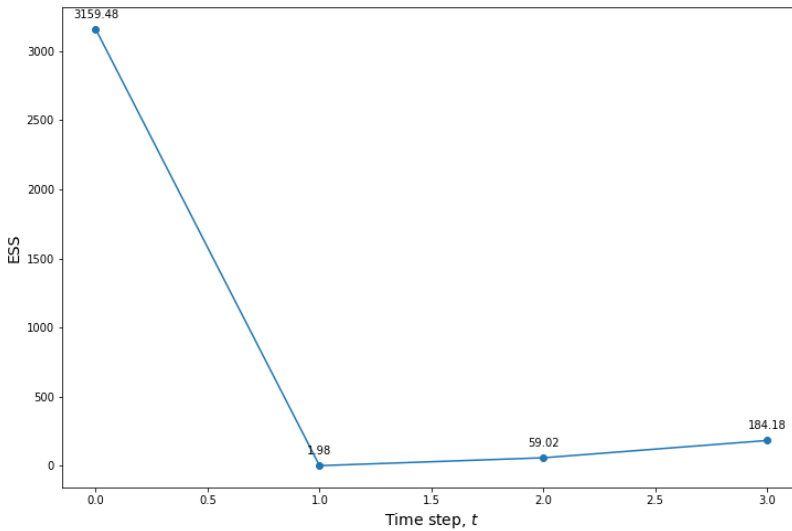
Figure 4.25: ESS at each time step using EnKPF with $\gamma = 0.9$.

position.

Figure 4.27 shows that at time step $t = 0$ the estimated velocity in both the x-direction and the y-direction fits well with the true velocity of the ship. At the remaining time steps the true velocity lays on the inside of the uncertainty bound of the estimated velocity in the y-direction. The true velocity in the x-direction lays on the outside of the uncertainty bound of the estimated velocity at time steps $t = 1$ and $t = 2$, but the difference between the true velocity and the estimated velocity is not very large at these time steps. At time step $t = 3$ the true velocity in the x-direction lays on the inside of the uncertainty bound of the estimated velocity. Overall the estimated velocity fits the true velocity of the ship quite well.

The results from applying real data and EnKPF with $\gamma = 0.9$ to track the ship are not very good, but not very bad either. The ESS is low, and the estimated path does not fit very well to the true path. However, the estimated velocity fits the true velocity quite well, and at the time steps when the estimated filtering distributions are biased compared to the true positions of the ship, the true positions of the ship are located on the edges of the estimated filtering distributions.
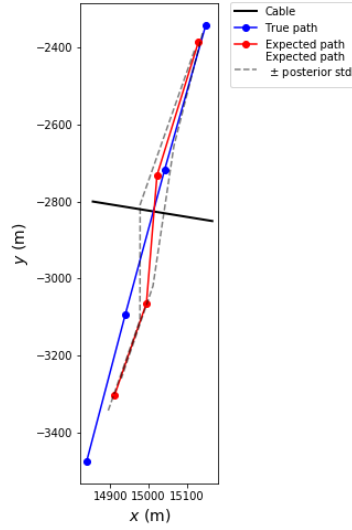
Figure 4.26: The expected path of the ship according to EnKPF with $\gamma = 0.9$.
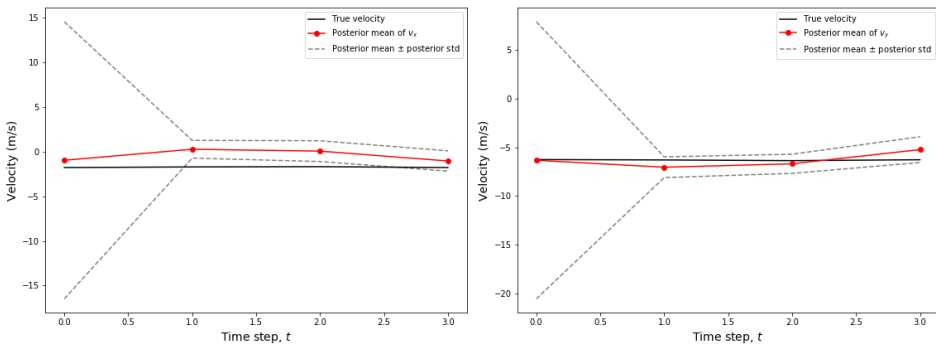

Figure 4.27: The estimated velocity of the ship according to EnKPF with $\gamma = 0.9$. The estimate of v_x is shown on the left, while the estimate of v_y is shown on the right.

Discussion

The results from applying SIR and EnKPF to the simulated and the real data are discussed in this chapter. The discussion is divided into two parts. The results for the simulated data are discussed in the first part, while the results for the real data are discussed in the second part.

5.1 Discussion of results for simulated data

The results from using the SIR method and the EnKPF method to track a ship using simulated fiber optic cable data that are presented in chapter 4 are based on optimal choices of values of the relevant parameters. The reasoning behind these choices are presented here. Also some results using alternative values of the parameters are presented and discussed. This section will provide a discussion concerning the suitability of using SIR and EnKPF to track a ship based on simulated fiber optic cable data.

5.1.1 Choice of parameters

For both the SIR method and the EnKPF method the number of particles used in the implementation is $N = 10000$ particles for all simulation cases. This value is chosen such that the methods are reliable and can be run in reasonable time. For SIR the number of particles could have been higher since degeneracy is a problem for several simulation cases. EnKPF, on the other hand, experience few problems with degeneracy and consequently it is expected that fewer particles than $N = 10000$ particles can be used in the implementation of the EnKPF method. However, $N = 10000$ is used such that the results from SIR and EnKPF are comparable.

For the simulated data the values of $\sigma_{\mathbf{T}}^2$, $\sigma_{\mathbf{P}}^2$ and s are chosen such that they are equal to the values used for simulation. The values of $\sigma_{\mathbf{T}}^2$ and $\sigma_{\mathbf{P}}^2$ that are chosen for simulation are chosen such that the noise of the simulated data seems to be of reasonable magnitude compared the signal of the simulated data. The value of s affects the magnitude of the

energy curve and for the simulation procedure s can be set to any value larger than zero, but $s = 500$ is chosen such that the value of $\sigma_\mathbf{P}^2$ does not have to be very small.

The prior for the first time step is given by Equation (3.11) with covariance matrix V_0 given by (3.5). For both methods and all simulation cases the elements of V_0 are given by $\sigma_{\text{pos},0} = 60$ m and $\sigma_{\text{vel},0} = 15$ m/s. These values reflect the uncertainty associated with the state of the ship prior to the collection of data. The values of $\sigma_{\text{pos},0}$ and $\sigma_{\text{vel},0}$ should be realistic, but which values that are a suitable or not depend on the situation. If one knows that a ship is operating in an area and one wants to know the exact path of the ship then $\sigma_{\text{pos},0}$ can be small. However, if one is very uncertain about where the ship is operating then $\sigma_{\text{pos},0}$ should be large. The level of uncertainty related to the velocity of the ship is dependent on the surroundings of the ship. For instance, if one knows that a ship is operating close to the shore, then one knows that the velocity might be smaller than if the ship was operating far off shore. Hence, $\sigma_{\text{vel},0}$ can be small if one knows that the ship is close to the shore, or operating in an area where there are limitations associated with the velocity of the ship.

If one has very little knowledge about the state of the ship prior to the collection of data, then it is not realistic that the expectation of the initial distribution of the particles is equal to the true state of the ship at time step $t = 0$. However, since $\sigma_{\text{pos},0}$ and $\sigma_{\text{vel},0}$ are not very small in this implementation, then choosing the expectation to be equal to the true state does not seem unreasonable.

For the remaining time steps the values of $\sigma_{\text{pos},t}$ and $\sigma_{\text{vel},t}$ are chosen such that they realistically represent the uncertainty one has about the movement of the ship. $\sigma_{\text{pos},t} = 50$ m is chosen for both methods for all simulation cases. It is preferred that the methods can handle large uncertainties, and the results in chapter 4 are quite good even though the value of $\sigma_{\text{pos},t}$ is large. $\sigma_{\text{vel},t} = 1$ m/s for simulation case 1 and 2 which indicates that for these simulation cases there is not much uncertainty associated with the velocity of the ship. For simulation case 3 and 4 $\sigma_{\text{vel},t} = 4$ m/s. This makes the method more suitable for detecting changes in the velocity of the ship.

5.1.2 Robustness to the choice of N

It is interesting to investigate how well the methods are able to estimate the states of the ship if fewer particles than $N = 10000$ particles are used in the implementation. If it is possible to use fewer particles then the run-time of the methods can be reduced. In order to explore the affect that the value of N has on the methods, simulation case 1 will be solved with different values of N. Since the EnKPF method with $\gamma = 0.1$ gave the best results for simulation case 1, results from this method along with results from the SIR method will be presented below.

The calculated evaluation metrics for the SIR method for simulation case 1 for different values of N are presented in Tables 5.1 and 5.2. For the results in these tables all other parameters than N are the same as those used in simulation case 1 in chapter 4. The values in the tables are only based on one run of the method.

Tables 5.1 and 5.2 show that for $N = 100$ and $N = 1000$ the SIR method is not able to produce a satisfying result for simulation case 1. In addition the method has collapsed due to degeneracy for these values of N. For $N = 5000$ and $N = 10000$ the minimal ESS is close to one. However, the values of $\text{RMSE}(x)$, $\text{RMSE}(y)$, $\text{CRPS}(x)$ and $\text{CRPS}(y)$

N	RMSE(x)	RMSE(y)	RMSE(v_x)	RMSE(v_y)	min(ESS)	min(ESS)/N
100	899.25	51.76	18.56	0.74	NaN	NaN
1000	213.47	41.27	4.94	2.23	NaN	NaN
5000	3.68	1.16	2.46	6.16	1.02	0.0002
10000	1.77	2.96	3.83	3.16	1.18	0.0001
20000	2.40	1.95	0.55	1.31	1.87	0.00009

Table 5.1: RMSE and minimal ESS of SIR for simulation case 1 for different values of N.

N	CRPS(x)	CRPS(y)	CRPS(v_x)	CRPS(v_y)
100	808642.49	2679.58	344.57	0.55
1000	45573.14	1707.00	30.16	17.37
5000	16.80	43.41	22.42	98.46
10000	7.14	69.19	34.38	42.95
20000	10.38	33.96	26.18	28.23

Table 5.2: Mean CRPS of SIR for simulation case 1 for different values of N.

indicates that the method seems to estimate the positions of the ship quite well for $N = 5000$ and $N = 10000$. The values of RMSE(v_x) and RMSE(v_y) indicate that SIR does not estimate the velocity of the ship very well for simulation case 1 for $N = 5000$ and $N = 10000$. From Table 5.1 it can be seen that the ratio min(ESS)/N is very low for both $N = 5000$ and $N = 10000$. For simulation case 1 it seems like the SIR method could have been run with $N = 5000$ and still give similar results to what was produced in simulation case 1 in chapter 4.

From Tables 5.1 and 5.2 it can be observed that if SIR is applied to simulation case 1 with $N > 10000$, namely $N = 20000$, then the bias and the uncertainty of the estimates are low, but the minimal ESS is close to one and degeneracy is a problem. Consequently, it seems like an extremely large N must be used if SIR is going to be able to track a ship without struggling with degeneracy.

The RMSE, minimal ESS and mean CRPS for four different values of N for EnKPF with $\gamma = 0.1$ for simulation case 1 are presented in Tables 5.3 and 5.4. For the implementation, all other parameters than N are the same as those used in simulation case 1 in chapter 4. The values in the tables are only based on one run of the method.

N	RMSE(x)	RMSE(y)	RMSE(v_x)	RMSE(v_y)	min(ESS)	min(ESS)/N
100	2.23	177.68	0.80	4.24	1.38	0.0138
1000	1.97	6.39	1.06	0.73	16.50	0.0165
5000	2.08	2.49	0.49	0.34	60.78	0.0122
10000	1.98	3.42	0.41	0.74	107.80	0.0108

Table 5.3: RMSE and minimal ESS of EnKPF with $\gamma = 0.1$ for simulation case 1 for different values of N.

Tables 5.3 and 5.4 show that with $N = 100$ the EnKPF method with $\gamma = 0.1$ does not produce a satisfying result. The values of RMSE(y) and CRPS(y) are high, and the minimal ESS is close to one. For the remaining values of N however, EnKPF with $\gamma = 0.1$ seems to be able to track the ship quite successfully. The ESS is high, and the RMSE and

N	CRPS(x)	CRPS(y)	CRPS(v_x)	CRPS(v_y)
100	78.04	31676.96	11.92	46.99
1000	114.53	351.65	40.89	41.80
5000	106.43	204.92	36.33	33.47
10000	108.31	234.17	33.93	35.34

Table 5.4: Mean CRPS of EnKPF with $\gamma = 0.1$ for simulation case 1 for different values of N.

CRPS is of similar size for all other values of N than $N = 100$. This indicates that for simulation case 1, the EnKPF method with $\gamma = 0.1$ can be used to track the ship with far fewer particles than $N = 10000$ which is used in simulation case 1 in chapter 4.

Table 5.3 shows that the ratio min(ESS)/N is approximately constant for EnKPF with $\gamma = 0.1$ for simulation case 1. It can also be observed that the variation of the RMSE and the CRPS is not very large for the different values of $N > 100$. Consequently, for simulation case 1 the number of particles N can be chosen such that the value of the minimal ESS is reasonable. The quality of the estimates of the states of the ship is then expected to be satisfying.

For infinitely many particles, that is $N \to \infty$, both the SIR method and the EnKPF method is expected to give results of high quality. As mentioned in chapter 3, the SIR method is exact in this case, while the EnKPF method is exact if $\gamma \to 0$. Hence, it is expected that as N increases, the RMSE and the CRPS of the methods stabilize around small values. It is not clear what these values are, but from Tables 5.1-5.4 it may seem like these values are reached for some of the elements of the state vector. For instance, the value of CRPS(y) for the EnKPF method seems to have stabilized around approximately 110. When N increases, the density of the estimated distributions increases, but the variance will not increase. This is the reason why the RMSE and CRPS stabilize when N increases.

Based on the results presented in Tables 5.1-5.4 it is safe to say that for simulation case 1 the EnKPF method is less sensitive to the choice of N than the SIR method is. It is assumed that this is true also for the other simulation cases. For simulation case 2-4 the minimal ESS of EnKPF with $\gamma = 0.1$ is smaller than the minimal ESS for simulation case 1. Consequently, it is expected that for simulation cases 2-4 the EnKPF alternatives can perform well with fewer particles than $N = 10000$, but that N may needs to be higher for these cases than for simulation case 1. For SIR it is assumed that for simulation case 2 it may be possible to use between $N = 5000$ and $N = 10000$ particles, which based on Table 5.3 is true for simulation case 1. For simulation case 3 and 4 in chapter 4 the results for SIR are bad, and it is not expected that the method would be able to give satisfying results if $N < 10000$.

5.1.3 Robustness to the expectation of the prior at time step $t = 0$

For all of the simulation cases, the prior at time step $t = 0$ is given by the distribution $\mathcal{N}_4(\mathbf{x}_{\text{true},0}, V_0)$. It is interesting to investigate how the results from the methods are affected by using an initial distribution that is biased compared to the true position of the ship at time step $t = 0$. This will be done for SIR and EnKPF with $\gamma = 0.1$ for simulation case 1. Two initial distributions will be considered, one with a smaller amount bias than the other.

Tables 5.5 and 5.6 show the evaluation metrics for SIR and EnKPF with $\gamma = 0.1$

for simulation case 1 where the expectation of the initial distribution is given by $\mathbf{x}_{\text{true},0} + [200, 100, 0, 0]^T$. Except from this, the parameters are the same as those specified for simulation case 1 in chapter 4. The values in the tables are based on three runs of the methods.

γ	RMSE(x)		RMSE(y)		RMSE(v_x)		RMSE(v_y)		min(ESS)	
	Mean	Std.	Mean	Std.	Mean	Std.	Mean	Std.	Min	Max
0	821.79	155.37	615.28	77.42	16.87	1.65	11.38	1.04	NaN	NaN
0.1	3.16	0.06	4.68	0.77	2.35	0.07	2.36	0.32	2.18	2.18

Table 5.5: RMSE and minimal ESS of SIR and EnKPF for simulation case 1 with an initial distribution with a small amount of bias..

γ	CRPS(x)		CRPS(y)		CRPS(v_x)		CRPS(v_y)	
	Mean	Std.	Mean	Std.	Mean	Std.	Mean	Std.
0	699480.86	254566.13	384565.99	98744.15	287.39	56.53	130.63	24.36
0.1	98.24	0.30	185.67	35.00	11.76	0.58	32.67	3.75

Table 5.6: Mean CRPS of SIR and EnKPF for simulation case 1 with an initial distribution with a small amount of bias.

Tables 5.7 and 5.8 show the evaluation metrics for SIR and EnKPF with $\gamma = 0.1$ for simulation case 1 where the expectation of the prior is given by $\mathbf{x}_{\text{true},0} + [400, 100, 0, 0]^T$. Except from this, the parameters are the same as those specified for simulation case 1 in chapter 4. The values in the tables are based on three runs of the methods.

γ	RMSE(x)		RMSE(y)		RMSE(v_x)		RMSE(v_y)		min(ESS)	
	Mean	Std.	Mean	Std.	Mean	Std.	Mean	Std.	Min	Max
0	706.84	139.32	115.08	25.64	22.00	2.55	4.45	0.95	NaN	NaN
0.1	42.00	24.32	151.08	51.13	25.63	1.88	4.25	0.95	NaN	NaN

Table 5.7: RMSE and minimal ESS of SIR and EnKPF for simulation case 1 with an initial distribution with a large amount of bias.

γ	CRPS(x)		CRPS(y)		CRPS(v_x)		CRPS(v_y)	
	Mean	Std.	Mean	Std.	Mean	Std.	Mean	Std.
0	519035.13	199731.77	13902.31	6233.23	490.4	116.08	20.78	9.06
0.1	2456.87	2323.81	25546.07	14465.22	660.51	97.73	19.06	8.50

Table 5.8: Mean CRPS of SIR and EnKPF for simulation case 1 with an initial distribution with a large amount of bias.

Tables 5.5-5.8 show that the SIR method collapses due to degeneracy both when the amount of bias is small and large. For the SIR method the RMSE and CRPS associated with the estimated position of the ship is very large for both variants of the initial distribution, and the results are not satisfying. The EnKPF method, on the other hand, gives satisfying results when the amount of bias is small, however the ESS is quite small. When the amount of bias is large, the EnKPF method is not able to give reasonable estimates of

the states of the ship and degeneracy is clearly a problem. From the tables it can also be observed that both of the methods seem to give more varying results when the bias of the initial distribution is large, compared to when it is small or non-existent.

The results of using the EnKPF method with $\gamma = 0.1$ for simulation case 1 when the expectation of the initial distribution is given by $\mathbf{x}_{\text{true},0} + [200, 100, 0, 0]^T$ are now presented more thoroughly. These results are based on one of the three runs of the method for which the values in Table 5.5 and Table 5.6 are calculated, and the run that the results are from is chosen randomly among the three runs. The estimated filtering distributions of the positions of the ship are shown in Figure 5.1. This figure is very similar to Figure 4.2, except that in Figure 5.1 the spread of the particles seems reasonable at time step $t = 1$.
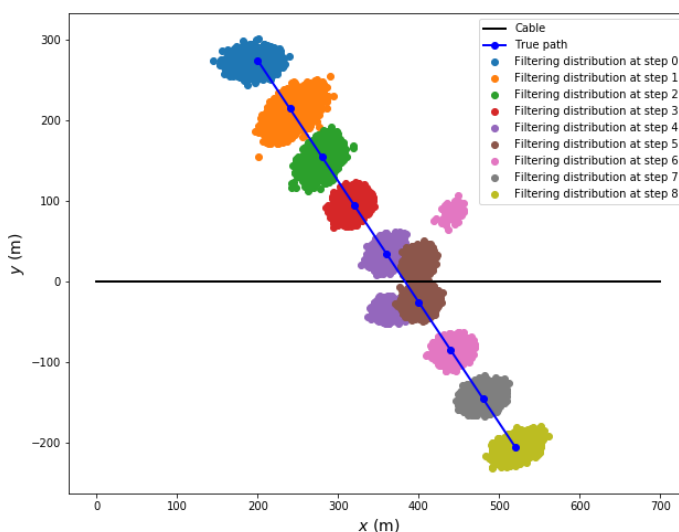

Figure 5.1: Estimated filtering distribution of the positions of the ship for simulation case 1 with a biased initial distribution according to the EnKPF method with $\gamma = 0.1$.

Figure 5.2 shows the ESS at each time step for EnKPF with $\gamma = 0.1$ for simulation case 1 with an initial distribution with a small amount of bias. The curve of the ESS in this figure is very similar to the curve of the ESS in Figure 4.3, but at time step $t = 0$, the ESS is very low when the initial distribution is biased. Also at time step $t = 1$ the ESS is smaller when the initial distribution is biased compared to when it is not. The minimal ESS of the EnKPF method with $\gamma = 0.1$ for simulation case 1 in chapter 4 is reached at time step $t = 5$. From Figure 5.2 it can be observed that the second smallest value of the ESS is reached at time step $t = 5$. This indicates that the biased initial distribution affects the ESS at time steps $t = 0$ and $t = 1$, but that for the remaining time steps the ESS is not affected by the bias of the initial distribution.

Based on a biased initial distribution and the EnKPF method with $\gamma = 0.1$ the expected
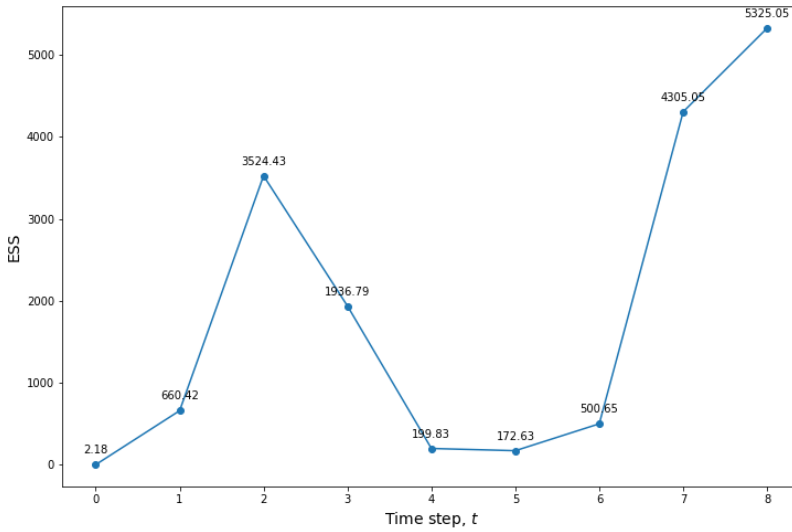
Figure 5.2: ESS at each time step for simulation case 1 with a biased initial distribution using EnKPF with $\gamma = 0.1$.

path for simulation case 1 is given in Figure 5.3. The true positions of the ship lay close to the expected positions of the ship for all time steps, and the true positions lay on the inside of the uncertainty bound of the estimated positions for all time steps. Consequently, it seems like the EnKPF method is able to estimate the positions of the ship for simulation case 1 very well even though the initial distribution is biased.

The estimated velocity based on the EnKPF method with $\gamma = 0.1$ for simulation case 1 with a biased initial distribution is presented in Figure 5.4. The true velocity in the y-direction lays on the inside of the uncertainty bound of the estimated uncertainty for all time steps, but at time step $t = 0$ the estimated velocity is much larger than the true velocity. At all of the remaining time steps the estimated velocity is close to the true velocity. The estimated velocity in the x-direction seems to converge towards the true velocity of the ship. Hence, the consequence of having a biased initial distribution is that quite a few steps of the EnKPF method needs to be performed before the estimated velocity fits the true velocity of the ship.

Based on Figures 5.1-5.4 the EnKPF with $\gamma = 0.1$ seem to provide good estimates of the states of the ship in simulation case 1 even though the initial distribution of the state of the ship is biased. This indicates that the EnKPF method is appropriate for state estimation also if the knowledge about the state of the ship is limited prior to the collection of data.
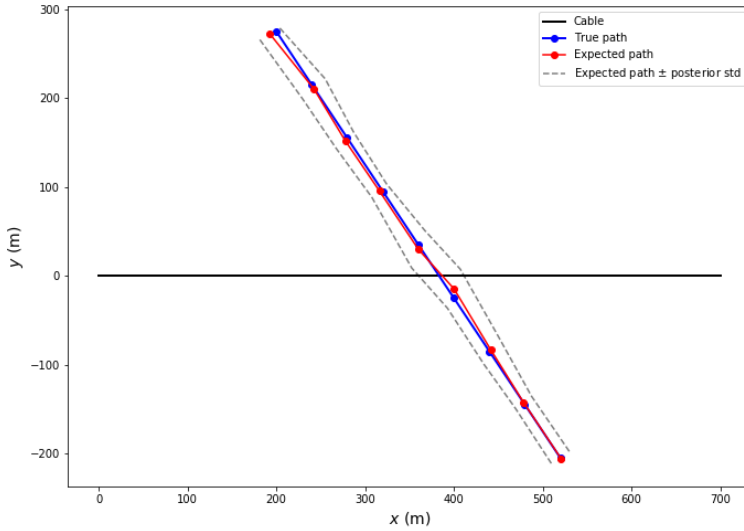
Figure 5.3: The expected path of the ship for simulation case 1 with a biased initial distribution according to EnKPF with $\gamma = 0.1$.
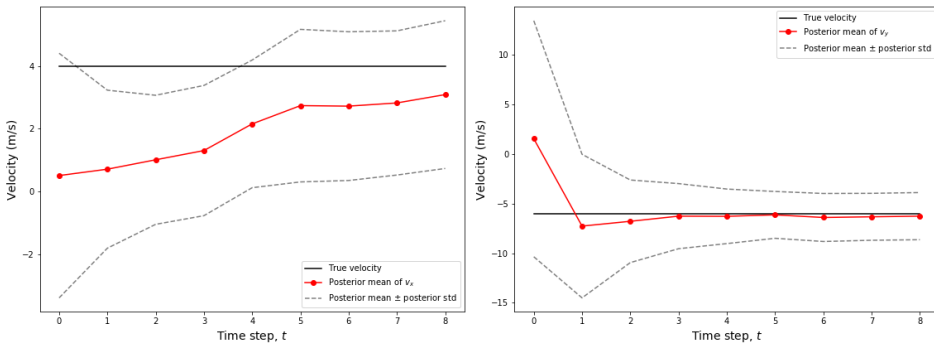

Figure 5.4: The estimated velocity of the ship for simulation case 1 with a biased initial distribution according to EnKPF with $\gamma = 0.1$. The estimate of v_x is shown on the left, while the estimate of v_y is shown on the right.

5.1.4 Robustness to the variance of the prior at time step $t = 0$

It may also be interesting to investigate how the SIR method and the EnKPF method perform for simulation case 1 when the standard deviation of the initial distribution is large. In this case the parameter $\sigma_{\text{pos},0}$ is increased from $\sigma_{\text{pos},0} = 60$ m, which is used in chapter 4, to $\sigma_{\text{pos},0} = 200$ m. The evaluation metrics for the SIR method and the EnKPF method with $\gamma = 0.1$ for simulation case 1 for an initial distribution with $\sigma_{\text{pos},0} = 200$ m is given in Table 5.9 and Table 5.10. The values in these tables are based on three runs of the methods, and all parameters except $\sigma_{\text{pos},0}$ are the same as those specified for simulation case 1 in chapter 4.

γ	RMSE(x)		RMSE(y)		RMSE(v_x)		RMSE(v_y)		min(ESS)	
	Mean	Std.	Mean	Std.	Mean	Std.	Mean	Std.	Min	Max
0	2.71	0.10	16.39	9.96	5.03	0.95	2.07	0.41	1.00	1.01
0.1	2.75	0.03	4.49	0.58	0.27	0.07	0.66	0.12	63.39	118.76

Table 5.9: RMSE and minimal ESS of SIR and EnKPF for simulation case 1 where the standard deviation of the initial distribution is large.

γ	CRPS(x)		CRPS(y)		CRPS(v_x)		CRPS(v_y)	
	Mean	Std.	Mean	Std.	Mean	Std.	Mean	Std.
0	11.66	0.38	381.76	244.62	33.55	9.02	30.13	6.29
0.1	163.73	1.36	621.29	51.54	33.04	0.78	39.74	1.04

Table 5.10: Mean CRPS of SIR and EnKPF for simulation case 1 where the standard deviation of the initial distribution is large.

Table 5.9 and Table 5.10 show that for simulation case 1 both the SIR method and the EnKPF method are able to estimate the states of the ship in a satisfying manner when the standard deviation of the initial distribution is large. Clearly, for the SIR method degeneracy is a problem. For the EnKPF method the minimal ESS is large, and it does not seem to be affected by the large uncertainty of the initial distribution. As in simulation case 1 in chapter 4 the SIR method seem to give more variable results than the EnKPF method. The results of ship tracking for simulation case 1 by EnKPF with $\gamma = 0.1$ for an initial distribution with large standard deviation are presented below. The results are based on one of the three runs of the method, and the run that the results are from is chosen randomly among the three runs.

Figure 5.5 shows the filtering distributions of the positions of the ship for simulation case 1 according to the EnKPF method with $\gamma = 0.1$ for an initial distribution with large standard deviation. The spread of the particles at time steps $t = 0, t = 1$ and $t = 2$ is large, but for the remaining time steps the distributions in Figure 5.5 are very similar to the distributions in Figure 4.2. This indicates that the large standard deviation of the initial distribution only affects the state estimation of the first states. The large spread of the particles at time steps $t = 0, t = 1$ and $t = 2$ makes sense when the values of CRPS(x) and CRPS(y) for $\gamma = 0.1$ in Table 5.10 are compared to the same evaluation metrics in Table 4.2 which concludes that the value of these evaluation metrics are larger when the standard deviation of the initial distribution is $\sigma_{\text{pos},0} = 200$ m than when it is $\sigma_{\text{pos},0} = 60$ m.
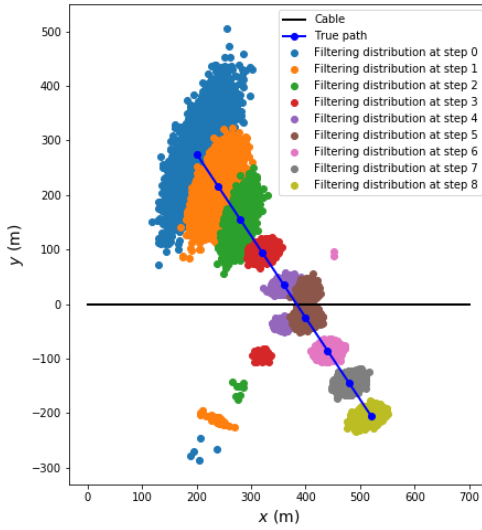
Figure 5.5: Estimated filtering distribution of the positions of the ship for simulation case 1 with an initial distribution with large standard deviation according to the EnKPF method with $\gamma = 0.1$.

The ESS of the EnKPF method with $\gamma = 0.1$ for simulation case 1 for an initial distribution with large standard deviation is given in Figure 5.6. For time steps $t = 0$, $t = 1$ and $t = 2$ the ESS is smaller in Figure 5.6 than in Figure 4.3, but for the remaining time steps the curve in Figure 5.6 is not very different from the curve in Figure 4.3. Consequently, also Figure 5.6 indicates that the large standard deviation of the initial distribution affects only the state estimation of the first steps of the EnKPF method.

Figure 5.7 shows the estimated path of the ship for simulation case 1 for an initial distribution with large standard deviation based on the EnKPF method with $\gamma = 0.1$. The estimated path fits the true path of the ship very well. It is clear that from time step $t = 0$ and forwards the uncertainty of the estimated positions decreases, while the uncertainty seems to stabilize at time step $t = 2$. This fits well with what was observed in Figure 5.5.

The estimated velocity of the ship according to EnKPF with $\gamma = 0.1$ for simulation case 1 with initial distribution with large standard deviation is displayed in Figure 5.8. The estimated velocity in both the x-direction and the y-direction fits well to the true velocity of the ship. This figure is very similar to Figure 4.5, which indicates that the estimation of the velocity of the ship is not affected by the large value of $\sigma_{\text{pos},0}$. This makes sense since $\sigma_{\text{vel},0}$ has the same value for both Figure 5.8 and Figure 4.5.

To conclude, both the SIR method and the EnKPF method is able to estimate the states of the ship quite well when the standard deviation of the initial distribution is large, but as when the standard deviation is small, the SIR method struggles with degeneracy. The affect of using a large value of $\sigma_{\text{pos},0}$ is that the uncertainty of the estimates of the positions
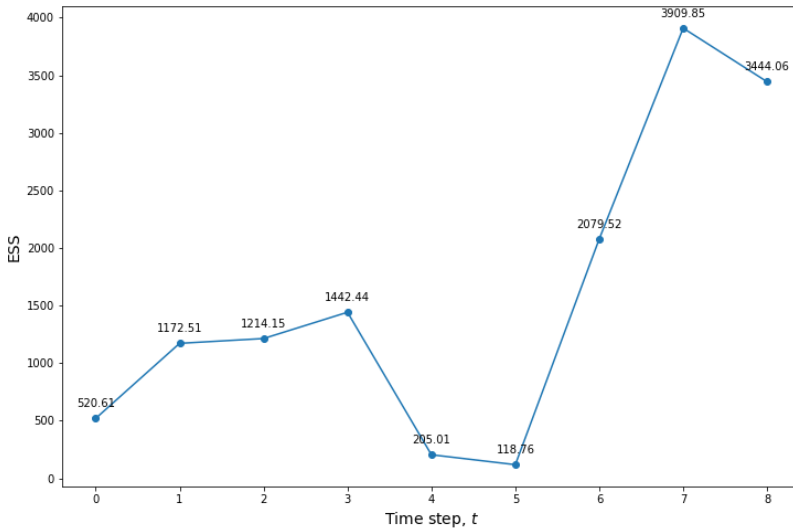
Figure 5.6: ESS at each time step for simulation case 1 with an initial distribution with large standard deviation using EnKPF with $\gamma = 0.1$.

of the ship is large for the three first time steps, and that the ESS is smaller for these time steps compared to when a smaller value of $\sigma_{\text{pos},0}$ is used. The estimated velocity is not affected by the large value of $\sigma_{\text{pos},0}$ and for time steps $t > 2$ the estimates of the positions of the ship are not significantly affected by the large value of $\sigma_{\text{pos},0}$.

Overall, the EnKPF method seems to be more appropriate for state estimation than the SIR method when the knowledge about the initial state of the ship is limited. The EnKPF method gives satisfying results both when the initial distribution is biased, and when the standard deviation of the initial distribution is large. The SIR method is able to track the ship when the standard deviation of the initial distribution is large, but when the initial distribution is biased the state estimates are not satisfying. When the bias of the initial distribution is large, none of the methods are able to track the ship properly.

Figure 5.7: The expected path of the ship for simulation case 1 with an initial distribution with large standard deviation according to EnKPF with $\gamma = 0.1$.
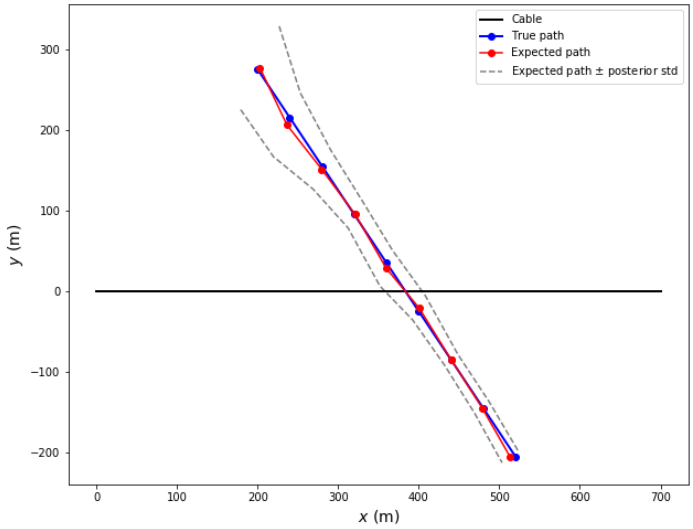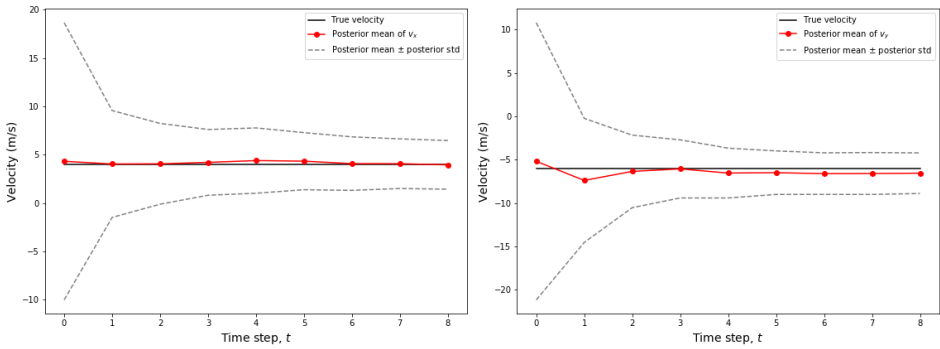

Figure 5.8: The estimated velocity of the ship for simulation case 1 with an initial distribution with large standard deviation according to EnKPF with $\gamma = 0.1$. The estimate of v_x is shown on the left, while the estimate of v_y is shown on the right.

5.1.5   Robustness to the choice of $\sigma_{\mathrm{vel},t}$ for $t > 0$

For simulation case 3 and 4 $\sigma_{\mathrm{vel},t} = 4$ m/s for $t > 0$. This choice was made such that it should be easy for the methods to detect the change in velocity during the tracking process. However, it is interesting to investigate how well the methods are able to track the ship if the value of $\sigma_{\mathrm{vel},t}$ is small. In this subsection, the EnKPF method with $\gamma = 0.9$ will be applied to simulation case 3, where all other parameters than $\sigma_{\mathrm{vel},t}$ are the same as in chapter 4. For the results that are presented here, $\sigma_{\mathrm{vel},t} = 1$ m/s for $t > 0$. The EnKPF method with $\gamma = 0.9$ is chosen for this analysis since this was the EnKPF alternative with the best performance in chapter 4. The SIR method is not a part of this analysis as the method collapsed for simulation case 3 in chapter 4.

Table 5.11 and Table 5.12 show the calculated evaluation metrics for EnKPF with $\gamma = 0.9$ for simulation case 3 where $\sigma_{\mathrm{vel},t} = 1$ m/s for $t > 0$. The evaluation metrics are calculated based on three runs of the method, and the results that are presented below are the results from one of these runs.

γ	RMSE(x)		RMSE(y)		RMSE(v_x)		RMSE(v_y)		min(ESS)	
	Mean	Std.	Mean	Std.	Mean	Std.	Mean	Std.	Min	Max
0.9	4.80	0.01	2.95	0.18	4.04	0.03	0.29	0.05	34.83	58.32

Table 5.11: RMSE and minimal ESS of EnKPF for simulation case 3 where the uncertainty associated with the velocity is small.

γ	CRPS(x)		CRPS(y)		CRPS(v_x)		CRPS(v_y)	
	Mean	Std.	Mean	Std.	Mean	Std.	Mean	Std.
0.9	54.32	0.44	63.46	2.60	43.17	0.30	26.53	1.37

Table 5.12: Mean CRPS of EnKPF for simulation case 3 where the uncertainty associated with the velocity is small.

By comparing Tables 5.11 and 5.12 to the last row of Tables 4.5 and 4.6 it seems like the EnKPF method with $\gamma = 0.9$ tracks the ship in simulation case 3 very well even if $\sigma_{\mathrm{vel},t}$ is small. Actually, most of the values of RMSE and CRPS are smaller in Tables 5.11 and 5.12 than in Tables 4.5 and 4.6. Also, the ESS in Table 5.11 is quite similar to the ESS in Table 4.5. The indication from the tables that the ship is tracked properly is confirmed by Figure 5.9, which shows the estimated filtering distributions of the positions of the ship in the case where the uncertainty associated with the velocity is small. The distributions are centered around the true positions of the ship, and the spread of the particles is of reasonable size. In fact, the spread of the particles seems to be smaller in Figure 5.9 than in Figure 4.12, which fits well with the values in Tables 5.11 and 5.12.

The ESS of EnKPF with $\gamma = 0.9$ for simulation case 3 with $\sigma_{\mathrm{vel},t} = 1$ m/s for $t > 0$ is shown in Figure 5.10. This figure is very similar to Figure 4.13, which shows the ESS of the EnKPF method with $\gamma = 0.9$ for simulation case 3 with $\sigma_{\mathrm{vel},t} = 4$ m/s for $t > 0$. Consequently, it seems like the decrease in uncertainty associated with the velocity does not affect the ESS of the EnKPF method.

The estimated path of the ship given by EnKPF with $\gamma = 0.9$ for simulation case 3 where $\sigma_{\mathrm{vel},t} = 1$ m/s for $t > 0$ is shown in Figure 5.11. The estimated path fits very well
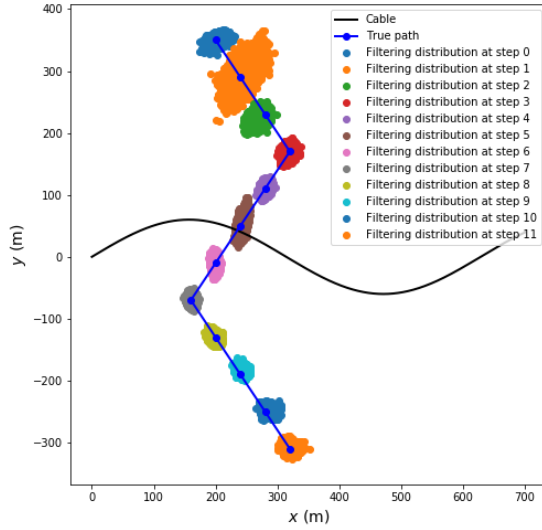
Figure 5.9: Estimated filtering distribution of the positions of the ship for simulation case 3 given by EnKPF with $\gamma = 0.9$ where the uncertainty associated with the velocity is small.

to the true path of the ship, which is not surprising based on the values of RMSE of x and y in Table 5.11. As was the case in Figure 4.14, the estimated position of the ship at time step $t = 2$ is a bit biased compared to the true position of the ship. The estimated path of the ship does not seem to be negatively affected by the decrease in uncertainty associated with the velocity of the ship.

Figure 5.12 shows the estimated velocity of the ship in simulation case 3 according to EnKPF with $\gamma = 0.9$ when $\sigma_{\text{vel},t} = 1$ m/s for $t > 0$. It is clear that when the uncertainty of the velocity has decreased, then also the quality of the estimated velocity has decreased. Compared to Figure 4.15, there are more time steps in Figure 5.12 at which the true velocity in the x-direction lays on the outside of the uncertainty bound of the estimated velocity. Consequently, the EnKPF method is not able to estimate the velocity of the ship in simulation case 3 in a satisfying manner when $\sigma_{\text{vel},t} = 1$ m/s for $t > 0$.

Based on Tables 5.11 and 5.12 and Figures 5.9-5.12 a few conclusions can be drawn on the topic of how robust the EnKPF method is to the value of $\sigma_{\text{vel},t}$ for $t > 0$. First of all, the method does not seem to have problems with small values of ESS when $\sigma_{\text{vel},t}$ is small, and the method estimates the path of the ship in an excellent manner. However, the EnKPF method is not able to detect the changes in the velocity of the ship when $\sigma_{\text{vel},t}$ is small. Consequently, if the EnKPF method is to be used in a situation where it is expected that the velocity of the ship is not constant, then a large value of $\sigma_{\text{vel},t}$ should be used for $t > 0$.
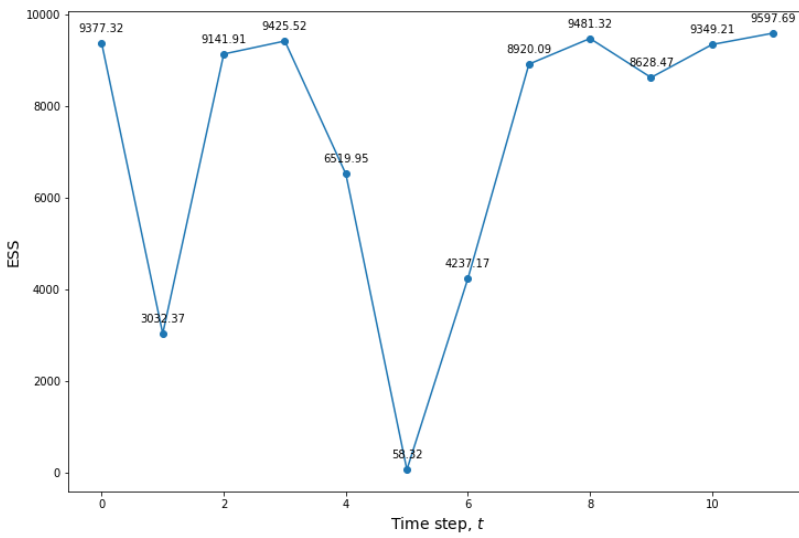
Figure 5.10: ESS of EnKPF with $\gamma = 0.9$ at each time step for simulation case 3 where the uncertainty associated with the velocity is small.

Figure 5.11: The expected path of the ship for simulation case 3 where the uncertainty associated with the velocity is small according to EnKPF with $\gamma = 0.9$.
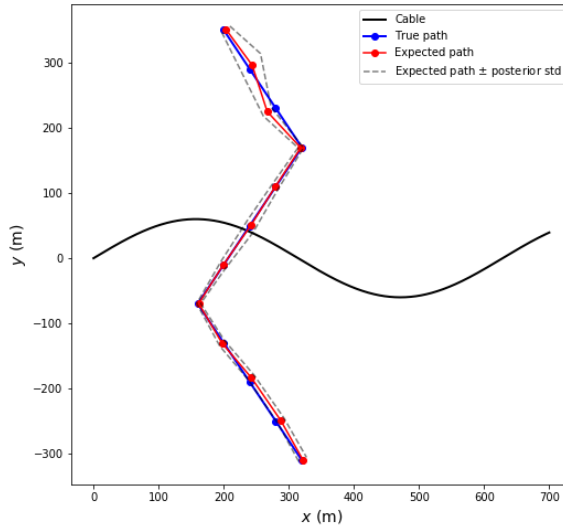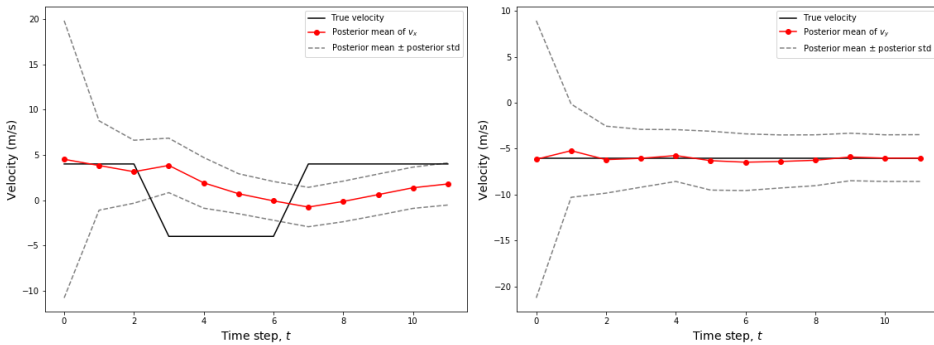

Figure 5.12: The estimated velocity of the ship for simulation case 3 where the uncertainty associated with the velocity is small according to EnKPF with $\gamma = 0.9$. The estimate of v_x is shown on the left, while the estimate of v_y is shown on the right.

5.1.6 Quality of results

Overall, the results from simulation cases 1-4 in chapter 4 are quite good. The results from the best alternative gives satisfying state estimates for all simulation cases. This indicates that in an idealized situation the EnKPF method is a good choice for ship tracking based on fiber optic cable data. If data is available from two cables, then the EnKPF is able to give highly accurate results. The EnKPF method has also proved to be able to give satisfying results with fewer particles than $N = 10000$, and the method can be applied to the tracking problem even if the knowledge about the ship prior to the collection of data is limited. In cases where it is not expected that a ship will move with constant velocity, it is necessary that the uncertainty associated with the velocity in the model is large. The SIR method experienced problems with degeneracy for all simulation cases, and consequently this method does not seem to be a good choice for ship tracking based on fiber optic cable data.

A positive aspect of the use of the SIR method and the EnKPF method is that the results that are achieved for the simulated data in this project are based on quite simple programming. The programming has been done in `Python`, and only the basic packages `NumPy`, `pandas`, `Matplotlib` and `pickle` are needed to simulate data and compute, save and visualize the results. This means that for the simulation cases anyone with basic programming skills, who are given Algorithm 2 and Algorithm 4, should be able to recreate the results that are presented for the simulated data in this project.

5.2 Discussion of results for real data

The reasons for the choices of values of parameters for the statistical methods applied to the real data are presented in this section. Also, some results associated with alternative values of parameters are presented and discussed, and the suitability of SIR and EnKPF for ship tracking based on real fiber optic cable data is discussed.

5.2.1 Choice of parameters

For the real data, both the SIR method and the EnKPF method use $N = 10000$ particles. This value is chosen by trial and error. The number of particles needs to be high enough for the methods to give satisfying results, and ideally avoid degeneracy. However, with many particles the run-time of the methods is high, and too many particles makes it very time consuming to run the methods. If the techniques presented here are to be used professionally then it is not appropriate to use a method with a large number of particles, and thereby an inconvenient run-time.

For the real data the normalization constant s is not the same for all time steps. The value of s for time step t is found by comparing the calculated energy curve for the true position at time step t to the extracted energy curve associated with the same position. s is chosen such that the magnitude of the two curves are as similar as possible. The values of $\sigma_{\mathbf{T}}^2$ and $\sigma_{\mathbf{P}}^2$ are then found by adding normally distributed noise, with variance given by these values, to curves of travel time and energy which are calculated using the chosen value of s. The noise should be of reasonable magnitude compared to the curvature of the calculated curves. Even though s is different for the different time steps, it was found by plotting the curves that $\sigma_{\mathbf{P}}^2$ can have the same value for all time steps.

For the real data at time step $t = 0$ $\sigma_{\mathrm{pos},0} = 60$ m and $\sigma_{\mathrm{vel},0} = 15$ m/s. These values are chosen based on what is realistic, but the choices are limited by the capability of the statistical methods. For the remaining time steps $\sigma_{\mathrm{pos},t} = 50$ m and $\sigma_{\mathrm{vel},t} = 1$ m/s. These values are chosen such that they could be realistic. For the real data, as for the simulated data, the expectation of the prior distribution of the particles at time step $t = 0$ is equal to the true state of the ship at time step $t = 0$.

The results for the real data are given for a path that is associated with time stamps *Time: 035539-Time: 035839*. At these time stamps the x-coordinate of the ship is located in, or at least very close to, the interval of x-coordinates which is defined by the 199 channels of the cable that the data is collected from. If states of the ship for other time stamps is to be estimated, then the data needs to be collected from more than the 199 channels closest to the point at which the ship crosses the cable.

5.2.2 Robustness to the choice of N

The small values of minimal ESS for the methods for the real case presented in Table 4.11 indicates that the methods maybe should have been run with more particles than $N = 10000$. The evaluation metrics for SIR for the real case for five different values of N are presented in Table 5.13 and Table 5.14, while the evaluation metrics for the EnKPF method with $\gamma = 0.9$ for the same values of N are presented in Table 5.15 and Table 5.16. For these results the values of all other parameters than N are the same as those specified

for the real case in chapter 4. The calculated evaluation metrics are based on one run of the methods.

N	RMSE(x)	RMSE(y)	RMSE(v_x)	RMSE(v_y)	min(ESS)	min(ESS)/N
100	158.56	150.79	2.73	4.07	NaN	NaN
1000	2780.48	1848.3	21.51	13.53	NaN	NaN
5000	49.29	81.70	1.23	0.78	1.00	0.0002
10000	60.97	96.52	0.64	1.20	1.09	0.0001
20000	62.51	104.81	1.14	0.61	1.05	0.00005

Table 5.13: RMSE and minimal ESS of SIR for the real case for different values of N.

N	CRPS(x)	CRPS(y)	CRPS(v_x)	CRPS(v_y)
100	25151.76	22748.58	10.88	77.44
1000	7731093.73	3416265.88	511.94	246.60
5000	2457.76	6748.38	51.41	56.19
10000	3753.19	9411.14	72.84	60.16
20000	3955.37	11418.31	65.33	53.56

Table 5.14: Mean CRPS of SIR for the real case for different values of N.

From Table 5.13 and Table 5.14 it can be observed that for the real data the SIR method collapses for $N = 100$ and $N = 1000$. For $N = 5000$, $N = 10000$ and $N = 20000$ the ESS is close to one. Also, for these values of N the values of RMSE and CRPS are similar. The ratio min(ESS)/N seems to decrease as N increases, and consequently it is difficult to decide a value of N that gives a value of minimal ESS that is not too small. The SIR method seems to need far more particles than $N = 20000$ in order to avoid degeneracy.

N	RMSE(x)	RMSE(y)	RMSE(v_x)	RMSE(v_y)	min(ESS)	min(ESS)/N
100	69.88	151.87	4.83	7.40	1.00	0.01
1000	49.42	110.01	0.44	1.51	2.00	0.002
5000	43.18	88.47	0.86	1.05	2.07	0.0004
10000	43.19	92.93	0.70	1.07	6.28	0.0006
20000	44.56	85.25	0.66	1.48	3.58	0.0002

Table 5.15: RMSE and minimal ESS of EnKPF with $\gamma = 0.9$ for the real case for different values of N.

Tables 5.15 and 5.16 show that for the EnKPF method with $\gamma = 0.9$ the results are very similar for the four largest values of N. For $N = 100$, the values of RMSE and CRPS are quite high compared to the values of the evaluation metrics for the larger values of N. The minimal ESS is small for all values of N, but it is larger than one for all $N > 100$. Based on the values in Tables 5.15 and 5.16 it seems like EnKPF with $\gamma = 0.9$ could produce the same results as in chapter 4 with fewer particles than $N = 10000$. Also, the method seems to require far more than $N = 20000$ particles in order to end up with a value of minimal ESS that is reasonable. For EnKPF for the real case, the ratio min(ESS)/N is not constant for different values of N. This makes it difficult to use the number of particles to estimate the value of the minimal ESS.

N	CRPS(x)	CRPS(y)	CRPS(v_x)	CRPS(v_y)
100	6275.03	27713.19	65.33	95.45
1000	3065.08	16554.71	50.26	55.21
5000	2622.36	8661.3	59.14	54.10
10000	2732.29	13393.55	57.38	59.19
20000	2659.83	9808.67	58.53	58.39

Table 5.16: Mean CRPS of EnKPF with $\gamma = 0.9$ for the real case for different values of N.

For smaller values of γ than $\gamma = 0.9$ the EnKPF method may have even smaller values of ESS for the different values of N than the values that are reported in Table 5.15. The reason is that for the real case in chapter 4 the minimal ESS is smaller for EnKPF with $\gamma = 0.1$ and $\gamma = 0.5$ than it is for EnKPF with $\gamma = 0.9$.

Tables 4.11 and 4.12 showed that for the real case both the SIR method and the EnKPF method give results that are highly variable. This also affects the results that are discussed in this subsection. For instance it can be observed from Table 5.15 that the minimal ESS of EnKPF with $\gamma = 0.9$ is smaller for $N = 20000$ than for $N = 10000$, which is not what one would expect. Consequently, the results in this subsection should be based on several runs of the methods such that the evaluation metrics that are compared for different values of N are less affected by the quality of one single run of the methods. However, because of the long run-time of the methods this has not been prioritized.

5.2.3   Robustness to the expectation of the prior at time step $t = 0$

For the results for the real data in chapter 4 the initial distribution of the particles is given by $\mathcal{N}_4(\mathbf{x}_{\text{true},0}, V_0)$ with the square root of the elements of V_0 given by $\sigma_{\text{pos},0} = 60$ m and $\sigma_{\text{vel},0} = 15$ m/s. Also for the real data it is interesting to investigate how the quality of the results change when the initial distribution is biased.

The evaluation metrics for the SIR method and the EnKPF method with $\gamma = 0.9$ for the real data for an initial distribution with a small amount of bias are presented in Tables 5.17 and 5.18. The expectation of the initial distribution is given by $\mathbf{x}_{\text{true},0} + [200, 100, 0, 0]^T$, and the values of all other parameters are the same as those used for the real case in chapter 4. The values in the tables are based on three runs of the methods.

γ	RMSE(x)		RMSE(y)		RMSE(v_x)		RMSE(v_y)		min(ESS)	
	Mean	Std.	Mean	Std.	Mean	Std.	Mean	Std.	Min	Max
0	1243.93	29.00	969.88	65.12	10.93	0.48	9.13	0.86	NaN	NaN
0.9	93.86	13.18	494.59	142.99	1.04	0.77	3.74	0.34	1.00	1.01

Table 5.17: RMSE and minimal ESS of SIR and EnKPF for the real case where the initial distribution contains a small amount of bias.

By comparing Tables 5.17 and 5.18 to Tables 4.11 and 4.12 it can be observed that the RMSE and CRPS seem to become worse as the initial distribution of the state of the ship is biased. In Table 5.17 the minimal ESS is approximately equal to one for the EnKPF method, and the SIR method has collapsed due to degeneracy. Overall, the biased initial

γ	CRPS(x)		CRPS(y)		CRPS(v_x)		CRPS(v_y)	
	Mean	Std.	Mean	Std.	Mean	Std.	Mean	Std.
0	1548199.07	71566.75	944917.45	123325.80	119.61	10.70	84.44	15.16
0.9	9615.92	2269.35	270904.72	125998.23	61.32	2.17	75.85	3.17

Table 5.18: Mean CRPS of SIR and EnKPF for the real case where the initial distribution contains a small amount of bias.

distribution makes both SIR and EnKPF with $\gamma = 0.9$ give worse results than when the expectation of the initial distribution is equal to the true state of the ship at time step $t = 0$.

The evaluation metrics for the SIR method and the EnKPF method with $\gamma = 0.9$ for the real data for an initial distribution with a large amount of bias are presented in Tables 5.19 and 5.20. The expectation of the initial distribution is given by $\mathbf{x}_{\text{true},0} + [400, 100, 0, 0]^T$, and the values of all other parameters are the same as those used for the real case in chapter 4. The values in the tables are based on three runs of the methods.

γ	RMSE(x)		RMSE(y)		RMSE(v_x)		RMSE(v_y)		min(ESS)	
	Mean	Std.	Mean	Std.	Mean	Std.	Mean	Std.	Min	Max
0	2506.28	77.46	1137.87	67.57	20.49	0.74	11.89	0.67	NaN	NaN
0.9	72.93	3.93	304.77	10.26	1.16	0.34	3.73	0.47	1.87	5.95

Table 5.19: RMSE and minimal ESS of SIR and EnKPF for the real case where the initial distribution contains a large amount of bias.

γ	CRPS(x)		CRPS(y)		CRPS(v_x)		CRPS(v_y)	
	Mean	Std.	Mean	Std.	Mean	Std.	Mean	Std.
0	6287415.55	391064.84	1299303.08	156951.13	420.47	30.35	141.72	16.18
0.9	6214.05	543.22	111095.23	15174.45	46.75	1.19	70.18	3.23

Table 5.20: Mean CRPS of SIR and EnKPF for the real case where the initial distribution contains a large amount of bias.

The minimal ESS in Table 5.19 shows that also when the bias of the initial distribution is large, the SIR method has collapsed. The values of RMSE and CRPS given in Tables 5.19 and 5.20 indicate that the quality of the estimated states is worse when the initial distribution contains a large amount of bias compared to when the bias is non-existent. This is true both for the SIR method and the EnKPF method for the real data. However, by comparing Tables 5.19 and 5.20 to Tables 5.17 and 5.18 it is clear that the quality of the results from EnKPF with $\gamma = 0.9$ is better when the amount of bias associated with the initial distribution is large compared to when the amount of bias is small. This is an unexpected result, and the reason for this result is not known.

The results from using the EnKPF method with $\gamma = 0.9$ for the real case where the expectation of the initial distribution is given by $\mathbf{x}_{\text{true},0} + [400, 100, 0, 0]^T$ are shown in the following figures. These figures are based on one of the three runs of the method, and that one run is chosen randomly among the three runs.

Figure 5.13 shows the estimated filtering distributions of the positions of the ship for the real case where the amount of bias added to the initial distribution is large. At time

steps $t = 0$, $t = 2$ and $t = 3$ the estimated filtering distributions do not surround the true positions, and at time step $t = 1$ the spread of the estimated filtering distribution is large. Also, at time steps $t = 1, t = 2$ and $t = 3$ the estimated filtering distributions cover both sides of the cable, and the estimated filtering distribution at time step $t = 3$ is bimodal.
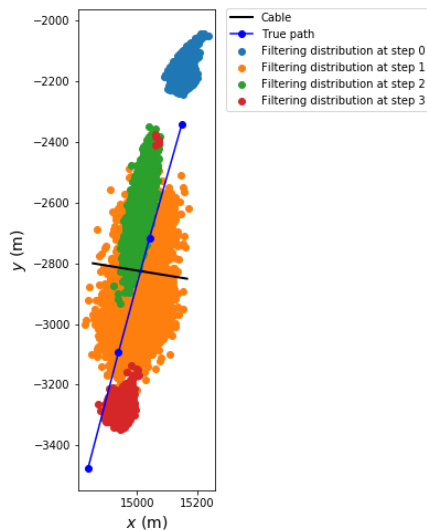

Figure 5.13: Estimated filtering distribution of the positions of the ship for the real case with a biased initial distribution according to the EnKPF method with $\gamma = 0.9$.

The ESS of EnKPF with $\gamma = 0.9$ for the real case where the initial distribution contains a large amount of bias is shown in Figure 5.14. The ESS is small at all time steps, also at time step $t = 0$, and the ESS is at its smallest at time step $t = 3$. This is different from what was observed in Figure 4.25 where the ESS was at its smallest at time step $t = 1$. By further comparisons to Figure 4.25, it seems like the ESS is negatively affected by the biased initial distribution at all time steps except at time step $t = 1$.

Figure 5.15 shows that as the initial distribution of the state of the ship is biased, the EnKPF method with $\gamma = 0.9$ is not able to produce an estimated path that fits the true path of the ship in a satisfying manner. At all time steps the estimated position of the ship is biased compared to the true position of the ship.

The estimated velocity of the ship according to EnKPF with $\gamma = 0.9$ for the real case where the initial distribution contains a large amount of bias is shown in Figure 5.16. The true velocity in the x-direction lays on the outside, or on the edge, of the uncertainty bound of the estimated velocity at time steps $t = 1$ and $t = 3$. At time steps $t = 1$ and $t = 2$ the true velocity lays on the outside of the uncertainty bound of the estimated velocity in the y-direction. At time step $t = 1$, the difference between the estimated velocity in the y-direction and the true velocity is very large.
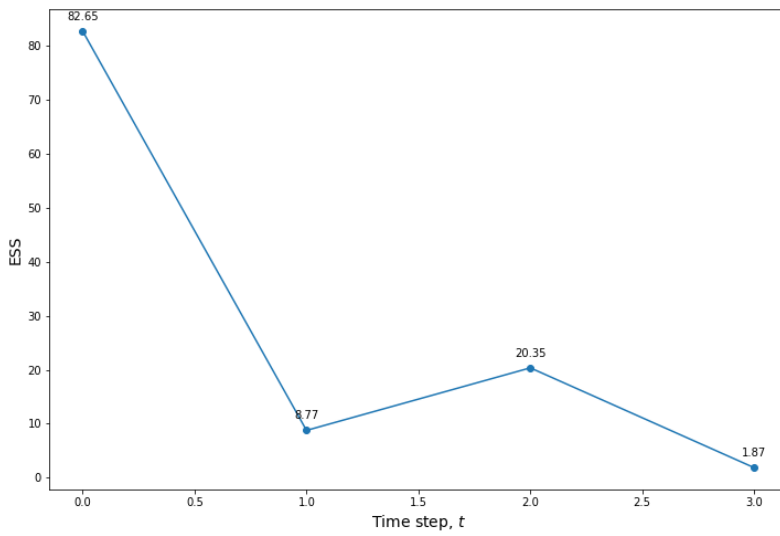
Figure 5.14: ESS at each time step for the real case with a biased initial distribution using EnKPF with $\gamma = 0.9$.
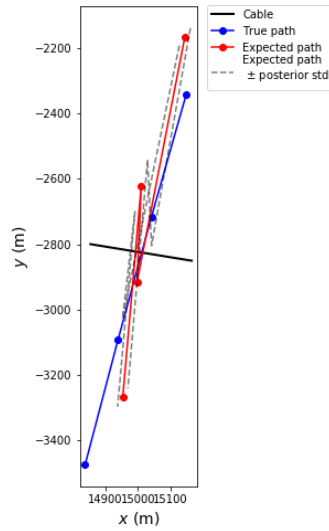
Figure 5.15: The expected path of the ship for the real case with a biased initial distribution according to EnKPF with $\gamma = 0.9$.
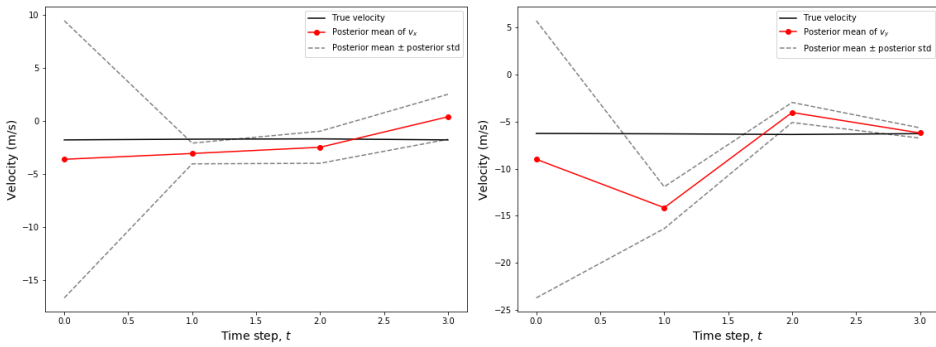

Figure 5.16: The estimated velocity of the ship for the real case with a biased initial distribution according to EnKPF with $\gamma = 0.9$. The estimate of v_x is shown on the left, while the estimate of v_y is shown on the right.

5.2.4 Robustness to the variance of the prior at time step $t = 0$

The results from applying the SIR method and the EnKPF method with $\gamma = 0.9$ to the real data for an initial distribution with large standard deviation are presented in Tables 5.21 and 5.22. In this case, $\sigma_{\text{pos},0} = 200$ m. For these results all other parameters than $\sigma_{\text{pos},0}$ are the same as those specified for the real case in chapter 4. The values in the tables are based on three runs of the methods.

γ	RMSE(x)		RMSE(y)		RMSE(v_x)		RMSE(v_y)		min(ESS)	
	Mean	Std.	Mean	Std.	Mean	Std.	Mean	Std.	Min	Max
0	93.82	28.53	255.78	113.33	2.21	0.86	4.08	0.11	1.00	1.00
0.9	71.1	32.24	274.54	228.50	0.74	0.20	2.88	2.12	1.00	6.01

Table 5.21: RMSE and minimal ESS of SIR and EnKPF for the real case where the standard deviation of the initial distribution is large.

γ	CRPS(x)		CRPS(y)		CRPS(v_x)		CRPS(v_y)	
	Mean	Std.	Mean	Std.	Mean	Std.	Mean	Std.
0	9663.78	5416.06	78451.30	53484.58	38.96	9.54	79.28	2.47
0.9	6977.87	5294.07	130514.74	162043.42	53.94	1.01	69.33	17.07

Table 5.22: Mean CRPS of SIR and EnKPF for the real case where the standard deviation of the initial distribution is large.

Compared to Tables 4.11 and 4.12 the values of RMSE and CRPS in Tables 5.21 and 5.22 indicate that the quality of the results of SIR and EnKPF has decreased as an initial distribution with large standard deviation is used for the state estimation procedures for real data. However, for some elements of the state vector, the RMSE and CRPS has decreased as the variance of the initial distribution has increased. The minimal ESS is small for both methods, but for EnKPF the upper limit of minimal ESS is larger in Table 5.21 than in Table 4.11. When the standard deviation of the initial distribution is large, the results from the statistical methods seem to be even more variable compared to when the standard deviation of the initial distribution is smaller.

The estimated filtering distributions of the positions of the ship for the real case given by the EnKPF method with $\gamma = 0.9$ for an initial distribution with large standard deviation are shown in Figure 5.17. This figure is based on one of the three runs of the EnKPF method for the real case where the standard deviation of the initial distribution is large. From the figure it can be observed that the estimated filtering distribution at time step $t = 1$ is bimodal and it is clear that when the standard deviation of the initial distribution is large, the EnKPF method with $\gamma = 0.9$ has problems with estimating the correct y-coordinate of the position of the ship at time step $t = 1$. The variance of the estimated filtering distributions of the positions of the ship is larger than the variance of the estimated filtering distributions of the positions of the ship given in Figure 4.24.

The ESS of the run that Figure 5.17 is based on is given in Figure 5.18. The ESS is at its lowest at time step $t = 1$, but at time steps $t = 1, t = 2$ and $t = 3$ the ESS is higher than the ESS at the corresponding time steps in Figure 4.25. At time step $t = 0$ the ESS is smaller in Figure 5.18 than in Figure 4.25. This indicates that the large variance of the initial distribution only affects the ESS negatively at time step $t = 0$.
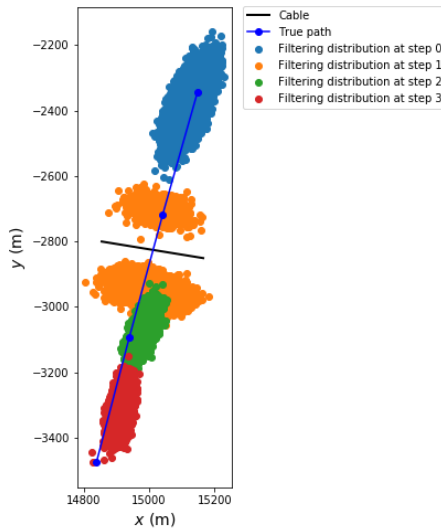
Figure 5.17: Estimated filtering distributions of the positions of the ship for the real case with an initial distribution with large standard deviation according to the EnKPF method with $\gamma = 0.9$.

The expected path of the ship according to EnKPF with $\gamma = 0.9$ given real data and an initial distribution with large standard deviation is given in Figure 5.19. Despite the large spread of the particles of the estimated filtering distributions in Figure 5.17, the expected path given by the EnKPF method for the real data and an initial distribution with large standard deviation is quite similar to the expected path associated with the real data in Figure 4.26. However, the uncertainty of the estimated path is larger in Figure 5.19 than in Figure 4.26. Also, in Figure 5.19 at time step $t = 1$, the estimated position is on the wrong side of the cable.

The estimated velocity of the ship according to EnKPF with $\gamma = 0.9$ for the real case for an initial distribution with large standard deviation is given in Figure 5.20. Compared to the results for the real case in chapter 4 and Figure 4.27 the estimated velocity in the x-direction seems to be improved as the true velocity lays on the inside of the uncertainty bound of the estimated velocity at all time steps. The estimated velocity in the y-direction fits the true velocity of the ship worse when the variance of the initial distribution is large, compared to when the variance is smaller.

It should be mentioned that it is difficult to know if the differences between the results in chapter 4 and the results in this subsection are due to the added variance of the initial distribution, or the high variability of the methods. Especially, this is true for the comparison of Figures 4.24-4.27 to Figures 5.17-5.20 since these figures are based on only one run of the methods. The comparison of Tables 4.11 and 4.12 to Tables 5.21 and 5.22 is more trustworthy as this comparison is based on three runs of the methods.
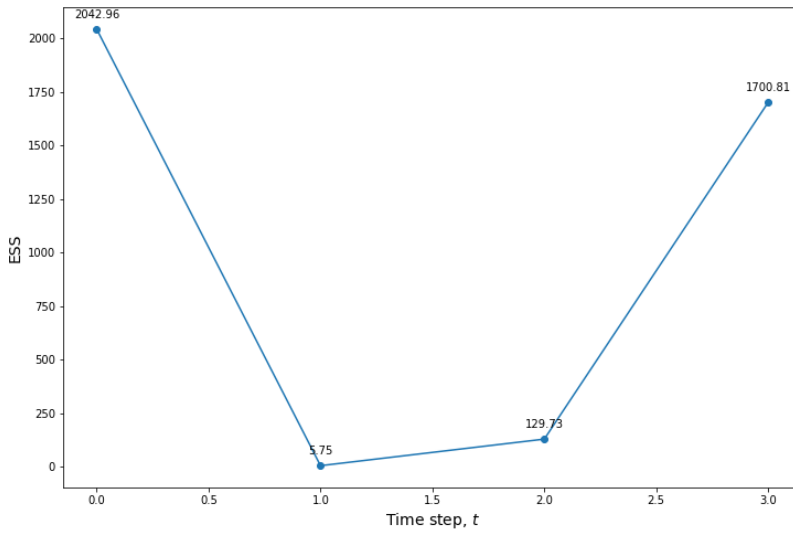
Figure 5.18: ESS at each time step for the real case with an initial distribution with large standard deviation using EnKPF with $\gamma = 0.9$.

Overall, the results from using the SIR method and the EnKPF method with a biased or large initial distribution are worse than the results that were obtained by using a non-biased or quite small initial distribution. The results are at its worst when the initial distribution is biased. The SIR method collapses if the initial distribution is biased, but this is not a problem if the variance of the initial distribution is large. Consequently, both of the methods are more robust to changes in the variance of the initial distribution than they are to changes in the expectation of the initial distribution. For the real case, the EnKPF method seem to be more robust than the SIR method.
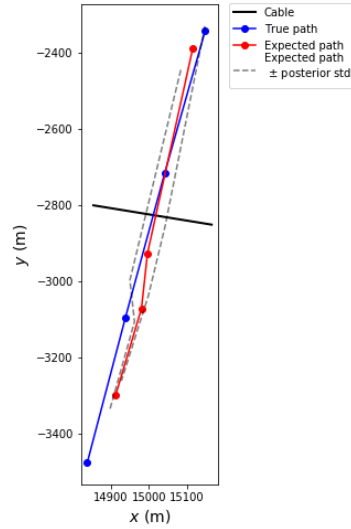
Figure 5.19: The expected path of the ship for the real case with an initial distribution with large standard deviation according to EnKPF with $\gamma = 0.9$.
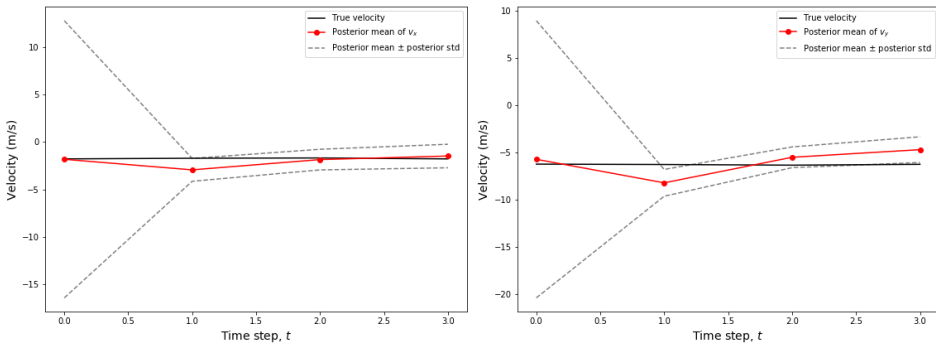

Figure 5.20: The estimated velocity of the ship for the real case with an initial distribution with large standard deviation according to EnKPF with $\gamma = 0.9$. The estimate of v_x is shown on the left, while the estimate of v_y is shown on the right.

5.2.5 Quality of results

The results for the real data are not very good, but not very bad either. At some time steps the estimated positions of the ship are biased compared to the true positions, and the minimal ESS is very small for the SIR method as well as for the EnKPF alternatives. The estimated velocity fits the true velocity quite well. The SIR method and the EnKPF alternatives provide very similar results, and the results have proved to be highly variable. The quality of the results of the methods decreases when the choices of parameters for the initial distribution are not optimal, and the EnKPF method seem to be more robust than the SIR method.

Based on the good results that are obtained for the simulation cases, it is reasonable to assume that the reason for the sub-optimal results for real data is possibly the curve extraction procedures along with the quality of the data. There are multiple aspects of the data that are problematic. As shown in Figure 2.10b the noise of the extracted energy curve is dominating at some time steps. In addition, Figure 2.10a shows that by using the travel time extraction procedure the minimum of the extracted travel time curve is not located where it is expected to be located. Since the location of the minimum of the travel time curve should represent the x-coordinate of the ship, it is very important that the minimum of the travel time curve has the correct location.

There is also a problem with the data that is not related to the extraction procedures of travel time curves and energy curves. From the structure of the data at time stamp *Time: 035839* in Figure 2.6 one would expect the minimum of the travel time curve to be located in the interval of channels given by $[75, 100]$. However, the x-coordinate of the ship given by AIS at time stamp *Time: 035839* indicates that the minimum of the travel time curve should be located at a channel not included in the collection of 199 channels used in this project. Consequently, the data from which the travel time curves and energy curves are extracted does not appear as one would expect.

Chapter 6

Further work

There are several ways in which the fiber optic cable data can be used to track a ship. For instance, other methods than particle filters can be used, and it might be possible to use the data in different ways than what has been done in this project. It is also possible to use other types of waves than direct waves. For instance, in some cases head waves may provide a more suitable representation of the vibrations from the ship than direct waves can. When the problem of ship tracking is solved like it is in this project there are several possible adjustments and extensions. Some of these adjustments and extensions are discussed in this chapter.

6.1 A dynamic EnKPF method

Instead of using the same γ for all time steps for the EnKPF method, a dynamic EnKPF method could have been applied to the tracking problem. At each time step t of Algorithm 4, when ESS_t is calculated, γ can be adjusted. The goal of this procedure is that at each time step the ratio $\alpha = \text{ESS}_t/N$ should be in a specified interval $[\alpha_1, \alpha_2]$. By achieving this, a value of minimal ESS close to one can be avoided. If $\alpha < \alpha_1$ then the method needs to be influenced more by the EnKF method and γ should be increased. On the other hand, if $\alpha > \alpha_2$ then γ should be decreased. Each time γ is adjusted line 3 and 4 of Algorithm 4 needs to be redone. The search for a γ which satisfies $\alpha \in [\alpha_1, \alpha_2]$ can be done in an effective way by using a binary search scheme. The procedure of the EnKPF method with a dynamic γ is presented by Shen and Tang (2015).

The reason why the dynamic version of the EnKPF method has not been applied to the ship tracking problem in this project is that the affect of γ was to be presented. However, this could also have been done by presenting the value of γ which satisfies $\alpha \in [\alpha_1, \alpha_2]$ at each time step. In addition, the run-time of the EnKPF method that is used in this project is long, and the fear of an even slower implementation of the method prevented the dynamic EnKPF method from being implemented.

Another reason why the dynamic EnKPF method has not been implemented is that in simulation case 1, a small value of γ resulted in a high minimal ESS while a large value

of γ resulted in a small minimal ESS. The reason for this was that the EnKF method has problems with estimating the state of the ship when there are several positions, one with a positive y-coordinate and one with a negative y-coordinate, that fits well with the measured data. This means that if a dynamic EnKPF method had been used for simulation case 1, then α would decrease when γ, and consequently the influence of the EnKF method, had been increased. This is the opposite performance of the expected performance of the dynamic EnKPF method.

It would be interesting to see if γ would have the same value for all time steps, or if it would vary from time step to time step. Hence, the use of a dynamic EnKPF method may be a suitable extension of this project, at least for simulation cases 2-4 and maybe also for the real case.

6.2 Alternative extraction procedures

Since a problem for the real case is that the minimum of the extracted travel time curves is not located where one would expect from looking at Figure 2.6, the results could maybe have been improved by using an extraction procedure that results in travel time curves that fits the expectation. It is difficult to know what changes would have to be applied to the current extraction procedure for the curves to fulfill the expectations, but one way may be to base the time shifting on the correlation between $\mathbf{q}_{t,j}$ and all other columns of Q_t, instead of basing the time shifting only on the correlation between $\mathbf{q}_{t,j}$ and $\mathbf{q}_{t,j-1}$. It may also be possible to use completely different extraction procedures than the one that is used in this project. Because of the mismatch between the structure of the data in Figure 2.6 and the coordinates given by AIS, it is not certain that a better extraction procedure would improve the results for the real case.

6.3 Using data from a larger part of the cable

In order to track the ship in the real case over a greater distance, it is necessary to use data from more than 199 channels. Even in the real case in chapter 4 a larger part of the cable should have been used as the true x-coordinate of the ship at time step $t = 3$ is outside of the interval of coordinates given by the 199 channels that have been used in this project. If more data from more channels had been used in the real case in chapter 4, then the results could maybe have been improved. If data from a larger part of the cable is used then it is possible to investigate how well the SIR method and the EnKPF method perform over more than four time steps. Hence, a natural next step in this project is to use data from more than the 199 channels closest to the point on the cable at which the ship crosses the cable.

6.4 Gathering more information about the placement of the cable

It is not clear why the data in Figure 2.6 does not appear as expected based on the coordinates given by AIS, but a hypothesis is that the cable is not as straight in the area where the ship crosses the cable as Figure 4.23 indicates. A cable which is not completely straight would give signals that is different from the signal associated with a straight cable, and certain curvatures of the cable may cause the structure of the data to be altered such that the minimum of the travel time curve is not located at the x-coordinate of the ship for which the data is measured.

For simulation case 2, the true travel time curve and the true energy curve associated with time step $t = 0$ are shown in Figure 6.1. From the plot of the travel time curve in Figure 6.1 it is clear that the minimum of the curve is not located at the x-coordinate of the ship, and from the plot of the energy curve it is clear that when the cable is curved the distance from the minimum to the maximum of the curve is not given by the distance $a_t = \sqrt{y_t^2 + z_{\text{true}}^2}$. This figure indicates that assuming a cable to be straight, when it actually is curved, results in calculating curves for the particles that does not match the data that is measured along the curved cable.
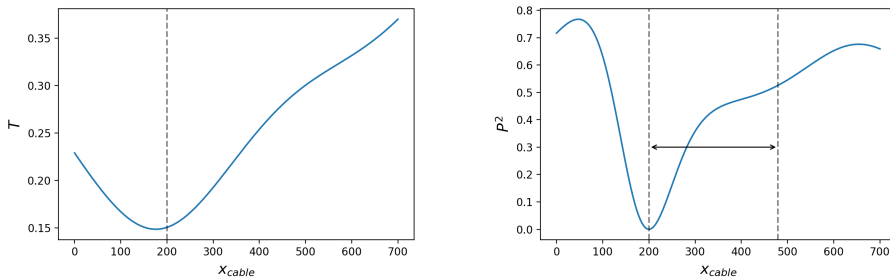
(a) Travel time curve of a direct wave where the cable is curved.

(b) Energy curve of a direct wave where the cable is curved.

Figure 6.1: Curves for travel time and energy for a direct wave from position $(x_t, y_t, z_{\text{true}}) = (200, 275, 50)$ where the cable is curved. The normalization constant is $s = 500$. The vertical dashed line in the plot on the left is placed at the x-coordinate of the ship. The double sided arrow in the plot on the right illustrates the distance a_t.

Figure 6.1 also indicates that there might not be a mismatch between the data and the AIS coordinates. If the cable is curved then the minimum of the travel time curve can be in a different position than the x-coordinate of the ship, which means that if the cable in the North Sea is curved then the peak of the structure of the data in Figure 2.6 does not have to be located at the channel which corresponds to the x-coordinate given by AIS.

In order to verify the hypothesis concerning the affect of a curved cable it is necessary to have more information about the placement of the cable along which the real data is measured. For this project, a list of coordinates for the cable is given. However, in the area where the ship crosses the cable too few coordinates are given to be able to know the

placement of the cable exactly. A plot of a segment of the cable, and the path of the ship for time stamps *Time: 035539-Time: 035839*, based on the available coordinates of the cable is shown in Figure 6.2.
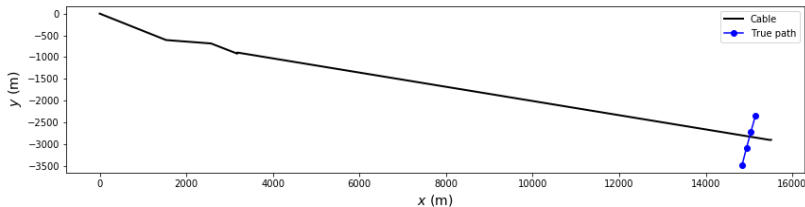

Figure 6.2: A segment of the cable in the North Sea as given by the available coordinates.

In the left end of Figure 6.2, several coordinates are given for the cable, and it is clear that the cable is not straight in this part of the figure. For the rest of the figure the cable seems to be straight, but it is reasonable to assume that this is not true, and that the reason for the straight cable is the lack of available coordinates. In this project the depth of the ocean at all points along the cable is not known, and the depth is assumed to be the same along the entire cable. This might also be a reason why the data does not appear as expected. In order to improve the results in this project, it seems important to have more detailed information about the placement of the cable.

6.5 Using more realistic assumptions for the state-space model

Another way of possibly improving the results for the real data is to use more realistic distributions for the noise of the observations. The analysis of the real data in chapter 2 clearly showed that several of the assumptions related to $\eta_{\mathbf{T},t}$ and $\eta_{\mathbf{P},t}$ were not realistic. By using more suitable distributions for these vectors, the calculated curves of the particles would be more similar to the curves extracted from the real data, and the results could perhaps be improved. A disadvantage of such assumptions is that the implementation of SIR and EnKPF would be more complicated, especially when it comes to calculating the weights of the particles.

According to Figure 4.26 there is some bias between the estimated positions and the true positions of the ship. As previously mentioned, the reason for this can be the curvature of the cable, but it is also a possibility that the data itself is biased. Because of this, it should be investigated how well the methods perform if bias is added to the observations in the state-space model. However, it is not clear exactly how this bias should be included in the model to best fit the possible bias of the data.

6.6 Some limitations of the project

For the simulated data, some changes in the implementations could have been performed in order to give more stable results. For instance, for simulation case 3 and 4 the RMSE and CRPS of the SIR method showed that the method is not able to estimate the path of the ship in a satisfying manner. Consequently, the methods should have been run with a larger number of particles. The reason why this has not been done is that a really large N is needed to give satisfying results from the SIR method. If the SIR method is to be run with $N >> 10000$ then also EnKPF needs to be run with the same large N for the results of the methods to be comparable. This means that for simulation cases 3 and 4 the four methods needs to be run with the large N. With $N = 10000$ the run-time of one run of the SIR method for simulation case 3 is approximately 20 minutes while the run-time of one run of the EnKPF method is approximately 50 minutes. For simulation case 4 the run-times of the methods are approximately equal to two times the run-times for simulation case 3. The run-time quickly becomes large when N increases and the consequence is that using a larger N than $N = 10000$ is not prioritized in this project.

Another improvement for the implementation that has not been prioritized in this project is to run the methods more than three times for the calculation of the evaluation metrics. This would make the calculated evaluation metrics more accurate and reliable. The reason why more than three runs has not been used is the long run-time of the methods. If more runs of the methods should be used to calculate RMSE and CRPS then much more time would have to be spent on running the code. Since the results of most of the methods for most of the simulation cases do not seem to be very variable it has not been prioritized to spend much more time on running the methods more than three times for each case. However, for the real case the results are highly variable, and the methods should have been run more than three times.

The run-times of the methods are recorded on a MacBook Pro from 2015. If a more powerful computer would had been available for running the methods, then it would be possible to prioritize to run the methods with more particles than $N = 10000$, and more than three runs of the methods could have been used for calculating the evaluation metrics.

6.7 Identifying the ships that are tracked

In contrast to the methods that are used in this project, the AIS is an identification system. This means that the AIS identifies the ships that are tracked by the system. It seems difficult to identify a ship that is tracked using a particle filter. However, it may be possible to classify which kind of boat is being tracked by examining the data. For instance, one can assume that a cargo ship would create different vibrations in the ocean than a fishing boat would. Consequently, the closest one comes to ship identification using particle filters seems to be ship classification.

It may also be possible to examine the data and in that way distinguish vibrations coming from different ships of the same kind. For instance, different cargo ships may create different vibrations. However, this seems more difficult than distinguishing vibrations from boats of different kinds. In order to distinguish these vibrations from each other it may be possible to save all unique vibrations in a data base, and use the data base for ship

identification. If two boats are identical in their structure, then it may be impossible to distinguish the vibrations coming from the two ships. The only way of identifying these ships would be to know their names or their identification numbers.

The possibilities of ship classification and ship identification that are discussed above seem quite difficult to implement. One problem is that one ship may create different vibrations in different scenarios. What may affect the vibrations is among others the weight of the ship and the velocity of the ship. This can make it problematic to save identities in a data base based on the vibrations that the ship makes.

The problem of distinguishing which vibrations are associated with which ship makes it difficult for the particle filters to track several ships at the same time. For this to be done one would have to know that the data that is being used at time steps t and $t+1$ has originated from the same ship. This seems like a difficult task, but if fiber optic cable data is to be used for ship tracking in the future, then one would have to be able to track several ships at the same time.

Conclusion

The goal of this project has been to track a ship based on simulated and real fiber optic cable data. This has been done by using the particle filters called SIR and EnKPF. The input to the methods has been the curves of travel time and energy associated with direct waves originating from the positions of the ship. Direct waves are a representation of the vibrations that a ship creates as it moves. The simulated curves were the product of adding normally distributed noise to curves given by the equations for travel time and energy associated with direct waves. The real data is measured using DAS, and for the real data, the curves of travel time and energy were extracted from the data. For the travel time curves, the extraction procedure was loosely based on a technique called DTW, and the energy curves were extracted based on the RMS of the data along the cable. The real data is measured along a fiber optic cable in the North Sea, and the data is provided by Tampnet and Sintef.

For the simulated data, the methods were used to track a ship in four different scenarios. The EnKPF method was applied to these problems with three different values of the tuning parameter γ, and for all of the four simulation cases, based on the evaluation metrics RMSE, minimal ESS and mean CRPS, one of the EnKPF alternatives proved to give the best results. The minimal ESS of the SIR method was close to one for the two simplest simulation cases, and for the remaining two cases, the SIR method collapsed and was not able to track the ship. Based on the results from the simulated data, it can be concluded that in an idealized situation the EnKPF method is suitable for ship tracking based on fiber optic cable data. If the vibrations caused by a ship are registered by two cables, then the EnKPF method is able to produce highly accurate state estimates.

The discussion of the results for simulated data showed that the EnKPF method is quite robust. At least for the simplest simulation case, the method is able to track the ship in a satisfying manner even if the knowledge of the state of the ship is limited prior to the collection of data. Furthermore, the number of particles used for estimation does not need to be very large for the EnKPF method to give satisfying results and avoid degeneracy. The SIR method is not as robust as the EnKPF method. Limited knowledge about the state of the ship prior to the collection of data causes the SIR method to experience degeneracy,

and the method needs a large amount of particles in order to be able to estimate the path of the ship in a satisfying manner.

The results from the real case were not as good as the results for the simulated data. The paths that the methods estimated were slightly biased compared to the true path of the ship, and the ESS was small. Because of the promising results for the simulated data, it was assumed that the reason for the sub-optimal results for the real case was the data and the extraction procedures. Especially for the extracted energy curves the signal to noise ratio is very low. In addition, for some of the extracted travel time curves the minimum is not located where one would expect from the plot of the real data. There is also a problem that the plot of the real data does not fit the expectations of the data based on the coordinates of the ship provided by AIS. This indicates that there are challenges in the data acquisition at cable location of the DAS system as well as in the processing of the data to extract physically relevant information.

The discussion of the results for the real data showed that the quality of the results of both of the methods seem to decrease as the choices of parameters are not optimal. Both of the methods are able to give satisfying state estimates when the number of particles is smaller than $N = 10000$, but the SIR method collapses if the number of particles is too small. Even by using more than $N = 10000$ particles, the minimal ESS is small for both methods. When the knowledge of the state of the ship prior to the collection of data is limited, the quality of the results is reduced for both methods, and when the initial distribution is biased, the SIR method collapses.

Overall, the results from this project are quite promising. In an idealized situation the EnKPF method is an excellent choice for ship tracking. However, for the real data that is used in this project the results are not as good as one could hope. The results could maybe have been better if the extraction procedure for travel time curves is improved. More reliable processing and inversion routines might be developed by incorporating complex noise characteristics, such as bias parameters or correlated noise in the state-space model. Also, the mismatch between the true coordinates of the ship and the plot of the data must be explained. A possible explanation may be found by gathering more information about the placement of the cable. If the problems with using real data are solved, the natural next steps of the project are to use data from more than 199 channels of the cable and to try to track several ships at the same time. Consequently, the results from this project indicate that by putting some more work into the field of fiber optic ship tracking, it may some time in the future be possible to use a particle filter together with fiber optic cable data to track ships.

Bibliography

Ajo-Franklin, J.B., Dou, S., Lindsey, N.J., Monga, I., Tracy, C., Robertson, M., Tribaldos, V.R., Ulrich, C., Freifield, B., Daley, T., Li, X., 2019. Distributed acoustic sensing using dark fiber for near-surface characterization and broadband seismic event detection. Scientific Reports 9. URL: `https://www.nature.com/articles/s41598-018-36675-8`.

Arulampalam, M.S., Maskell, S., Gordon, N., Clapp, T., 2002. A tutorial on particle filters for online nonlinear/non-gaussian bayesian tracking. IEEE Transactions on Signal Processing 50, 174–188. doi:`10.1109/78.978374`.

Baldwin, C.S., 2014. Brief history of fiber optic sensing in the oil field industry. Fiber Optic Sensors and Applications XI 9098, 1 – 9. URL: `https://doi.org/10.1117/12.2050550`, doi:`10.1117/12.2050550`.

Brockwell, P.J., Davis, R.A., 2016. Introduction to Time Series and Forecasting. 3 ed., Springer.

Doucet, A., de Freitas, N., Gordon, N., 2001. An Introduction to Sequential Monte Carlo Methods. Springer.

Evensen, G., 2003. The ensemble kalman filter: theoretical formulation and practical implementation. Ocean Dynamics 53, 343–367. URL: `https://doi.org/10.1007/s10236-003-0036-9`.

Evensen, G., 2009. Data Assimilation: The Ensemble Kalman Filter. 2 ed., Springer.

Frei, M., Künsch, H.R., 2013. Bridging the ensemble Kalman and particle filters. Biometrika 100, 781–800. URL: `https://doi.org/10.1093/biomet/ast020`, doi:`10.1093/biomet/ast020`.

Hersbach, H., 2000. Decomposition of the continuous ranked probability score for ensemble prediction systems. Weather and Forecasting 15, 559–570. URL: `https://doi.org/10.1175/1520-0434(2000)015<0559:DOTCRP>2.0.CO;2`, doi:`10.1175/1520-0434(2000)015<0559:DOTCRP>2.0.CO;2`.

Keogh, E.J., Pazzani, M.J., 2001. Derivative Dynamic Time Warping. pp. 1–11. URL: `https://epubs.siam.org/doi/abs/10.1137/1.9781611972719.1`, doi:`10.1137/1.9781611972719.1`.

Kystverket, 2019. Ais. URL: `https://www.kystverket.no/Maritime-tjenester/Meldings--og-informasjonstjenester/AIS/`.

Rezaie, J., Eidsvik, J., 2012. Shrinked $(1-\alpha)$ ensemble kalman filter and α gaussian mixture filter. Computational Geosciences 16, 837–852. URL: `https://doi.org/10.1007/s10596-012-9291-5`.

Shen, Z., Tang, Y., 2015. A modified ensemble kalman particle filter for non-gaussian systems with nonlinear measurement functions. Journal of Advances in Modeling Earth Systems 7, 50–66. URL: `https://agupubs.onlinelibrary.wiley.com/doi/abs/10.1002/2014MS000373`, doi:`10.1002/2014MS000373`.

Sheriff, R., Geldart, L., 1995. Exploration Seismology. 2 ed., Cambridge University Press.

Silixia, 2019. What is distributed sensing? URL: `https://silixa.com/resources/what-is-distributed-sensing/`.

Skare, O., Bølviken, E., Holden, L., 2003. Improved sampling-importance resampling and reduced bias importance sampling. Scandinavian Journal of Statistics 30, 719–737. URL: `http://www.jstor.org/stable/4616798`.

Särkkä, S., 2013. Bayesian Filtering and Smoothing. Cambridge University Press.

Tampnet, 2019. Tampnet in the north sea. URL: `https://www.tampnet.com/north-sea/`.

TeleGeography, 2019. Submarine cable map. URL: `https://www.submarinecablemap.com/`.

Maia Haugen Tømmerbakk

Ship Tracking Based on Fiber Optic Cable Data

NTNU
Norwegian University of
Science and Technology